


FOREWORD

This report was prepared for the Prototype Division of the Air Force Flight Dynamics Laboratory by the Los Angeles Aircraft Division, Rockwell International. The work was performed as part of the STOL tactical aircraft investigation program under USAF contract F33615-71-C-1760, project 643A0020. Daniel E. Fraga, AFFDL/PTA, was the Air Force program manager, and Garland S. Oates, Jr., AFFDL/PTA, was the Air Force technical manager. Marshall H. Roe was the program manager for Rockwell.

This investigation was conducted during the period from 10 June 1971 through 9 December 1972. This final report is published in six volumes and was originally published as Rockwell report NA-72-868. This report was submitted for approval on 9 December 1972.

This technical report has been reviewed and is approved.



E. J. Cross, Jr.
Lt Col, USAF
Chief, Prototype Division

ABSTRACT

The basic objective of the work reported herein was to provide a broader technology base to support the development of a medium STOL Transport (MST) airplane. This work was limited to the application of the externally blown flap (EBF) powered lift concept.

The technology of EBF STOL aircraft has been investigated through analytical studies, wind tunnel testing, flight simulator testing, and design trade studies. The results obtained include development of methods for the estimation of the aerodynamic characteristics of an EBF configuration, STOL performance estimation methods, safety margins for takeoff and landing, wind tunnel investigation of the effects of varying EBF system geometry parameters, configuration definition to meet MST requirements, trade data on performance and configuration requirement variations, flight control system mechanization trade data, handling qualities characteristics, piloting procedures, and effects of applying an air cushion landing system to the MST.

From an overall assessment of study results, it is concluded that the EBF concept provides a practical means of obtaining STOL performance for an MST with relatively low risk. Some improvement in EBF performance could be achieved with further development - primarily wind tunnel testing. Further work should be done on optimization of flight controls, definition of flying qualities requirements, and development of piloting procedures. Considerable work must be done in the area of structural design criteria relative to the effects of engine exhaust impingement on the wing and flap structure.

This report is arranged in six volumes:

Volume I - Configuration Definition

Volume II - Design Compendium

Volume III - Performance Methods and Takeoff and Landing Rules

Volume IV - Analysis of Wind Tunnel Data

Volume V - Flight Control Technology

Part I - Control System Mechanization Trade Studies

Part II - Simulation Studies/Flight Control System Validation

Part III - Stability and Control Derivative Accuracy

Requirements and Effects of Augmentation System Design

Volume VI - Air Cushion Landing System Trade Study

Contrails

TABLE OF CONTENTS

Section		Page
I	INTRODUCTION	1
II	MAJOR CORRELATING PARAMETERS	3
	2.1 Blowing Coefficient	3
	2.2 Jet Turning Angle	5
	2.3 Effects of Flap Impingement on Jet Turning Angle	6
	2.4 Jet Turning Efficiency	13
III	LIFT	19
	3.1 Geometric Parameters	21
	3.1.1 Flap Deflection Angle	21
	3.1.2 Aspect Ratio Factor	22
	3.1.3 Effective Wing Area	22
	3.1.4 Mean Aerodynamic Chord of Effective Wing Area	22
	3.1.5 Wing Thickness Ratio	22
	3.2 Lift at Zero Incidence	25
	3.3 Lift Due to Angle of Attack	29
	3.4 Total Lift Estimation	32
	3.5 Maximum Lift Coefficient	33
	3.6 Angle of Attack for Maximum Lift	38
	3.7 Effects of Aspect Ratio	41
	3.8 Effects of Flap Span	43
	3.9 Effects of Wing Sweep	45
	3.10 Effects of Flap Configuration	47
	3.11 Effects of Leading Edge Devices	54
	3.12 Effects of Nacelle Location and Engine Orientation	59
	3.13 Effects of Asymmetric Thrust	62
IV	DRAG	65
	4.1 Drag Due to Lift	66
	4.2 Thrust Reaction Force	70
V	PITCHING MOMENT	73
	5.1 Thrust Reaction Moment	75
	5.2 Moment Due to Circulation Lift at Zero Incidence	78
	5.3 Pitching Moment Due to Angle of Attack	79
	5.4 Ram Drag Moment	80

Contrails

Section		Page
	5.5 Total Pitching Moment	81
	5.6 Effect of Leading Edge Devices	83
VI	TAIL ENVIRONMENT EFFECTS	87
	6.1 Downwash at Zero Incidence	87
	6.2 Downwash Factor	93
	6.3 Configuration Effects	94
	6.4 Tail Dynamic Pressure	103
VII	ASYMMETRIC POWER EFFECTS ON LATERAL CHARACTERISTICS	105
	7.1 Rolling Moment Due to Engine Failure	105
	7.2 Yawing Moment Due to Engine Failure	111
VIII	POWER EFFECTS ON AERODYNAMIC DERIVATIVES	113
	8.1 Longitudinal Derivatives	113
	8.1.1 Change in Forward Velocity Derivatives	113
	8.1.2 Change in Angle of Attack Derivatives	114
	8.1.3 Rate of Pitch Derivatives	114
	8.1.4 Linear Acceleration Derivatives	114
	8.1.5 Longitudinal Control Derivatives	115
	8.2 Power Effect on Lateral-Directional Derivatives	115
	8.2.1 Change in Sideslip Derivatives	115
	8.2.2 Rate of Roll Derivatives	117
	8.2.3 Rate of Yaw Derivatives	118
	8.2.4 Lateral Acceleration Derivatives	118
	8.2.5 Lateral-Directional Control Derivatives	118
IX	SAMPLE CALCULATIONS	121
APPENDIX	FORTAN IV PROGRAM FOR CALCULATING AERODYNAMIC CHARACTERISTICS OF EXTERNALLY BLOWN FLAP POWERED LIFT SYSTEMS	129

LIST OF ILLUSTRATIONS

Figure	Title	Page
1	Definition of Jet Turning Angle.	5
2	Definition of Impingement Parameter.	6
3	Jet Turning Angle Ratio for Double Slotted Flaps - 0° Sweep.	9
4	Jet Turning Angle Ratio for Double Slotted Flaps - 25° Sweep	10
5	Jet Turning Angle Ratio for Triple Slotted Flaps - 25° Sweep	11
6	Jet Turning Angle - Design Curves.	12
7	Jet Turning Efficiency for Double Slotted Flaps - 0° Sweep	14
8	Jet Turning Efficiency for Double Slotted Flaps - 25° Sweep.	15
9	Jet Turning Efficiency for Triple Slotted Flaps - 25° Sweep.	16
10	Jet Turning Efficiency for Single Slotted Flaps - 33° Sweep.	17
11	Jet Turning Efficiency - Design Curves	18
12	Definition of Flap Deflection Angle.	21
13	Aspect Ratio Correction Factor	23
14	Effective Wing Area.	24
15	Definition of MAC With Flaps Extended.	24
16	$(\partial C_L / \partial \theta)_{\infty}$ and $(\partial C_L / \partial \alpha)_{\infty}$ for a Jet Flap	27
17	Correlation of Lift Increment Due to Power at Zero Incidence	28
18	Lift Curve Slope Correction for Partial Span Blowing	30
19	Correlation of Lift Curve Slope	31
20	Correlation of $\Delta C_{L_{max}}$ Due to Power According to Equation 3.22.	36
21	Correlation of $\Delta C_{L_{max}}$ Due to Power According to Equation 3.23.	37
22	Definition of $\alpha \Delta_{MAX}$	38
23	Correlation of Maximum Angle of Attack Data.	39
24	Effects of Aspect Ratio on Lift Due to Power	42
25	Correlation of Effects of Flap Span on Lift Due to Power	44
26	Correlation of Effects of Wing Sweep on Lift Due to Power.	46
27	Effects of Flap Configuration on Lift Increment Due to Power.	48
28	Flap Details for Comparison of Flap Chord Effects.	49
29	Effect of Flap Configuration on Lift - Power Off	50
30	Effect of Flap Configuration on Lift Due to Power.	51
31	Effect of Flap Configuration on Total Lift Coefficient	52
32	Effect of Flap Gap on Optimum Lift	53
33	Effect of Leading Edge Flap Span on Lift Due to Power.	55
34	Effect of Leading Edge Flap Span on $C_{L_{max}}$	56
35	Effect of Leading Edge Flap Span on $(\Delta C_{L_{max}})$ Due to Power	57
36	Alternate Nacelle Positions Tested in Reference 13	58
37	Effects of Nacelle Location and Nozzle Deflection on Lift Due to Power - Versus δ_N	60

Contrails

Figure	Title	Page
38	Effects of Nacelle Location and Nozzle Deflection on Lift Due to Power.	61
39	Effect of Asymmetric Thrust on Powered Lift Increment	63
40a	Correlation of Induced Drag Data.	67
40b	Correlation of Induced Drag Data.	68
41	Summary of Induced Drag Data.	69
42	Uncertainty of Jet Turning Efficiency Parameter, η	71
43	Chordwise Pressure Distribution of an Externally Blown Flap .	74
44	Spanwise Loading Distribution of an Externally Blown Flap . .	74
45	Definition of Thrust Reaction Moment Arm.	77
46	Correlation of Pitching Moment Coefficient Data	82
47	Effect of Leading Edge Blowing on Center of Pressure Location of Power Effect	84
48	Effect of Leading Edge Configuration Variation on Center of Pressure Location of Power Effect	85
49	Downwash Angle at Zero Incidence, Summary Curves.	88
50	Effect of Tail Length on Downwash Variation With Lift Coefficient at Zero Incidence	89
51	Effect of Tail Height and Engine Deflectors on Downwash Variation With Lift Due to Power at Zero Angle of Attack. .	90
52	Effect of Flap and Nozzle Angles on Downwash Variation With Lift Change Due to Power.	91
53	Effect of Spanwise Engine Location and Leading Edge Devices on Downwash Variation With Lift Change Due to Power.	92
54	Gradient of Downwash Angle With Lift Coefficient and Tail Height.	95
55	Sample Estimated Downwash Factor.	96
56	Experimental Downwash Factor Data	97
57	Tail Dynamic Pressure Characteristics	104
58	Lateral Center of Pressure For Span Loading Due to Power With One Engine Not Operating	106
59	Maximum Lift Loss Due to One Engine Out	107
60	Engine Failure Effect on Maximum Lift	108
61	Roll Characteristics With Left Engine Inoperative	109
62	Roll Characteristics With Left Outboard Engine Inoperative. .	110
63	Yaw Characteristics With Left Engine Inoperative.	112
64	Sample Determination of Power Effects on Forward Velocity Derivatives	119
65a	Comparison of Estimated and Experimental Results.	125
65b	Comparison of Estimated and Experimental Results.	126
65c	Comparison of Estimated and Experimental Results.	127

Contrails

LIST OF SYMBOLS

A	Aspect ratio
A _j	Nozzle exhaust area per engine, ft ²
b	Wing span, ft
c	Local chord, ft
c'	Wing chord on engine centerline, or midway between engines on four engine configurations, ft
\bar{c}	Mean aerodynamic chord, ft
\bar{c}_F	MAC of flapped area of wing, developed chord length, ft
C _D	Total drag coefficient, D/qS
(ΔC_D) _R	Ram drag coefficient, D _r /qS
C _{D_i}	Drag coefficient due to lift with jet reaction force removed
C _L	Total lift coefficient, L/qS
C _{L_{max}}	Maximum lift coefficient, L _{MAX} /qS
C _l	Rolling moment coefficient, \mathcal{L} /qSb
C _m	Pitching moment coefficient, M/qS \bar{c}
C _n	Yawing moment coefficient, \mathcal{N} /qSb; section load coefficient
C _p	Pressure coefficient, P/qS
C _R	Chordwise distance from intersection of jet reaction vector with reference plane to leading edge of chord at thrust centerline, ft
C _μ	Blowing coefficient, T/qS
C _{μ'}	Sectional blowing coefficient, equal to $C_{\mu}/\lambda = C_{\mu} \left(\frac{S}{S'} \right)$
D _j	Diameter of exhaust nozzle, ft
E _j	Energy of jet exhaust per unit volume, lb/ft ²
F	Aspect ratio correction factor
F _A	Static axial jet reaction force, lb
F _N	Static normal jet reaction force, lb
F _R	Resultant static jet reaction force, lb
δ _F	Flap deflection angle, degrees. The angle formed by the wing reference line and a line bisecting the flap trailing edge closing angle (see Figure 12). Nearly all deflection angles quoted in the data sources were revised to conform with the present definition.
g	Acceleration due to gravity, ft/sec ²
h	Height of horizontal tail above wing reference plane, ft
l	Tail arm, distance from 0.25 \bar{C}_W to 0.25 \bar{C}_H , ft
Δ _{l_R}	Height of c.g. above centerline of engine inlet, ft
Δ _{l_T}	Length of moment arm of engine thrust axis about moment reference center, ft
N	Normal force or number of engines
δ _N	Deflection angle of engine exhaust deflector, or nozzle, degrees

Contrails

LIST OF SYMBOLS - Continued

Δp	Exhaust pressure differential across nozzle exit, lb/ft ²
q	Freestream dynamic pressure, $1/2\rho V^2$, lb/ft ²
R	Radius of jet plume at flap trailing edge, ft
S	Wing reference area, ft ²
S'	Wing area affected by flap blowing, ft ²
t/c	Airfoil thickness ratio
T	Nozzle exhaust static thrust, lb
δT	Angle between freestream and engine nozzle centerline, degrees
USB	Upper surface blowing
V	Velocity, ft/sec
W _a	Rate of engine airflow, lb/sec
x	Chordwise dimension, ft
x _{c.p.}	Location of center of pressure, ft
x _{L.E.c'}	Location of leading edge of c', ft
x _{L.E.c_f}	Location of leading edge of c _f , ft
x _{REF}	Location of moment reference center, ft
y	Spanwise dimension, ft
z	Vertical dimension, ft
z _F	Distance which flap trailing edge extends into jet plume perpendicular to engine centerline, ft
α	Angle of attack, degrees or radians
Γ	Circulation
γ	Flight path angle, degrees
Δ	Incremental value
δ	Deflection angle, degrees
ϵ	Downwash angle, degrees
η	Jet turning efficiency factor
θ	Effective jet turning angle, radians
λ	Area ratio, S'/S
Λ	Wing sweep of 0.25 chord, degrees
ν	Lift slope correction for partial span blowing
π	Ratio of circumference of a circle to its diameter
ρ	Density, slugs/ft ³
ψ	Yaw angle, degrees
ϕ	$(C_{L\alpha})_{PO}/C_{L\alpha}$

SUBSCRIPTS

()B	Baseline power-off data
()EST	Estimated
()EXP	Experimental data
()H	Horizontal tail
()j	Jet exhaust
()L.E.	Leading edge
()MAX.	Maximum value

SUBSCRIPTS (Continued)

- ()MEAS. Measured value
- ()MIN. Minimum value
- ()0 Zero angle of attack
- ()PL Powered lift
- ()P.O. Power off
- ()R Due to jet reaction
- ()RD Ram drag
- ()REF About moment reference center
- ()TEST Test data
- ()V At forward speed
- () θ Due to jet deflection
- () ∞ Two dimensional value
- () α Due to angle of attack
- () Γ Circulation lift
- ()F Flaps

Contrails

Contrails

Section I

INTRODUCTION

The externally blown flap lift-propulsion system has recently evolved in design studies of advanced short takeoff and landing (STOL) aircraft. This lift-propulsion system is attractive because it generates a significant amount of wing lift at typical STOL speeds while it is not as complex as other lift-propulsion systems.

Because STOL aerodynamic data for this lift-propulsion system are relatively new it has been extremely difficult for the aerodynamicist to estimate effects of geometric perturbations that are normally encountered during preliminary design phases. It is therefore appropriate to collect and organize the basic aerodynamic information into a manual and to develop methods of estimation. This will give improved credence to STOL performance data for this lift-propulsion system and better comparison with the performance of other lift-propulsion systems. To provide such a manual is a purpose of the present design compendium.

The design compendium presents methods to determine the power effects on lift, drag, pitching moment, downwash, lateral and directional moments, and some dynamic derivatives. The methods are presented for possible inclusion in the DATCOM stability and control handbook. Increments due to power are given, so that these can be added to power off data from existing sections of DATCOM. Occasionally, when insufficient data were available to generate a method, some guidelines for the fairing of curves are given.

The general approach used here is based on jet flap theory with some empirically guided interpretations in application to the externally blown flap. Although the jet flap theory strictly applies only to inviscid, incompressible flow at small incidence angles, small jet turning angles, and a thin jet sheet, surprisingly good agreement is found with experimental data where these conditions are rather grossly exceeded.

The data and methods in this compendium are often given for the determination of characteristics at zero angle of attack, rather than for the angle at zero lift that is commonly used in conventional aerodynamics. The zero angle of attack is chosen because the zero lift angle results in extreme negative values for STOL airplanes in the power mode. These negative angles are generally unattainable in flight because of flow separation at the lower wing surface. On the other hand, STOL takeoff and landings are often made with angles of attack relatively close to zero.

Contracts

Section II

MAJOR CORRELATING PARAMETERS

The forces developed by flap blowing are functions of the total jet momentum, the turning angle of the jet, and the geometry of the wing-flap system. The jet momentum is usually expressed as a coefficient, C_{μ} , and in conformance with jet flap theory the momentum exiting from the flap trailing edge is used in estimation methods. Where C_{μ} is the jet nozzle momentum, the flap exit momentum is defined as ηC_{μ} , where η is an efficiency factor accounting for energy losses incurred in the turning process. The turning angle, θ , is the effective angle at which the jet leaves the flap. Derivation of these parameters, and methods of estimation are discussed below.

2.1 BLOWING COEFFICIENT

The lift and normal force at forward speed appear to be affected predominantly by the ratio of the energy of the freestream air and the energy exhausted by the blowing nozzle, as well as by geometric relations. The energy from the exhaust nozzle is, expressed in terms of unit exhaust volume:

$$E_j = \frac{1}{2} \rho_j v_j^2 \quad 2.1$$

The use of the freestream dynamic pressure $q = 1/2 \rho v^2$ to nondimensionalize this energy yields the parameter

$$\frac{\rho_j v_j^2}{\rho v^2}$$

Herein, $\rho_j v_j^2$ can be expressed in terms of the nozzle exhaust thrust. Denoting T_v as the nozzle exhaust thrust at forward speed, and introducing the symbol A_j as the nozzle exhaust area, a relation between $\rho_j v_j^2$ and the nozzle thrust is obtained as follows:

$$T_v = (\rho_j v_j A_j) v_j + \Delta p A_j \quad 2.2$$

Contrails

Herein Δp is the exhaust pressure differential across the nozzle exit, which is zero for unchoked exhaust typical for external blowing, so that

$$\frac{\rho_j v_j^2}{\rho v^2} = \frac{T_v / A_j}{2 q} \quad 2.3$$

or

$$\frac{\rho_j v_j^2}{\rho v^2} = \frac{T_v}{q S} \left(\frac{S}{2 A_j} \right)$$

Because for a given configuration the value of $\frac{S}{2 A_j}$ is fixed, it is seen that the energy ratio is proportional to $C_{\mu v}$:

$$\frac{\rho_j v_j^2}{\rho v^2} = \text{constant} \cdot C_{\mu v} \quad 2.4$$

where, per definition

$$C_{\mu v} = \frac{T_v}{q S} \quad 2.5$$

The validity that the force characteristics correlate with the energy ratio, i.e., the blowing parameter, has been substantiated by several investigations wherein engine thrust and q were varied, and C_{μ} held constant.

It should be noted that T_v is the exhaust thrust of the nozzle, and not the net engine thrust. The net engine thrust is equal to the exhaust thrust minus the intake momentum drag. Only the exhaust thrust is used in this section because it is assumed that only the energy from the exhaust is determining the airfoil lifting characteristics from blowing regardless of the engine inlet flow characteristics.

The exhaust thrust, T_v , generally increases slightly with increase in speed. Often, the increase of T_v with speed is not quantitatively known, and therefore only the static thrust is taken as the reference thrust. Advantages of this procedure lie in the fact that the thrust used is a constant which makes it very suitable for use as a reference and no intake momentum drag exists in this condition. Thus, the use of the definition of the coefficient

$$C_{\mu} = \frac{T}{q S} \quad 2.6$$

is favored, where T is the static thrust.

2.2 JET TURNING ANGLE

The jet turning angle, θ , is the effective direction at which the jet leaves the trailing edge of the flap system and defines the direction of the total reaction force vector, F_R (see Figure 1). The jet turning angle and reaction force components are determined for the static condition, since the effects of forward velocity on these values are **not** known, and would be very difficult to define. By definition, then:

$$\theta = \tan^{-1} F_N/F_A \quad 2.7$$

F_N = static normal force

F_A = static axial force

$$F_R = (F_N^2 + F_A^2)^{1/2} = \text{resultant reaction force.} \quad 2.8$$

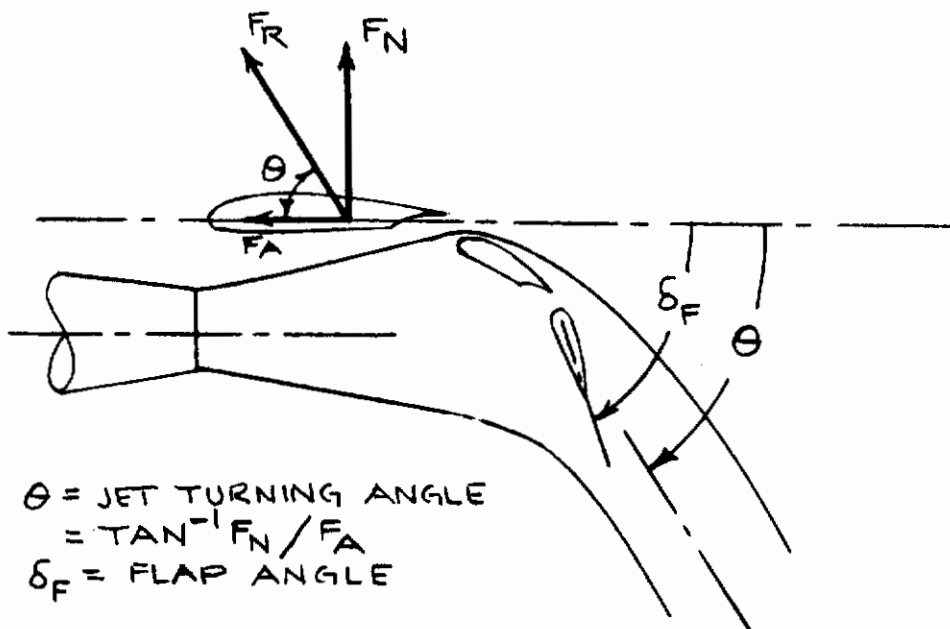


Figure 1. Definition of Jet Turning Angle

2.3 EFFECTS OF FLAP IMPINGEMENT ON JET TURNING ANGLE

Direct application of the jet flap theory to the externally blown flap would assume that the jet turning angle, θ , is equal to the flap deflection angle, δ_F . This has proved to be a good assumption for the case where the flap system captures the entire jet efflux; however, where the flap intercepts only a part of the jet, the effective turning angle will be less than the flap angle. The following section presents an approach to estimating the jet turning angle for externally blown flaps, including those cases where there is less than full impingement of the jet exhaust on the flap.

Using a heuristic approach, it was assumed that the effective jet turning angle is related to the flap angle and to the portion of jet momentum that is intercepted by the flap. Following this reasoning correlations were made of experimental values of jet turning angle as a function of flap angle, θ/δ_F , and the extent of flap penetration into the jet. The results of these correlations are shown in Figures 3 through 5 for various types of flaps and wing sweep angles. In these figures the extent of flap penetration into the jet is given in terms of the ratio Z_F/R , where Z_F is the distance that the flap penetrates into the jet, and varies in value from $-R$ to $+R$ as the flap traverses the entire jet. The definition of this parameter, Z_F/R , is illustrated in Figure 2. The value of the radius, R , of the jet at the location of the flap trailing edge can be estimated by the relation:

$$\frac{R}{D_j/2} = 1 + \frac{x/D_j}{2.3} \quad 2.9$$

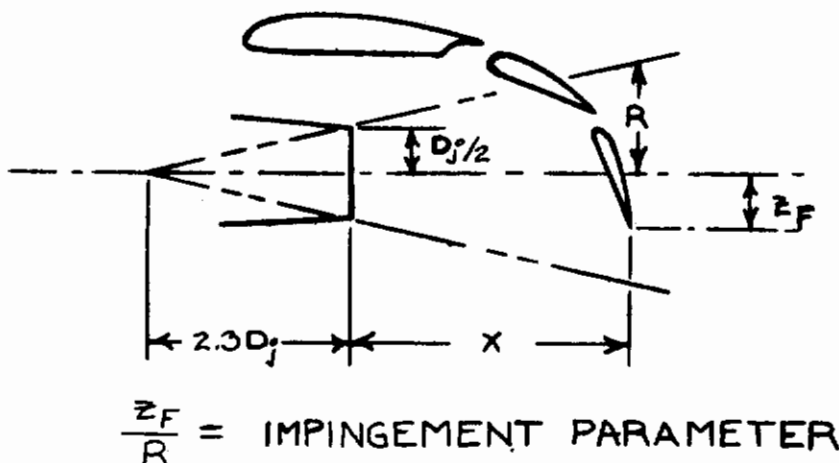


Figure 2. Definition of Impingement Parameter

Contrails

where D_j is the diameter of the exhaust nozzle, and X is the distance of the flap trailing edge behind the nozzle exhaust, Figure 2. The effective source length, $2.3 D_j$, used here is based on a jet expansion envelope where the jet velocity is essentially zero at the edge of the jet wake profile. Other definitions such as one percent or five percent of the maximum jet velocity could be used, which would only change the scale of the Z_F/R parameter. Only an average spreading angle is used here, although according to Ribner, Reference 7, the spreading depends to some extent on the thrust coefficient.

The data from these correlation plots Figures 3 through 5, were used to develop a set of design curves, shown in Figure 6, for estimating jet turning angle values. These design curves represent envelopes of the better performance data from the individual correlation plots. The data correlations have considerable scatter resulting from non-optimum flap geometry and variations in experimental technique. However, values of jet turning angle from these design curves have been used in substantiation calculations of the methods for prediction of aerodynamic characteristics of externally blown flaps in later sections of this report, with generally very good results (Section III, IV and V).

It is noted in the design curves, Figure 6, that the only flap geometry parameter that appears is the number of flap segments (double and triple slotted flaps). Other variables such as wing sweep, and perhaps aspect ratio, would be expected to influence the jet turning angle. However, the effects of these other variables are evidently of lower order and are lost in the data scatter.

Separate curves are shown for data with jet deflectors. These devices have been tested in several investigations and found to improve the lift augmentation of externally blown flaps (References 4, 8, 16, 20). These deflectors are simple flat plates that deflect the jet exhaust upward to increase the degree of impingement of the jet on the flap. In effect the deflectors are increasing the impingement ratio, Z_F/R , which has been shown above to influence the effective jet turning angle.

For purposes of predicting the effectiveness of jet deflectors, the procedure described above utilizing the impingement parameter, can not be used directly since the deflectors change the characteristic shape of the jet expansion envelope in some undefined manner so the impingement ratio of the deflected jet is not known. However, results of tests of deflectors from the referenced tests have provided effective turning angle data as shown in Figures 3 through 5, which are shown as a function of the impingement ratio of the undeflected jet, which can be determined.

The available data on the effectiveness of jet deflectors in terms of effective jet turning angle have been summarized in Figure 6. Here, a

Contrails

recommended design curve for EBF systems utilizing jet deflectors is presented as a function of the impingement parameter of the undeflected jet. As indicated by this plot, there is no distinguishable difference between the effectiveness of double or triple slotted flaps when utilizing the deflector. The procedure for estimating the effective jet turning angle with deflectors is, then, to define the impingement ratio of the undisturbed jet, as described above, and then utilize the design curve labeled "with jet deflectors."

The effects of engine location relative to the flap, and the effects of nacelle incidence and nozzle deflection are all accounted for in this use of the impingement parameter.

Test data show nearly complete jet turning with flap immersion of $Z_F/R > 0.65$ except for cases where flow separation over the flaps is suspected. It is concluded then, that in the design of the propulsion-lift system that the design goal should be to attain impingement of at least $Z_F/R = 0.6$ for high lift performance.

Those data that fall significantly below the design curves are in some cases extreme flap angles (75° to 95°) which apparently did not have proper blowing to maintain flow attachment, and in other cases rather unconventional flap segment arrangements which evidently resulted in separation. In view of these results it would probably be prudent to not apply these methods to flap angles exceeding 65° unless experimental verification can be obtained.

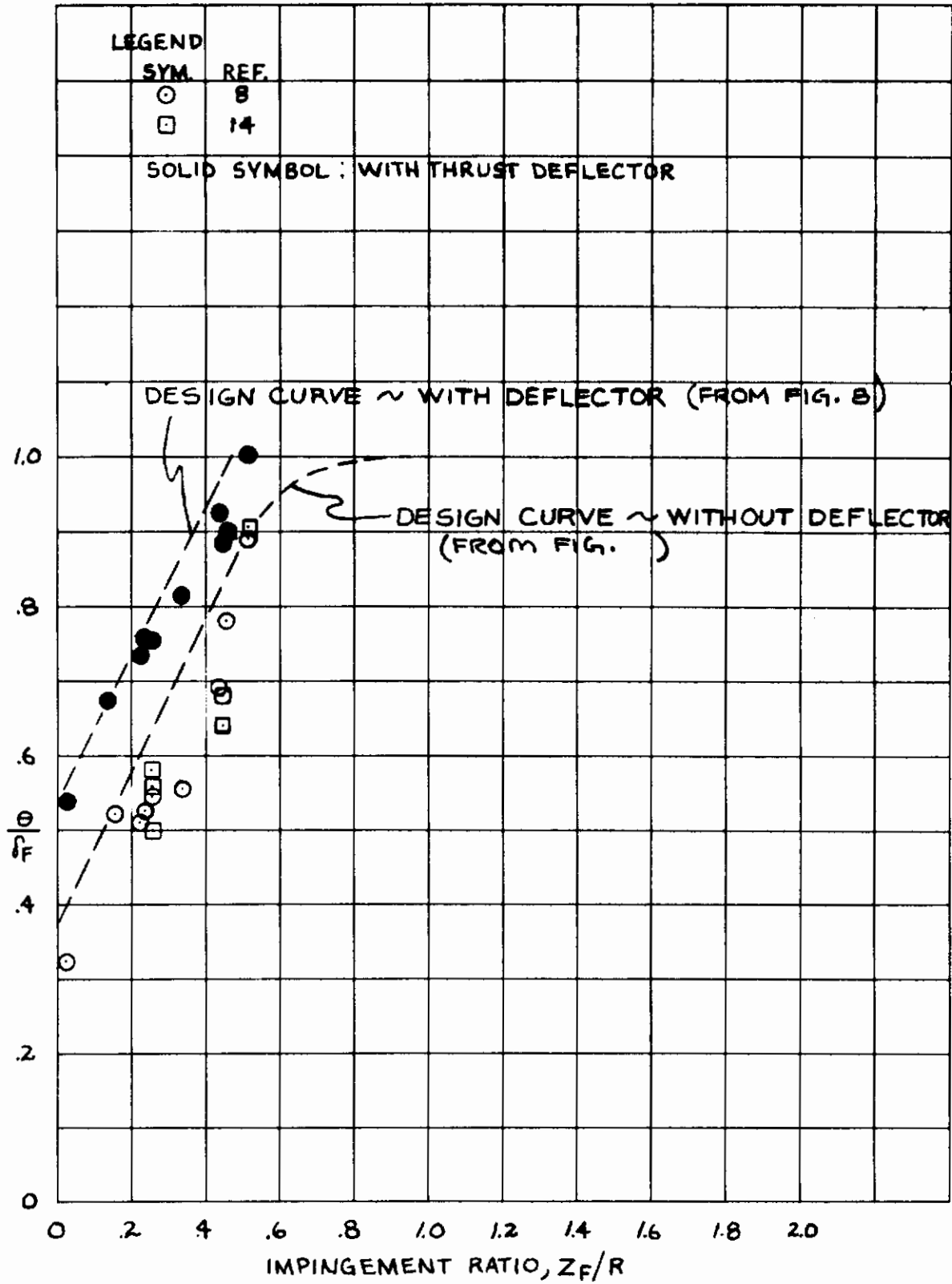


Figure 3. Jet Turning Angle Ratio for Double Slotted Flaps - 0° Sweep

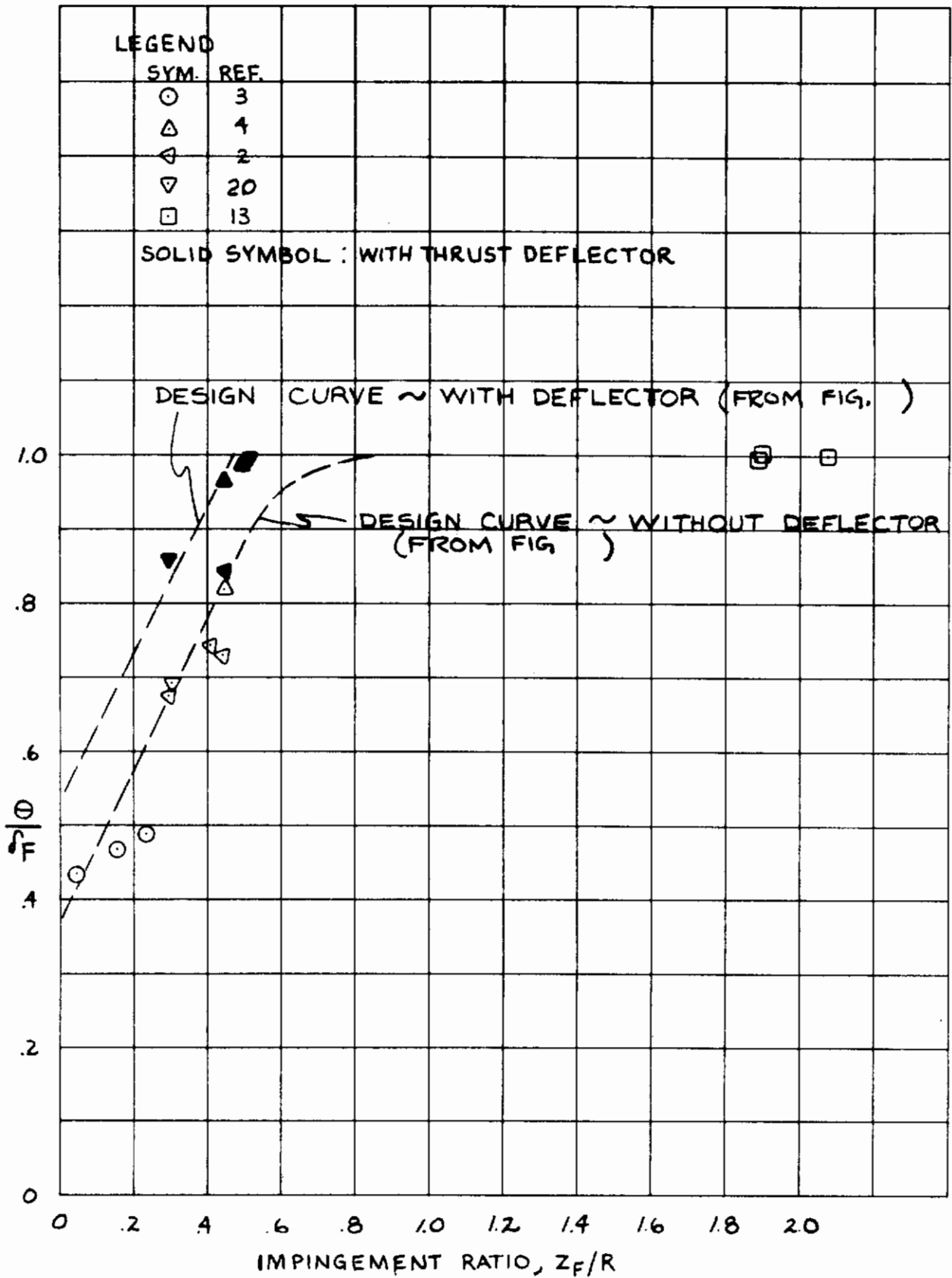


Figure 4. Jet Turning Angle Ratio for Double Slotted Flaps - 25° Sweep

Contrails

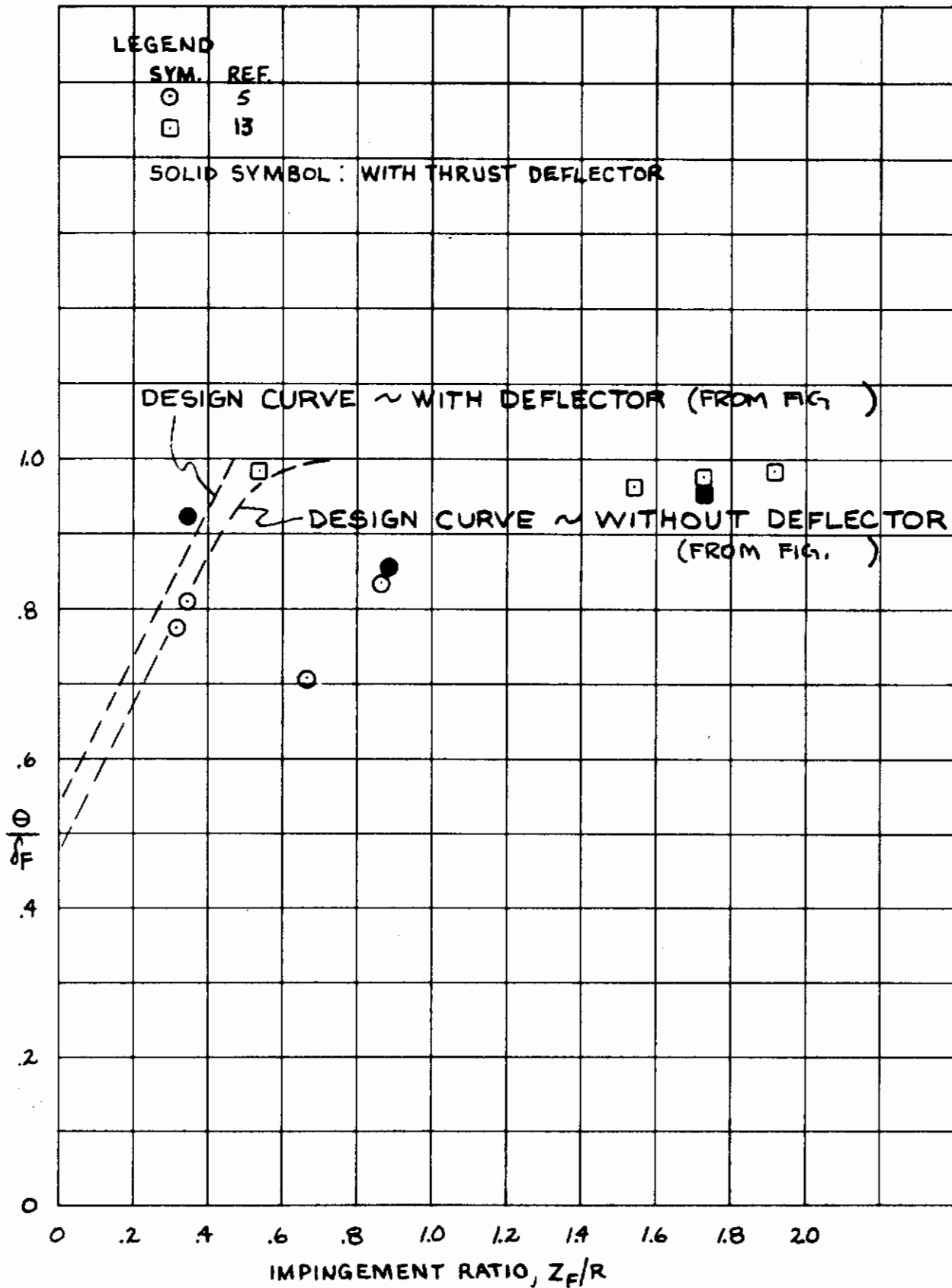


Figure 5. Jet Turning Angle Ratio for Triple Slotted Flaps - 25° Sweep

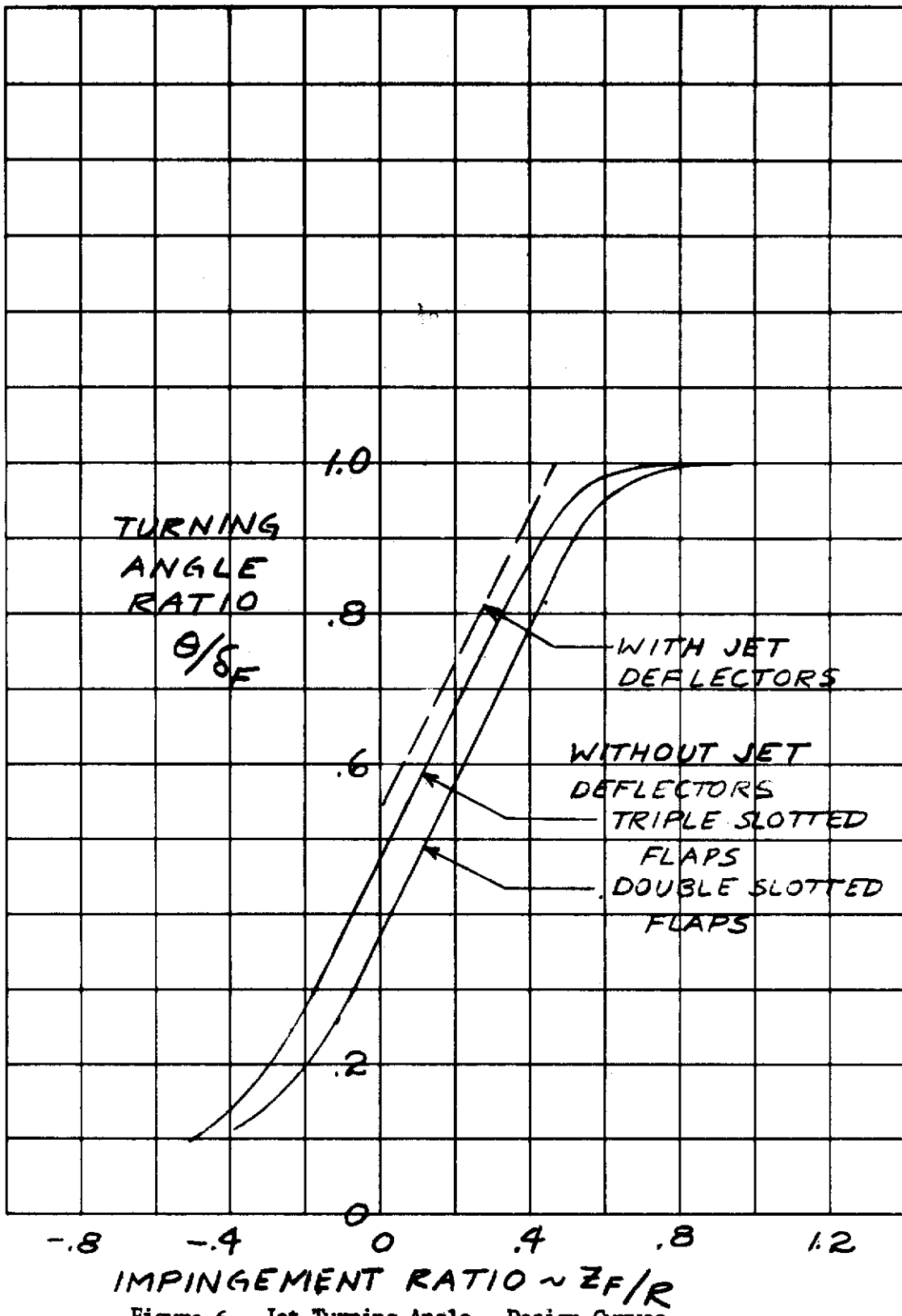


Figure 6. Jet Turning Angle - Design Curves

2.4 JET TURNING EFFICIENCY

In applying the relationships of jet flap theory to the externally blown flap, the blowing momentum leaving the flap trailing edge should be used. This exiting momentum is defined as ηC_{μ} , where the factor η accounts for all of the losses in the jet turning process. The turning efficiency can be determined from static tests, where it is defined as:

$$\eta = F_R / T \quad 2.10$$

where $F_R = (F_N^2 + F_A^2)^{1/2}$

F_N = static normal force

F_A = static axial force

T = nozzle thrust

It would be expected that the turning losses would depend on the degree of turning and the details of the flap geometry.

For use in prediction methods, data correlations have been made of the turning efficiency versus effective turning angle where effects of the number of flap slots (single, double, triple), and of wing sweep are apparent. Considerable scatter in the test results exists which no doubt is due to details of slot gaps, various amounts of separation on the flap segments, differences in flap segment contours, and experimental techniques (Figures 7 through 10). Curves have been established on Figure 11 for design use which are considered to be representative of better designed externally blown flap systems.

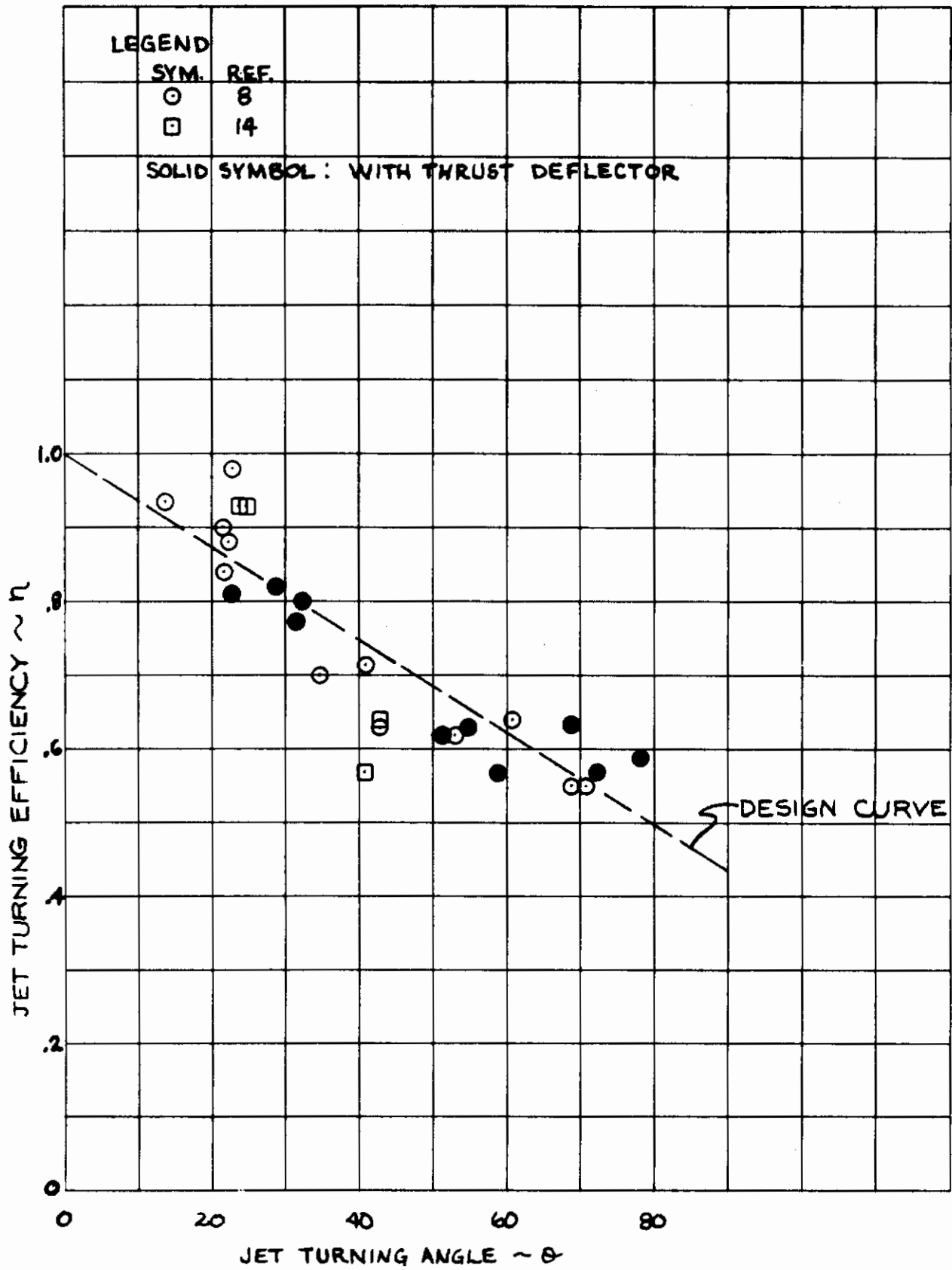


Figure 7. Jet Turning Efficiency for Double Slotted Flaps - 0° Sweep

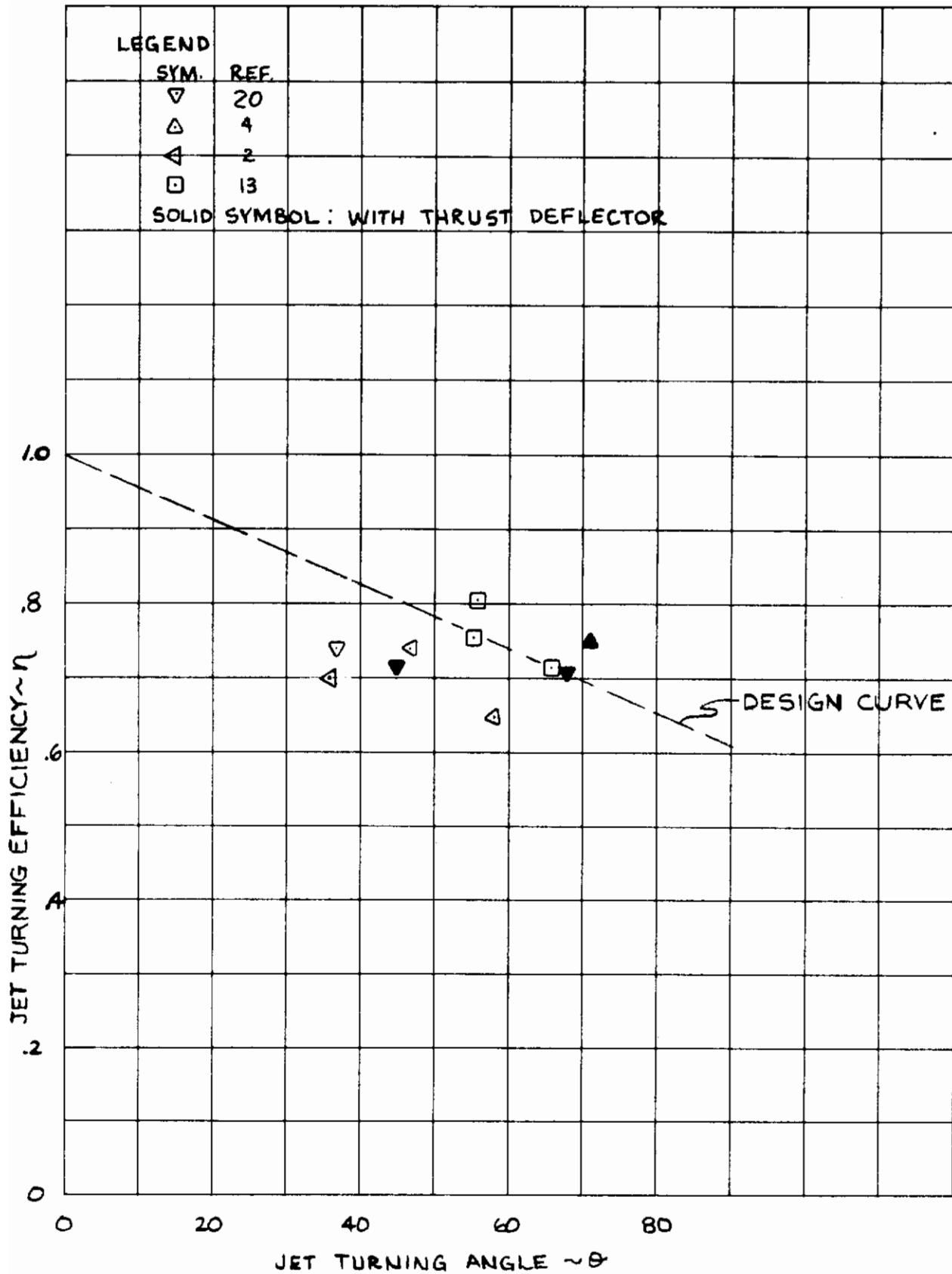


Figure 8. Jet Turning Efficiency for Double Slotted Flaps - 25° Sweep

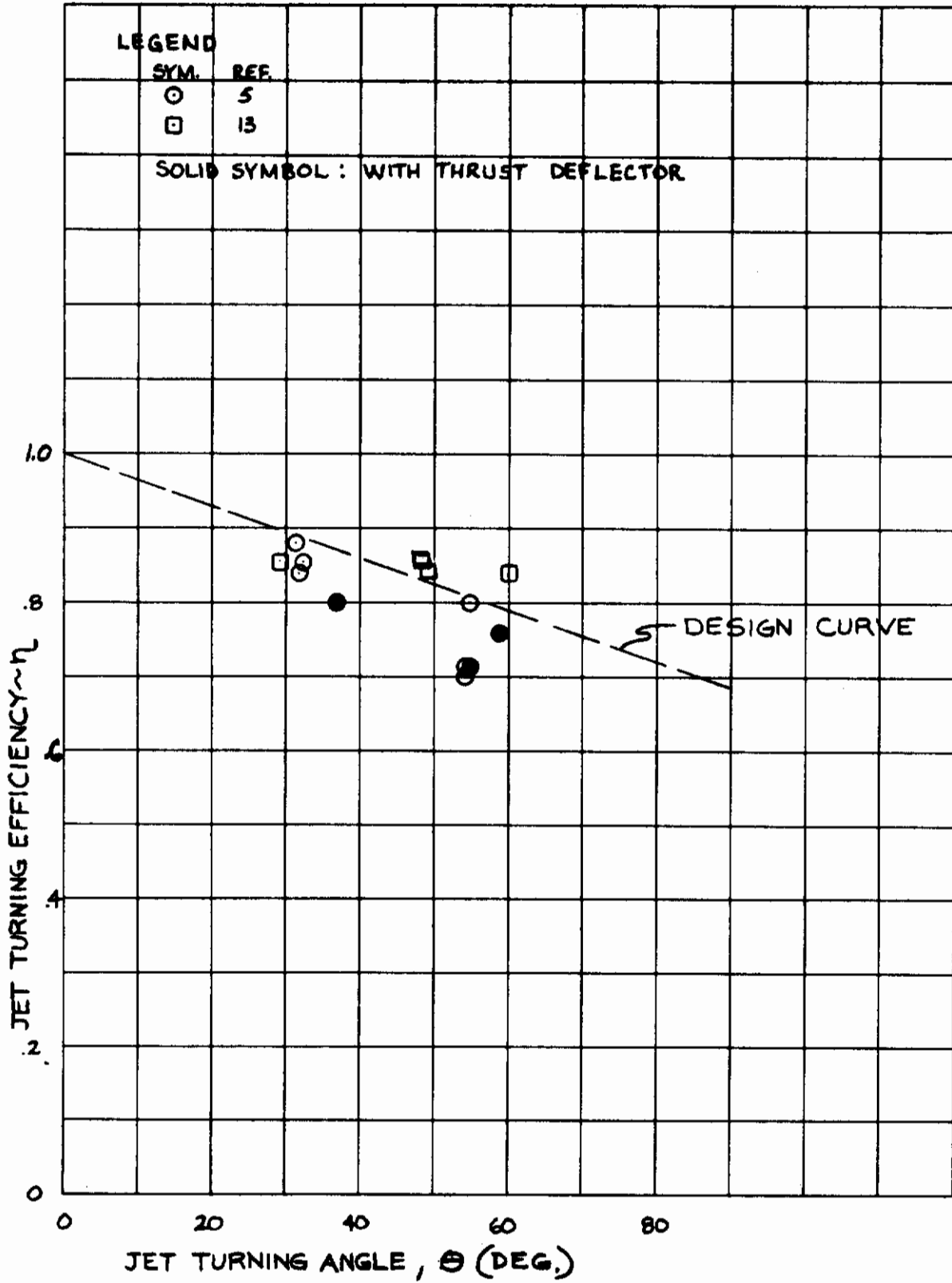


Figure 9. Jet Turning Efficiency for Triple Slotted Flaps - 25° Sweep

Contrails

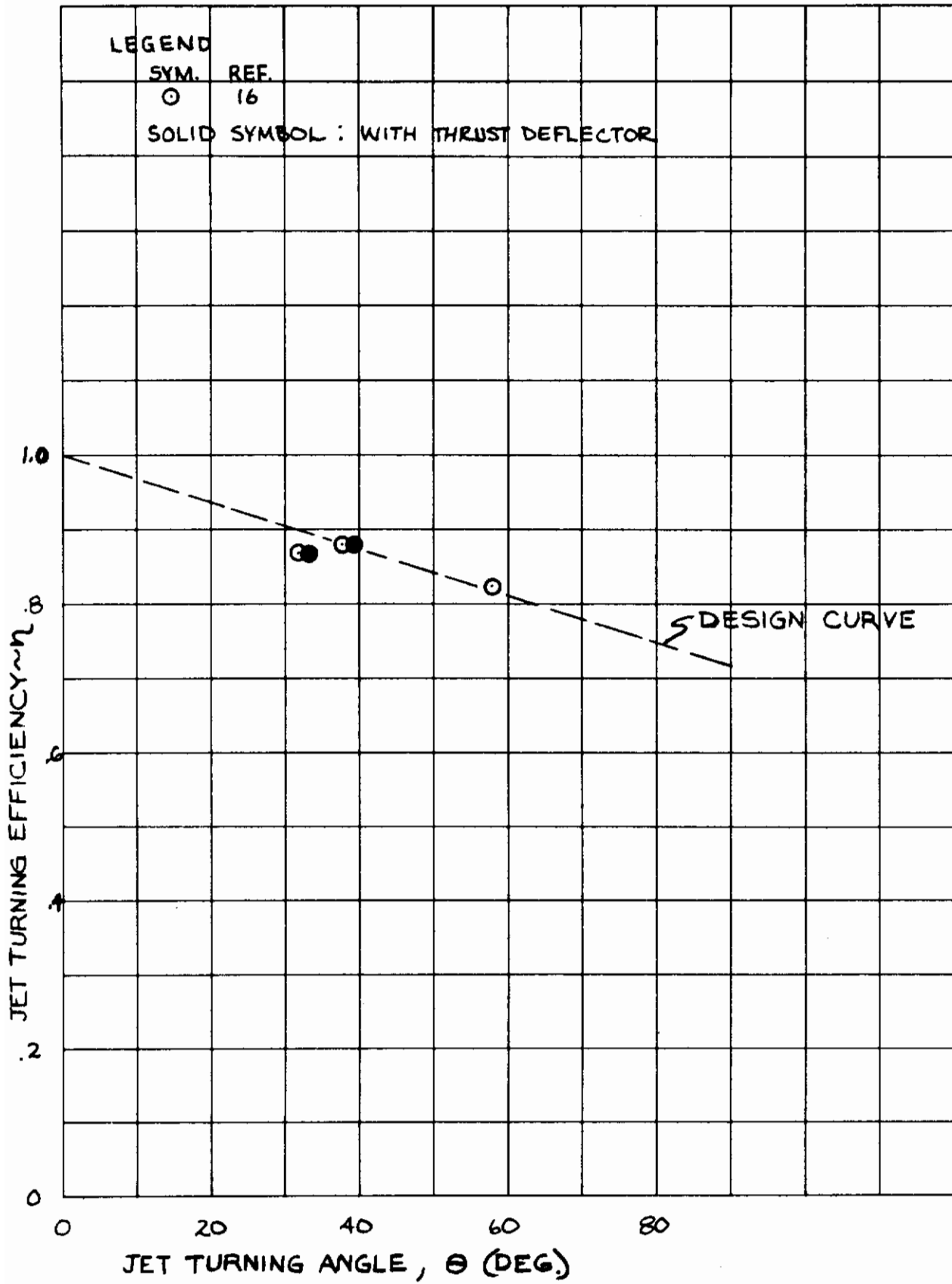


Figure 10. Jet Turning Efficiency for Single Slotted Flaps - 33° Sweep

Contrails

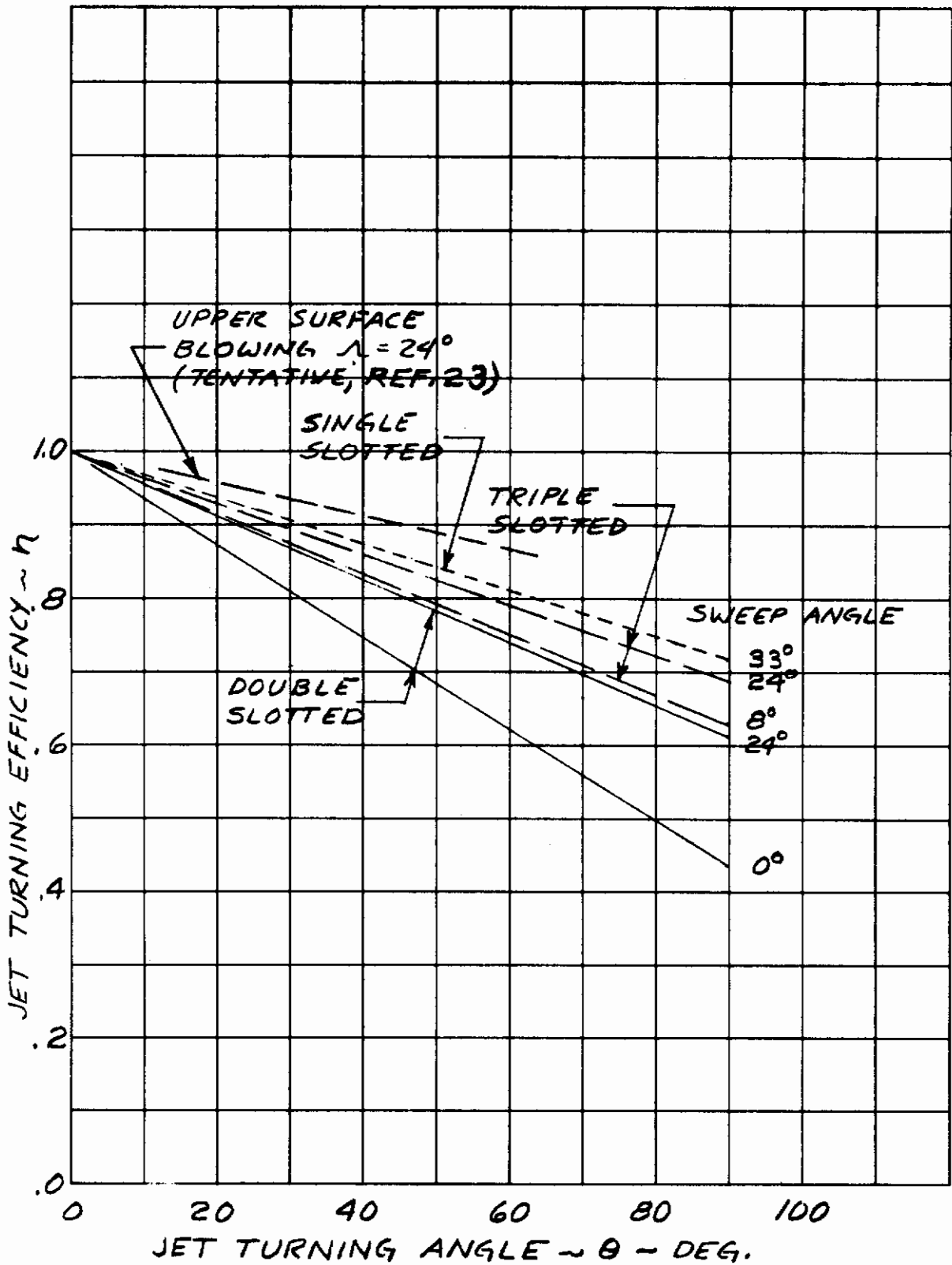


Figure 11. Jet Turning Efficiency - Design Curves

Section III

LIFT

The tail-off lift of an airplane with an externally blown flap is estimated by adding the effects of blowing to the power-off lift at zero angle of attack with flap deflected. The power-off lift is estimated by conventional methods, such as DATCOM, or is based on unpowered wind tunnel data.

(NOTE: Estimation of the power-off lift due to flap deflection at zero angle of attack can be included in the present methods, as will be discussed later; however, accuracy should be improved by use of conventional methods as stated above.)

$$C_L = (C_L)_B + (\Delta C_L)_{PL} \quad 3.1$$

where $(C_L)_B$ is the baseline lift at $\alpha = 0$, flaps deflected, power-off; $(\Delta C_L)_{PL}$ = powered lift increment due to jet deflection and angle of attack.

Estimation of the powered lift increment is based on the jet flap theory developed by Spence (Reference 10), which gives for the lift of a two-dimensional thin airfoil with a jet flap:

$$C_L = (C_{L\theta})_{\infty} \theta + (C_{L\alpha})_{\infty} \alpha \quad 3.2$$

where $(C_{L\theta})_{\infty}$ is the two-dimensional lift gradient with jet deflection angle, θ , and $(C_{L\alpha})_{\infty}$ is the two-dimensional gradient of lift with angle of attack, α .

In application of this theory to an airfoil of finite thickness and finite aspect ratio, the pressure lift terms are modified for thickness by the factor $(1 + t/c)$, and for aspect ratio by a factor F , derived by Maskell and Spence (Reference 11). The derivation of the aspect ratio correction factor is based on the assumption of elliptical spanwise distribution of chord length and blowing coefficient. The resulting expression for the lift of a three-dimensional wing with a full span jet flap, as given in Reference (11), is:

$$C_L = F \left[\left(1 + \frac{t}{c}\right) \left\{ (C_{L\theta})_{\infty} \theta + (C_{L\alpha})_{\infty} \alpha \right\} - \frac{t}{c} (\theta + \alpha) C_{\mu} \right] \quad 3.3$$

Further development by Williams, Butler, and Wood (Reference 12) to account for partial span blowing provided correction factors λ and ν for the jet deflection term and angle of attack term, respectively.

Adaptation of these methods for the jet flap to the case of the externally blown flap is based on the following considerations: The lift increment due to power is estimated by the jet flap methods and added to the power-off lift of the wing with flaps deflected; in calculation of the lift due to jet deflection the sine of the turning angle is used rather than the angle, since the theory was developed on the basis of small angles for which $\sin \theta \approx \theta$; the aspect ratio correction factor which is based on elliptical spanwise distribution of blowing, is not strictly applicable to the concentrated blowing technique of the EBF, but its use gives better results than the unpowered factor, $A/(A + 2)$; the thickness correction factor is applied to the entire lift increment due to power rather than excluding the direct jet lift which results in a small discrepancy with the theory but improves the experimental correlations and simplifies the calculations.

With the above considerations, the expression for the lift increment due to power for an externally blown flap airplane is:

$$(\Delta C_L)_{PL} = F \left(1 + \frac{t}{c}\right) \left[\lambda (C_{L\theta})_{\infty} \sin \theta + \nu (C_{L\infty})_{\infty} \infty \right] \quad 3.4$$

It is more convenient to treat the total lift increment due to power in its components due to jet deflection and angle of attack:

$$(\Delta C_L)_{PL} = (\Delta C_L)_{\theta} + (\Delta C_L)_{\infty} \quad 3.5$$

$$(\Delta C_L)_{\theta} = F \left(1 + \frac{t}{c}\right) \lambda (C_{L\theta})_{\infty} \sin \theta \quad 3.6$$

$$(\Delta C_L)_{\infty} = F \left(1 + \frac{t}{c}\right) \nu (C_{L\infty})_{\infty} \infty \quad 3.7$$

Further development of procedures for calculating these lift increments is given in Sections 3.2 and 3.3. A discussion of the geometrical parameters involved in these calculations is given in the next section.

3.1 GEOMETRIC PARAMETERS

The methods of estimation in the following sections make use of various geometrical parameters which will be defined here.

3.1.1 FLAP DEFLECTION ANGLE

The flap deflection angle, δ_F , as used herein for under the wing blowing is defined as the angle from the wing reference plane to the bisector of the trailing segment of the flap. For over the wing blowing the deflection angle is taken from the wing reference plane to the upper surface of the trailing edge of the flap. These angles are illustrated in Figure 12.

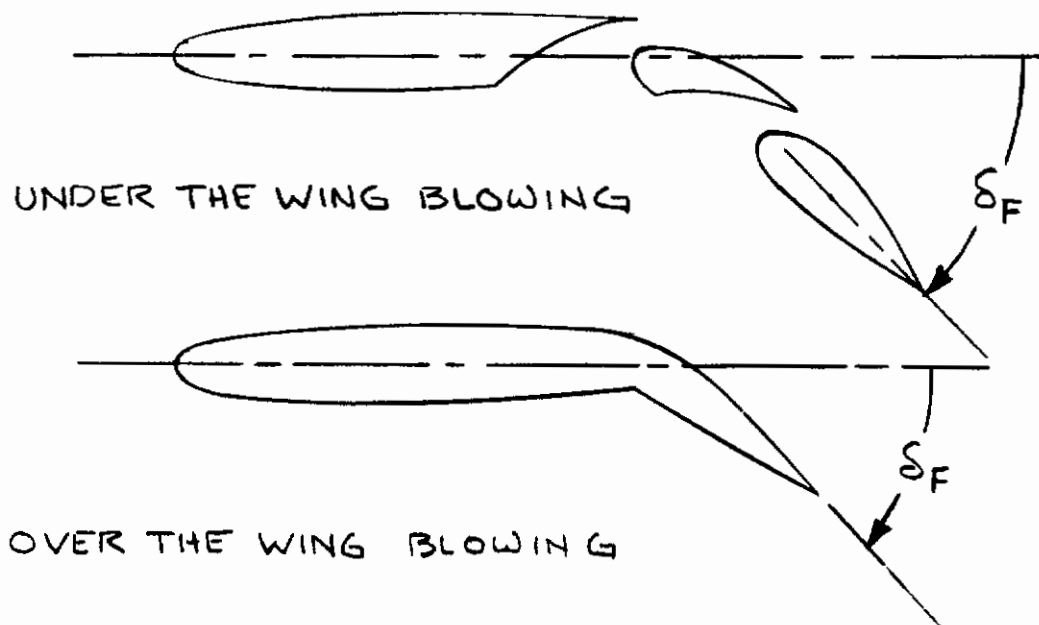


Figure 12. Definition of Flap Deflection Angle

3.1.2 ASPECT RATIO FACTOR

An approximate relation for the aspect ratio correction factor, F , given in Reference (12), and replacing C_{μ} with $\eta C'_{\mu}$, is:

$$F \approx \frac{A + 2\eta C'_{\mu} \pi}{A + 2 + 0.604 (\eta C'_{\mu})^2 + 0.876 \eta C'_{\mu}} \quad 3.8$$

where C'_{μ} is the sectional thrust coefficient = $C_{\mu} \left(\frac{S}{S'} \right)$.

A plot of this factor for various values of A and $\eta C'_{\mu}$ is shown in Figure 13.

For the case of part span flaps, the aspect ratio is taken as that of the wing excluding half of the area outboard of the flaps.

3.1.3 EFFECTIVE WING AREA

The effective wing area, S' , is defined as the area of the wing between the inboard station and outboard station of the flap (see Figure 14). If the wing has part span flaps the effective wing area includes one-half of the area outboard of the flaps. This definition was derived from consideration of pressure data from Reference (14), which shows carry over on the wing outboard of the flap of about one-half the loading on the flapped portion of the wing. Use of this definition in estimating characteristics of part span configurations has produced good correlations with test data (see Section 3.8). (NOTE: Limited data for upper surface blowing configurations indicate that only that portion of the wing surface that is in the exhaust flow should be included in the definition of S' for upper surface blowing. For example, S'/S for the configuration of Reference 22 is approximately 0.5.)

3.1.4 MEAN AERODYNAMIC CHORD OF EFFECTIVE WING AREA

The MAC of the effective wing area, \bar{c}_F , is determined by conventional methods applied to the effective wing area, S' , as described above, but the chord length is taken as the developed chord length with the flaps extended as shown in Figure 15.

For full span flaps \bar{c}_F can be taken as the MAC of the basic wing, \bar{c} , corrected for flap chord extension.

3.1.5 WING THICKNESS RATIO

The wing thickness ratio, t/c , is taken as the thickness ratio of the MAC of the flapped portion of the wing.

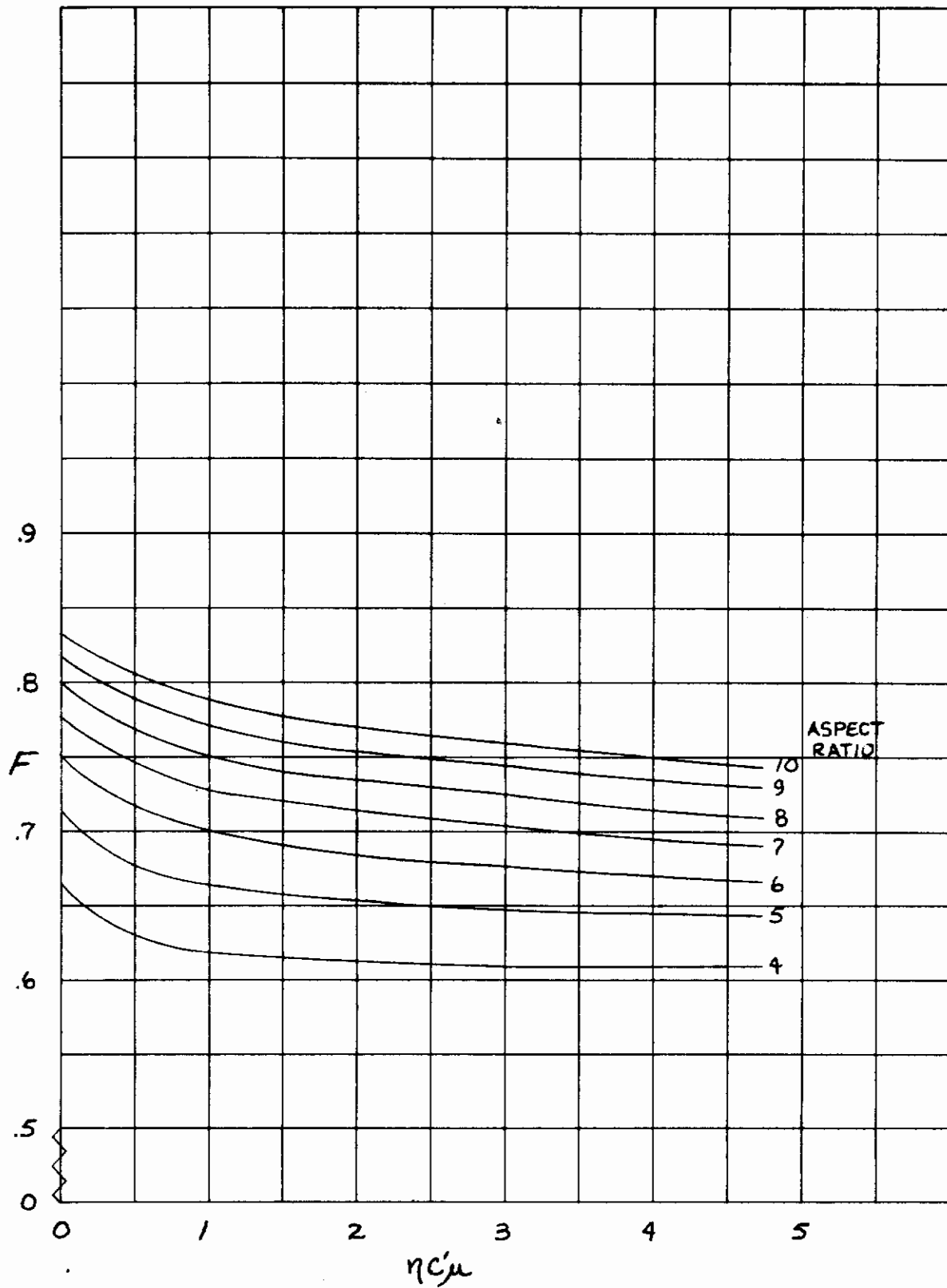


Figure 13. Aspect Ratio Correction Factor

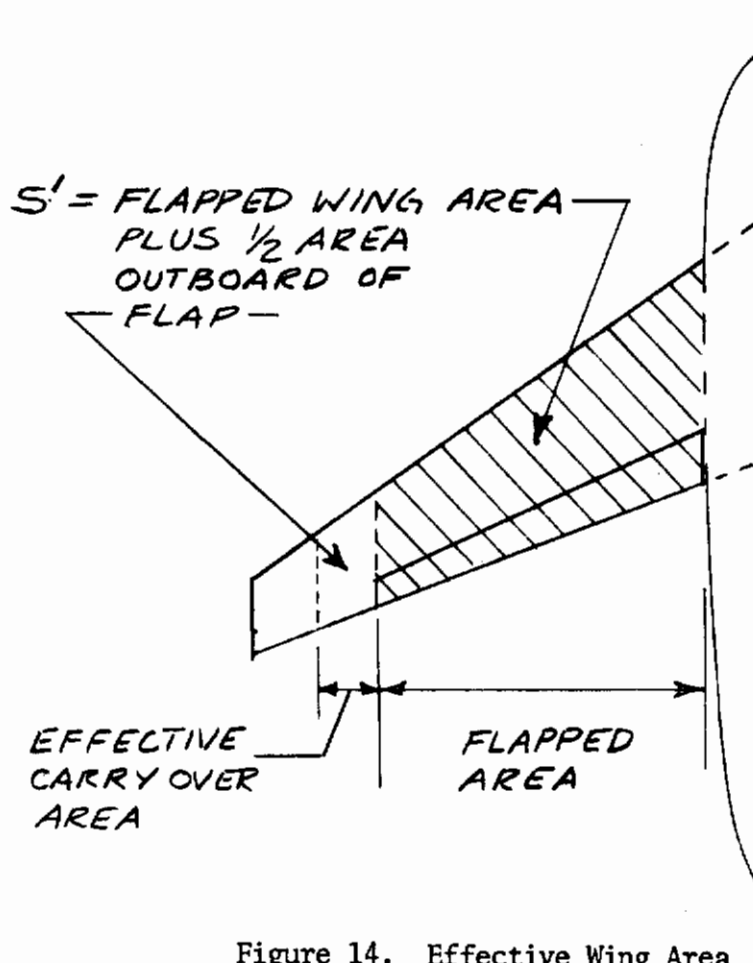


Figure 14. Effective Wing Area

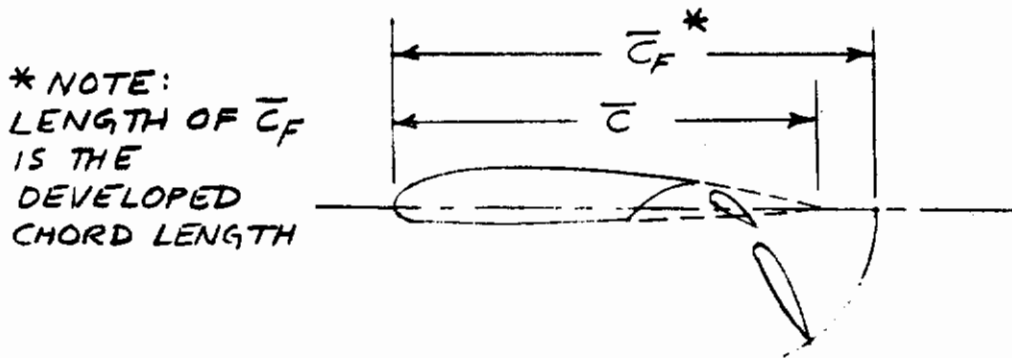


Figure 15. Definition of MAC With Flaps Extended

3.2 LIFT AT ZERO INCIDENCE

The lift increment due to power at zero angle of attack is defined by:

$$(\Delta C_L)_\theta = F \left(1 + \frac{t}{c}\right) \lambda (\partial C_L / \partial \theta)_\infty \sin \theta \quad 3.6$$

where F , η , t/c , and θ have been defined in previous sections, and

$\lambda = S'/S =$ area ratio defined in Section 3.1.3

$(\partial C_L / \partial \theta)_\infty =$ two-dimensional lift due to jet turning angle.

A plot of $(\partial C_L / \partial \theta)_\infty$ as defined in Reference (10) is shown in Figure 16. The curve for $C_F/C = 0$, corresponding to a pure jet flap, should be used in these estimation procedures. An approximate interpolation formula for the $C_F/C = 0$ case, given in Reference (11) is, substituting $\eta C'_\mu$ for C_μ :

$$(\partial C_L / \partial \theta)_\infty \approx \left[4\pi \eta C'_\mu \left\{ 1 + 0.151(\eta C'_\mu)^{1/2} + 0.139 \eta C'_\mu \right\} \right]^{1/2} \quad 3.9$$

where C'_μ , again, is the sectional thrust coefficient = $C_\mu (S/S')$.

NOTE: The power-off increment of lift due to flap deflection can be included in the methods of estimation by using the relation of $(\partial C_L / \partial \theta)_\infty$ as a function of flap chord as shown in Figure 16. In this case the ratio of flap chord to wing chord should be defined in the flap-extended condition. The lift increment calculated by this method should be added to the flaps-up, power-off, lift to obtain total lift at $\alpha = 0^\circ$. It is believed, however, that other methods of estimation of the power-off lift due to flap deflection, such as DATCOM, or wind tunnel data, will give better accuracy.

The expression here for $(\Delta C_L)_\theta$ was developed from a small angle theory; however, it is used herein for jet turning angles, θ , exceeding one radian. It is therefore believed to be more appropriate to use $\sin \theta$ rather than θ in the use of these expressions. This substitution has been made in all subsequent calculations.

It is more convenient in the pitching moment calculations to separate the components of the lift increment at zero incidence into the thrust reaction term, $\eta C'_\mu \sin \theta$, and the circulation lift component $(\Delta C_L)_\theta$:

Contrails

$$(\Delta CL)_\theta = (\Delta CL)_r + \eta C_\mu \sin \theta \quad 3.10$$

$$\begin{aligned} \text{then } (\Delta CL)_r &= (\Delta CL)_\theta - \eta C_\mu \sin \theta \\ &= F(1 + t/c) \lambda (CL_\theta)_\infty \sin \theta - \eta C_\mu \sin \theta \end{aligned} \quad 3.11$$

It should be noted that the factor F, and the two dimensional CL_θ are based on the sectional blowing coefficient, ηC_μ . The thrust reaction term represents a discrete force and is defined by the blowing coefficient, C_μ , based on the wing reference area, and the static values of η and θ .

Comparisons are shown in Figure 17 of estimated and experimental values of $(\Delta CL)_\theta$ for a wide range of model configurations. The results show reasonably good agreement, being better than +10 percent in most cases. The lift estimation is quite sensitive to the parameters η and θ , so these must be determined as closely as possible. As discussed in Section II, the methods presented here for estimating η and θ tend to represent well designed lift systems that produce good performance; whereas some of the wind tunnel models used in these correlations perform below average.

It should be noted in these correlations that in those cases where the nozzle thrust was inclined relative to the wing to improve impingement on the flap, the measured lift data were corrected for the downward thrust reaction force by:

$$(\Delta CL)_{\theta \text{ EXP}} = (\Delta CL)_{\theta \text{ MEAS.}} + C_\mu \sin \delta_T$$

where δ_T is the angle between the nozzle centerline and the reference plane.

Contrails

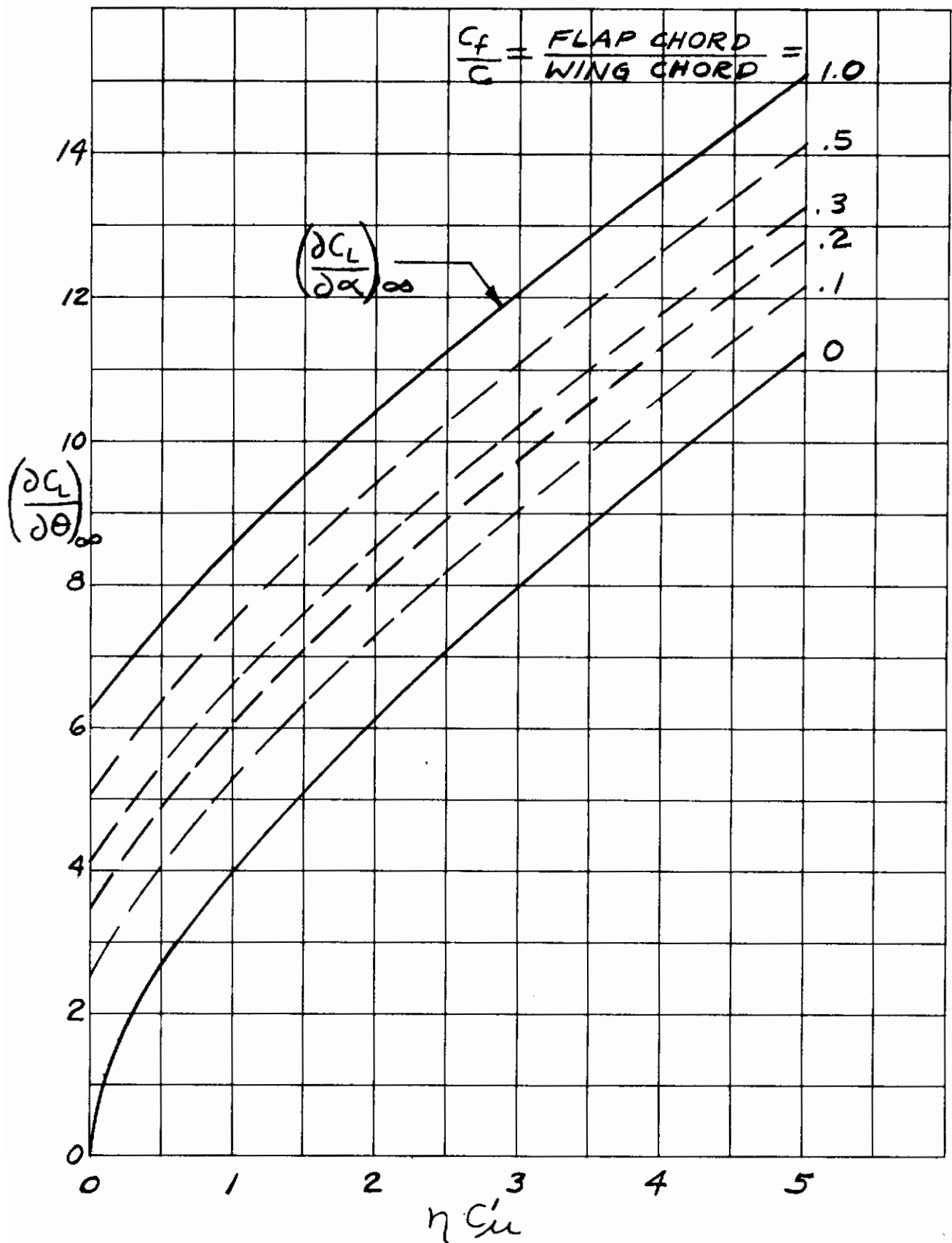


Figure 16. $\left(\frac{\partial C_L}{\partial \theta}\right)_{\infty}$ and $\left(\frac{\partial C_L}{\partial \alpha}\right)_{\infty}$ for a Jet Flap

Contrails

SYM	TEST CASE	REF	A	$\Delta c_{l\alpha}$	L. E. FLAP % SPAN	T. E. FLAP % SPAN
0	22a	14	7	0	100	75
x	61a	9	7	25	100	75
y	91a	22	7.84	25	50	50(USB)
o	1a	13	7	24	100	100
△	1b	13	7	24	100	100
□	1d	13	7	24	100	100
◇	1f	13	7	24	100	100
▽	14a	13	7	24	80	75
⊖	21a	14	7	0	100	100
△	10a	13	6.6	30	80	100
▽	11a	13	10	24	80	100
∇	9a	13	8	9.3	80	100
+	81a	5	7.23	24	100	100

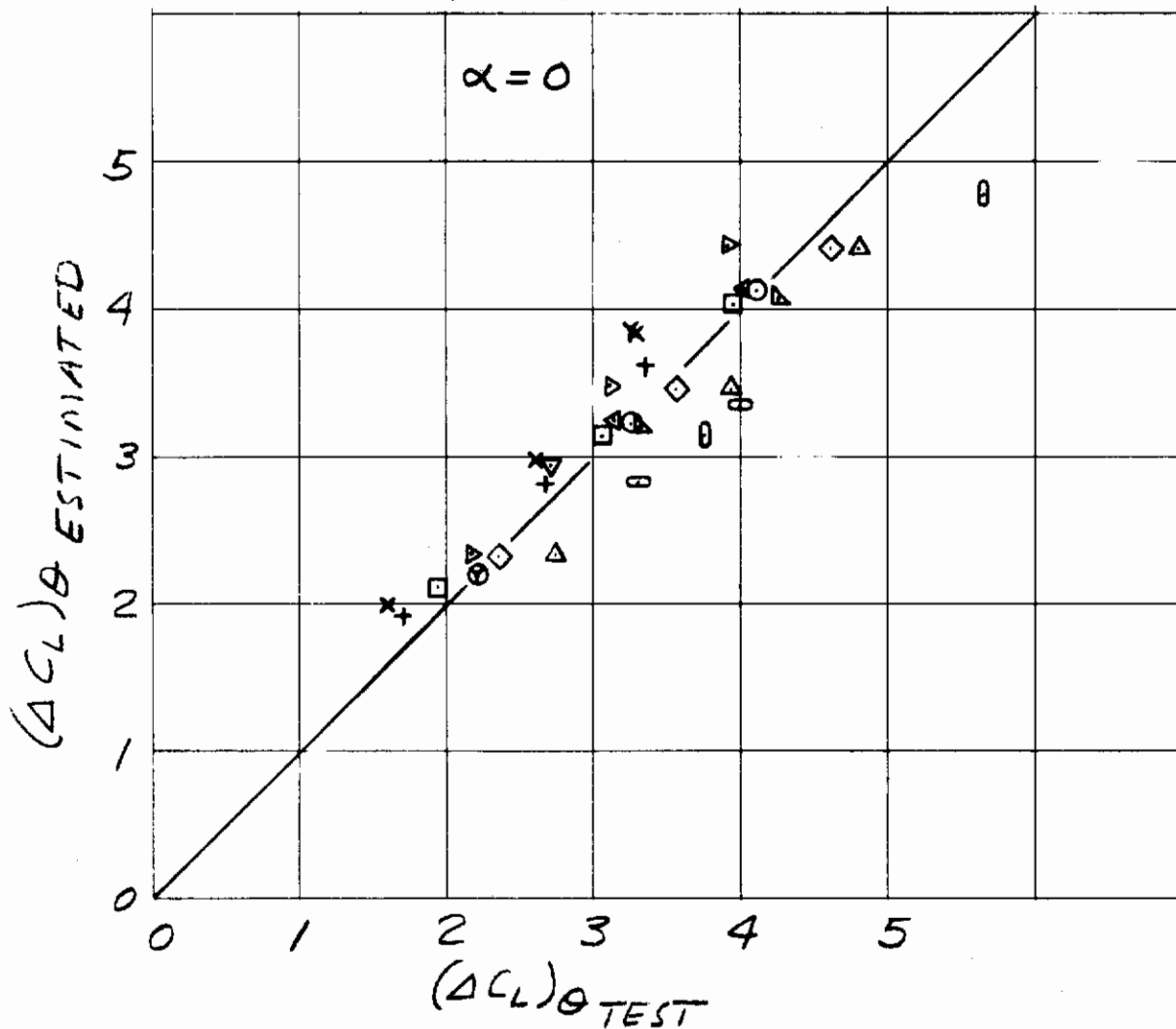


Figure 17. Correlation of Lift Increment due to Power at Zero Incidence

3.3 LIFT DUE TO ANGLE OF ATTACK

The powered lift increment due to angle of attack is estimated by:

$$(\Delta C_L)_\alpha = \left[F \left(1 + \frac{t}{c}\right) \nu \left(\frac{\partial C_L}{\partial \alpha}\right)_\infty \right] \alpha \quad 3.7$$

where F , η , θ and t/c have been defined in previous sections. The correction factor for partial span blowing, ν , from Reference (12), is:

$$\nu = s'/s + (1 - s'/s) 2\pi / \left(\frac{\partial C_L}{\partial \alpha}\right)_\infty \quad 3.12$$

This function is plotted in Figure 18.

$\left(\frac{\partial C_L}{\partial \alpha}\right)_\infty$ = two dimensional lift due to angle of attack (Reference (10)). A plot of $\left(\frac{\partial C_L}{\partial \alpha}\right)_\infty$ versus $\eta C'_{mu}$ is shown in Figure 16. An approximate analytical expression from Reference (11), again substituting $\eta C'_{mu}$ for C'_{mu} , is:

$$\left(\frac{\partial C_L}{\partial \alpha}\right)_\infty \approx 2\pi \left[1 + 0.151 (\eta C'_{mu})^{1/2} + 0.217 \eta C'_{mu} \right] \quad 3.13$$

This procedure is of course limited to the linear range of lift with angle of attack. The extent of the linear range is strongly dependent on leading edge treatment, and varies also with flap deflection, thrust coefficient, aspect ratio, and sweep.

Correlations of estimated versus experimental values of the lift curve slope as defined by $(\Delta C_L)_\alpha / \alpha$ are shown in Figure 19 for a wide range of test configurations. It appears that on the average the method of estimation slightly over-estimates the value of the lift curve slope, although the agreement is within +10 percent for nearly all of the data.

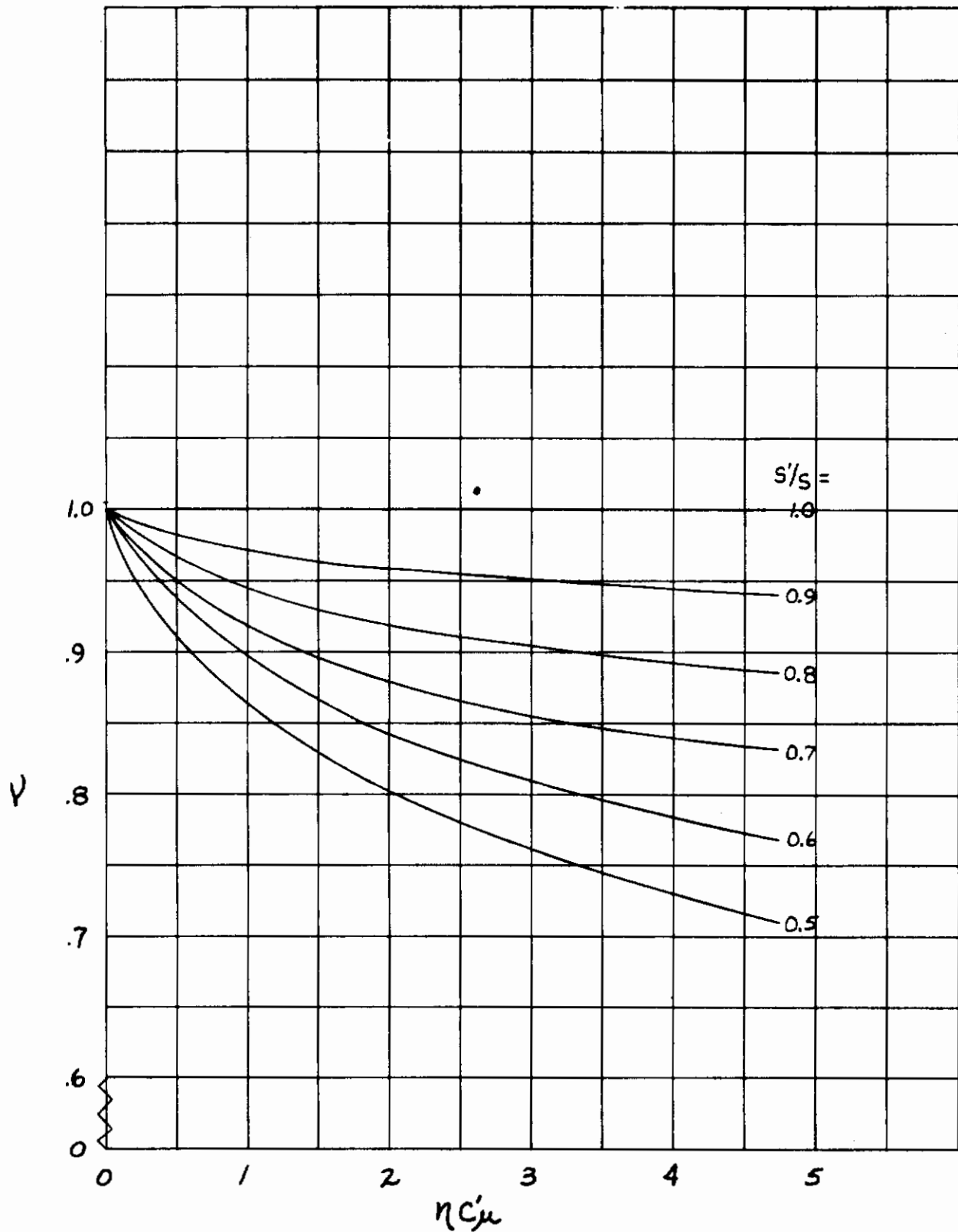


Figure 18. Lift Curve Slope Correction for Partial Span Blowing

Contrails

SYM	TEST CASE	REF	A	$\Lambda \bar{c}/4$	L. E. FLAP % SPAN	T. E. FLAP % SPAN
0	22a	14	7	0	100	75
x	61a	9	7	25	100	75
Y	91a	22	7.84	25	50	50(USB)
○	1a	13	7	24	100	100
△	1b	13	7	24	100	100
□	1d	13	7	24	100	100
◇	1f	13	7	24	100	100
▽	14a	13	7	24	80	75
◻	21a	14	7	0	100	100
△	10a	13	6.6	30	80	100
▽	11a	13	10	24	80	100
∇	9a	13	8	9.3	80	100
+	81a	5	7.23	24	100	100

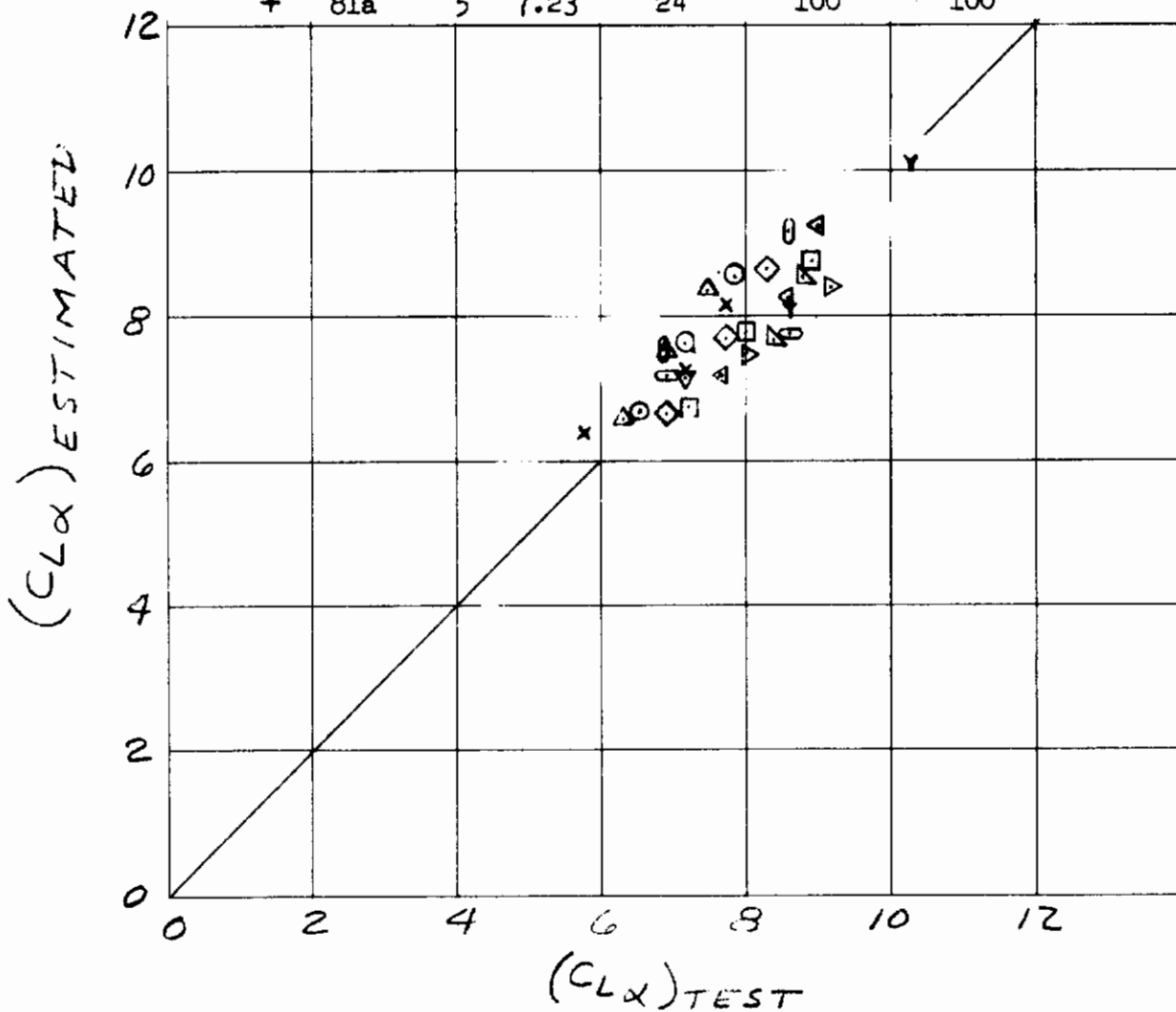


Figure 19. Correlation of Lift Curve Slope

3.4 TOTAL LIFT ESTIMATION

The recommended procedure for estimating the lift coefficient is to determine power-off lift at zero angle of attack by other conventional methods of estimation; then add the power effects due to jet turning, angle of attack and nozzle incidence:

$$C_L = (C_L)_B + (\Delta C_L)_\theta + (\Delta C_L)_\alpha - C_{\mu} \sin \delta_T \quad 3.14$$

where detailed description of the lift increments are given by:

$(\Delta C_L)_\theta$ from Section 3.2

$(\Delta C_L)_\alpha$ from Section 3.3

3.5 MAXIMUM LIFT COEFFICIENT

A relationship for the maximum lift coefficient of a two-dimensional wing with a jet augmented flap, based on the maximum lift of the unflapped wing, and assuming a leading edge stall for both wings, is given by D.N. Foster in Reference (15), as:

$$C_{L_{MAX}} = C_{L_{MAX}}_{\delta, c_{\mu}} - \frac{\Delta C_{L_{\delta, c_{\mu}}}}{2} - \frac{\Delta C_{L_{c_{\mu}}}}{4} \quad 3.15$$

where, in the nomenclature of Reference 15, $C_{L_{MAX}}$ is the maximum lift coefficient of the unflapped, unaugmented wing; $C_{L_{MAX}}_{\delta, c_{\mu}}$ is the maximum lift coefficient of the wing with flap deflected and jet augmentation; $\Delta C_{L_{\delta, c_{\mu}}}$ is the increment of lift due to flap deflection and jet augmentation; and, $\Delta C_{L_{c_{\mu}}}$ is the increment of lift due to jet augmentation only, with the flap already deflected

The increment in maximum lift coefficient due to flap deflection and jet augmentation is, then:

$$\begin{aligned} \left(\Delta C_{L_{MAX}} \right)_{\delta, c_{\mu}} &= C_{L_{MAX}}_{\delta, c_{\mu}} - C_{L_{MAX}} \\ &= 1/2 \left[\Delta C_{L_{\delta, c_{\mu}}} + 1/2 \Delta C_{L_{c_{\mu}}} \right] \end{aligned}$$

by definition $\Delta C_{L_{\delta, c_{\mu}}} = \Delta C_{L_{\delta}} + \Delta C_{L_{c_{\mu}}}$ 3.16

$$\begin{aligned} \text{so } \left(\Delta C_{L_{MAX}} \right)_{\delta, c_{\mu}} &= 1/2 \left[\Delta C_{L_{\delta}} + \Delta C_{L_{c_{\mu}}} + 1/2 \Delta C_{L_{c_{\mu}}} \right] \\ &= 1/2 \left[\Delta C_{L_{\delta}} + 3/2 \Delta C_{L_{c_{\mu}}} \right] \end{aligned} \quad 3.17$$

Contrails

Now according to Reference 24, the increment in maximum lift coefficient due to flap deflection only is equal to one-half the increment in lift at constant angle of attack due to flap deflection:

$$\left(\Delta C_{L_{MAX}}\right)_{\delta} = 1/2 \Delta C_{L_{\delta}} \quad 3.18$$

So, defining $\left(\Delta C_{L_{MAX}}\right)_{C_{\mu}}$ as the increment in maximum lift coefficient due to jet augmentation only, with the flap already deflected:

$$\begin{aligned} \left(\Delta C_{L_{MAX}}\right)_{C_{\mu}} &= \left(\Delta C_{L_{MAX}}\right)_{\delta} - \left(\Delta C_{L_{MAX}}\right)_{\delta, C_{\mu}} \\ &= 1/2 \left[\Delta C_{L_{\delta}} + 3/2 \Delta C_{L_{C_{\mu}}} \right] - 1/2 \Delta C_{L_{\delta}} = 3/4 \Delta C_{L_{C_{\mu}}} \end{aligned} \quad 3.19$$

In the derivation of $C_{L_{MAX}}$ in Reference 15, the term $\Delta C_{L_{C_{\mu}}}$ is defined as the increment in lift due to jet augmentation at "constant angle of attack," and is then further interpreted as being at $\alpha = 0$. However, it is believed that the value of $\left(\Delta C_L\right)_{C_{\mu}}$ to be used here should be defined at the angle of attack for stall with flap deflected and with blowing, as suggested by Moorhouse in Reference 23. The reason for this, on which the analysis of Reference 15 is based, is that the leading edge loading of a blown flapped wing is the same as that of an unblown flapped wing when the C_L of the unblown wing is equal to $C_L - 3/4 \left(\Delta C_L\right)_{C_{\mu}}$ of the blown wing.

In applying this approach to the estimation of $C_{L_{MAX}}$ for the finite aspect ratio case, it is reasoned that the $\left(\Delta C_L\right)_{C_{\mu}}$ used in the calculation should be the two-dimensional value, since it is the section loading that determines $C_{L_{MAX}}$. However, it is usually the three-dimensional data that are available, so the three-dimensional value of $\left(\Delta C_L\right)_{C_{\mu}}$ should be modified for aspect ratio by the factor, $1/F$. This procedure was first suggested by McRae in Reference 24.

The maximum lift increment due to flap blowing for the finite aspect ratio case is then:

$$\left(\Delta C_{L_{MAX}}\right)_{PL} = \frac{3}{4F} \left(\Delta C_L\right)_{PL, \alpha_{MAX}} \quad 3.20$$

Now since the value of α_{MAX} is not known, the above expression has been defined in terms of known values, based on the simplified lift curves illustrated in Figure 22:

$$\left(C_{L_{MAX}}\right)_{PL} = \frac{3/(4F) \left[\left(\Delta C_L\right)_{\theta} \phi - \left(C_L\right)_{PO, \alpha = 0} (1-\phi) \right] + \left(C_{L_{MAX}}\right)_{PO} - C_{\mu} \sin \delta_T}{1 - \frac{3}{4F} (1-\phi)} \quad 3.21$$

Contrails

where: $\phi = \frac{(C_{L\alpha})_{PO}}{C_{L\alpha}}$

and $-C_{\mu} \sin \delta_T$ is a correction to $C_{L_{MAX}}$ for those EBF systems which incorporate jet nozzle incidence to improve lift augmentation.

A correlation of experimental data versus estimates using equation 3.2.1 has been made representing many variations of aspect ratio, sweep angle, flap configuration, blowing coefficient, and leading edge devices. The results show a fairly consistent underestimation of $\Delta C_{L_{MAX}}$ of about 15 percent. Application of a multiplying factor of 1.15 to the first term of equation 3.2.1 was found to bring the data into reasonably good agreement, as shown in figure 20, although it caused the upper surface blown data to spread. The resulting expression for estimation of $C_{L_{MAX}}$ for EBF systems is, then:

$$\left(C_{L_{MAX}} \right)_{PL} = \frac{\frac{3}{4F} \left\{ [1.15 (\Delta C_L)_{\theta} \phi - (C_L)_{PO, \alpha=0} (1-\phi)] + (C_{L_{MAX}})_{PO} \right\} - C_{\mu} \sin \delta_T}{1 - \frac{3}{4F} F (1-\phi)} \quad 3.22$$

It should be remembered that this relation assumes similar type stall for both power on and power off, which is often not the case for powered lift wind tunnel tests.

It has been found from test data correlations that an adequate approximation for the estimation of $\Delta C_{L_{MAX}}$ is:

$$\left(\Delta C_{L_{MAX}} \right)_{PL} \approx 1/F (\Delta C_L)_{\theta} - C_{\mu} \sin \delta_T \quad 3.23$$

This expression is much more amenable to quick "hand calculated" estimations, and gives equally good correlation with test data as the relation given in equation 3.22.

Contrails

SYM	TEST CASE	REF	A	$\Delta c_{\frac{1}{4}}$	L.E. FLAP % SPAN	T.E. FLAP % SPAN
0	22a	14	7	0	100	75
x	61a	9	7	25	100	75
Y	91a	22	7.84	25	50	50(USB)
o	1a	13	7	24	100	100
△	1b	13	7	24	100	100
□	1d	13	7	24	100	100
◇	1f	13	7	24	100	100
▽	14a	13	7	24	80	75
▢	21a	14	7	0	100	100
△	10a	13	6.6	30	80	100
▽	11a	13	10	24	80	100
▽	9a	13	8	9.3	80	100
+	81a	5	7.23	24	100	100

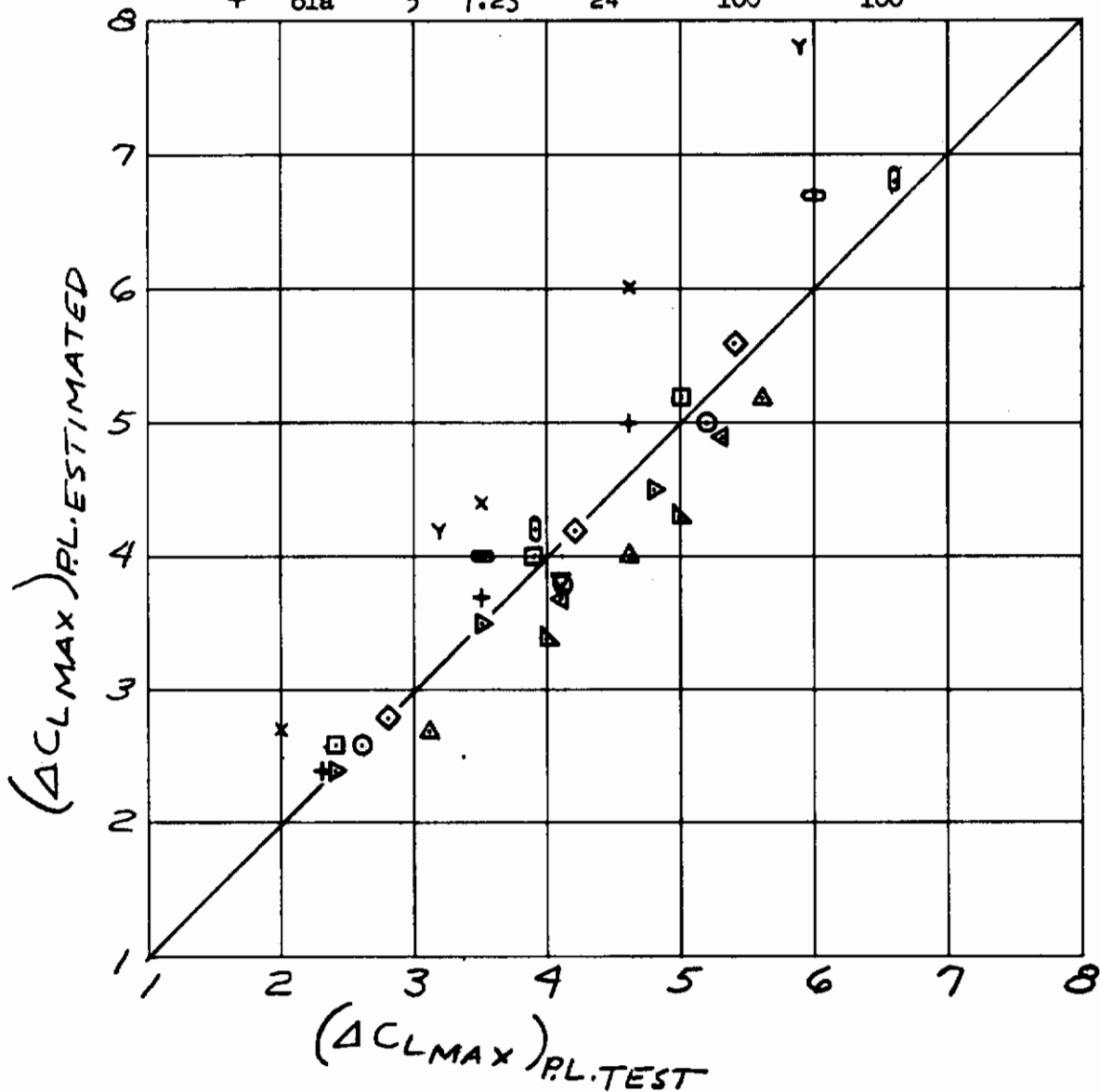


Figure 20. Correlation of ΔC_{LMAX} Due to Power According to Equation 3.22

Contrails

SYM	TEST CASE	REF	A	$\Delta c_{l\alpha}$	L.E. FLAP % SPAN	T.E. FLAP % SPAN
0	22a	14	7	0	100	75
x	61a	9	7	25	100	75
y	91a	22	7.84	25	50	50(USB)
1a	13	7	7	24	100	100
1b	13	7	7	24	100	100
1d	13	7	7	24	100	100
1f	13	7	7	24	100	100
14a	13	7	7	24	80	75
21a	14	7	7	0	100	100
10a	13	6.6	6.6	30	80	100
11a	13	10	10	24	80	100
9a	13	8	8	9.3	80	100
+	81a	5	7.23	24	100	100

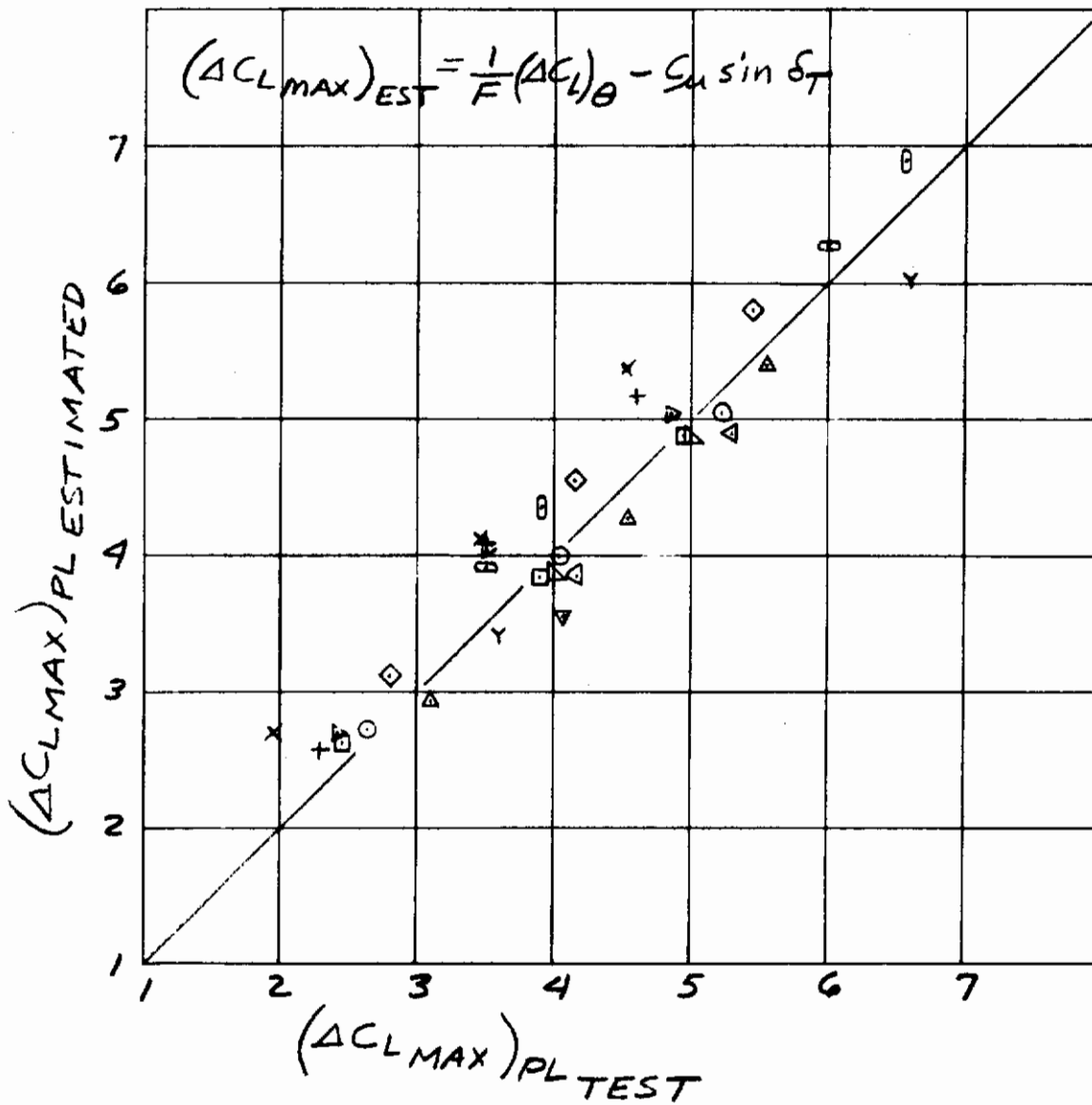


Figure 21. Correlation of $\Delta C_{L\max}$ Due to Power According to Equation 3.23

3.6 ANGLE OF ATTACK FOR MAXIMUM LIFT

The change in angle of attack at maximum lift due to jet augmentation can be estimated using the characteristics of idealized lift curves as illustrated in Figure 22, and the relations for $(C_{LMAX})_{PL}$ of the previous section.

$$(\Delta\alpha)_{MAX} = \frac{(C_{LMAX})_{PL} - (C_L)_{\alpha=0}}{C_{L\alpha}} - \frac{(C_{LMAX})_{PO} - (C_L)_{PO, \alpha=0}}{(C_{L\alpha})_{PO}} \quad 3.24$$

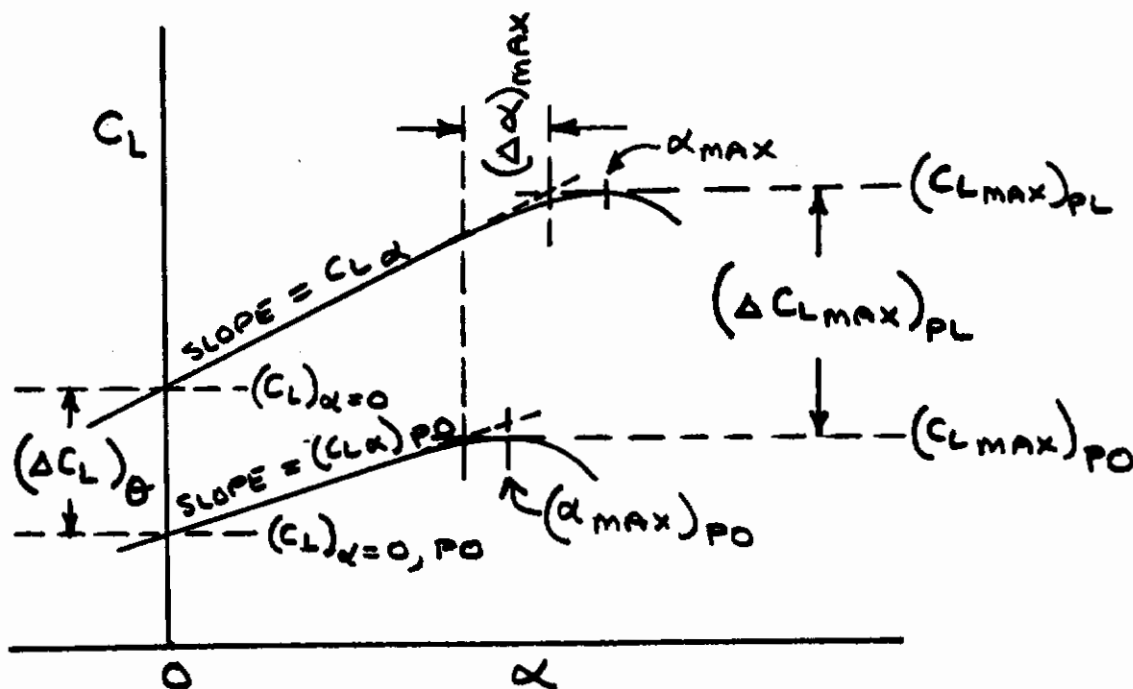


Figure 22. Definition of α_{MAX}

The angle of attack at maximum lift power on is approximated by:

$$\alpha_{MAX} = (\alpha_{MAX})_{PO} + (\Delta\alpha)_{MAX} \quad 3.25$$

A correlation of estimated and experimental α_{MAX} data is shown in Figure 23. Reasonably good agreement is observed, with some notable exceptions. Again, the theoretical approach assumes a similar type of stall for both the power-on and power-off cases, whereas examination of wind tunnel test results indicates obvious variances in the type of stall for

Contrails

SYM	TEST CASE	REF	A	$\Lambda c/4$	L. E. FLAP % SPAN	T. E. FLAP % SPAN
0	22a	14	7	0	100	75
x	61a	9	7	25	100	75
Y	91a	22	7.84	25	50	50(USB)
0	1a	13	7	24	100	100
Δ	1b	13	7	24	100	100
\square	1d	13	7	24	100	100
\diamond	1f	13	7	24	100	100
∇	14a	13	7	24	80	75
0	21a	14	7	0	100	100
Δ	10a	13	6.6	30	80	100
∇	11a	13	10	24	80	100
∇	9a	13	8	9.3	80	100
+	81a	5	7.23	24	100	100

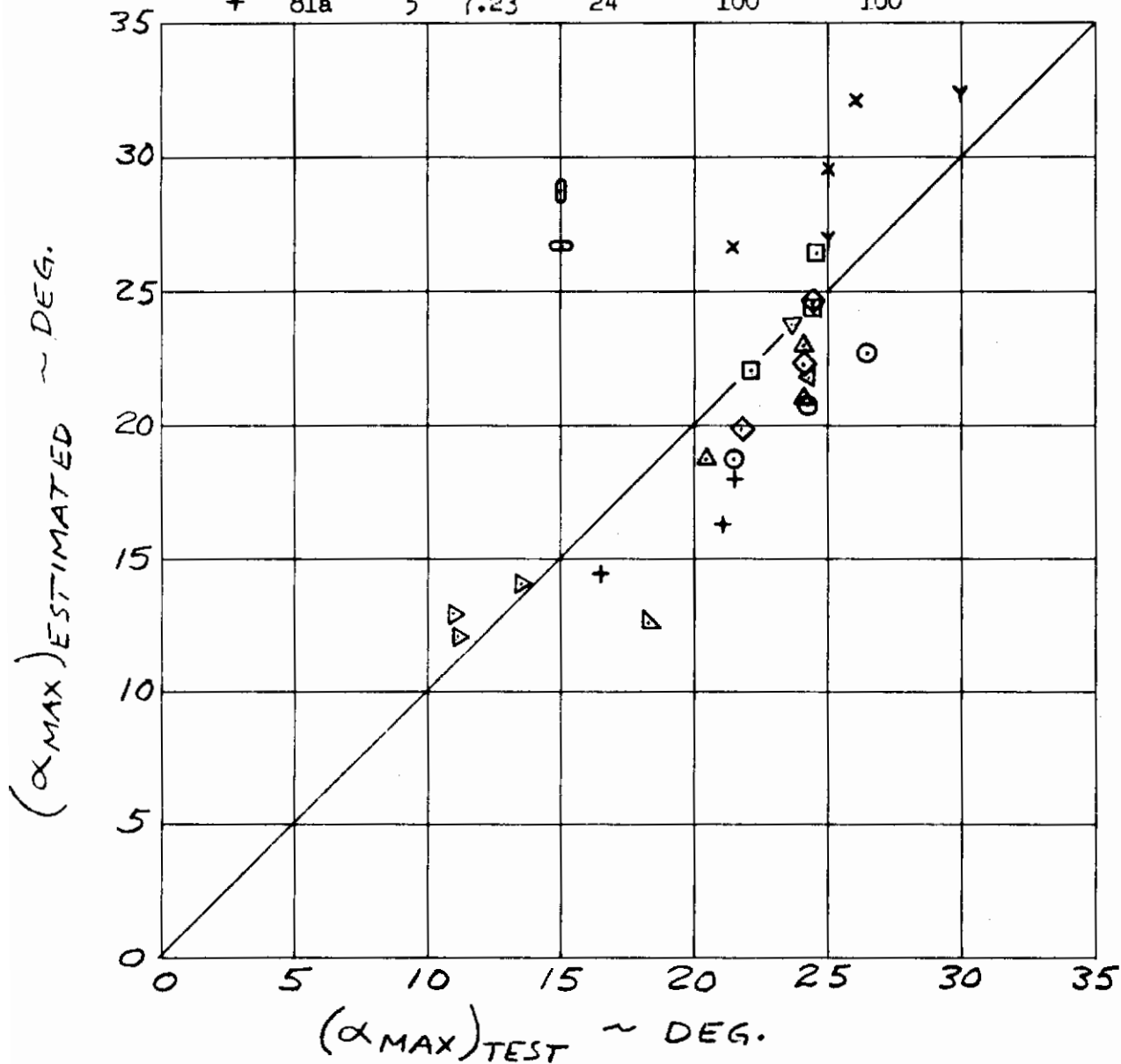


Figure 23. Correlation of Maximum Angle of Attack Data

Contrails

different values of the blowing coefficient. When this condition exists agreement can not be expected between estimated and experimental data. It would be expected that the estimated values of α_{MAX} would be in better agreement with flight test results of a well designed full scale, EBF system, than with wind tunnel results of small scale models.

3.7 EFFECTS OF ASPECT RATIO

The theoretical aspect ratio correction factor, F , discussed in Section 3.1.2 was developed on the assumption that the jet blowing was distributed elliptically spanwise. In the case of the externally blown flap the blowing is concentrated at the engine nozzle and the lift distribution peaks in the vicinity of the thrust centerline, which violates considerably the assumptions under which the aspect ratio factor was derived. However, better results are obtained by using the aspect ratio factor, F , than are obtained by using the power-off factor, $A/(A + 2)$.

Experimental data from Reference (13), shown in Figure 24, illustrates a negligible effect in varying aspect ratio by 40 percent. Estimated values of lift increment due to blowing for these same model configurations show a larger predicted effect of aspect ratio than that observed in the test data. The error in lift increment is not large, but these results indicate that the aspect ratio factor better accounts for the spanwise loading effects at aspect ratio 7 than at 10.

The comparison of experimental effects of aspect ratio with the theoretical prediction indicates that as the blowing coefficient is increased the effective aspect ratio is decreased. This trend would be expected due to higher loading of the inboard portion of the wing span with the higher blowing coefficients and with the typical EBF configuration.

It is believed that an aspect ratio correction factor could be developed based on loading distributions more typical of EBF systems, which would more accurately predict the aspect ratio effects on powered lift. However the factor, F , used herein is recommended for prediction methods until improved factors can be developed.

Contrails

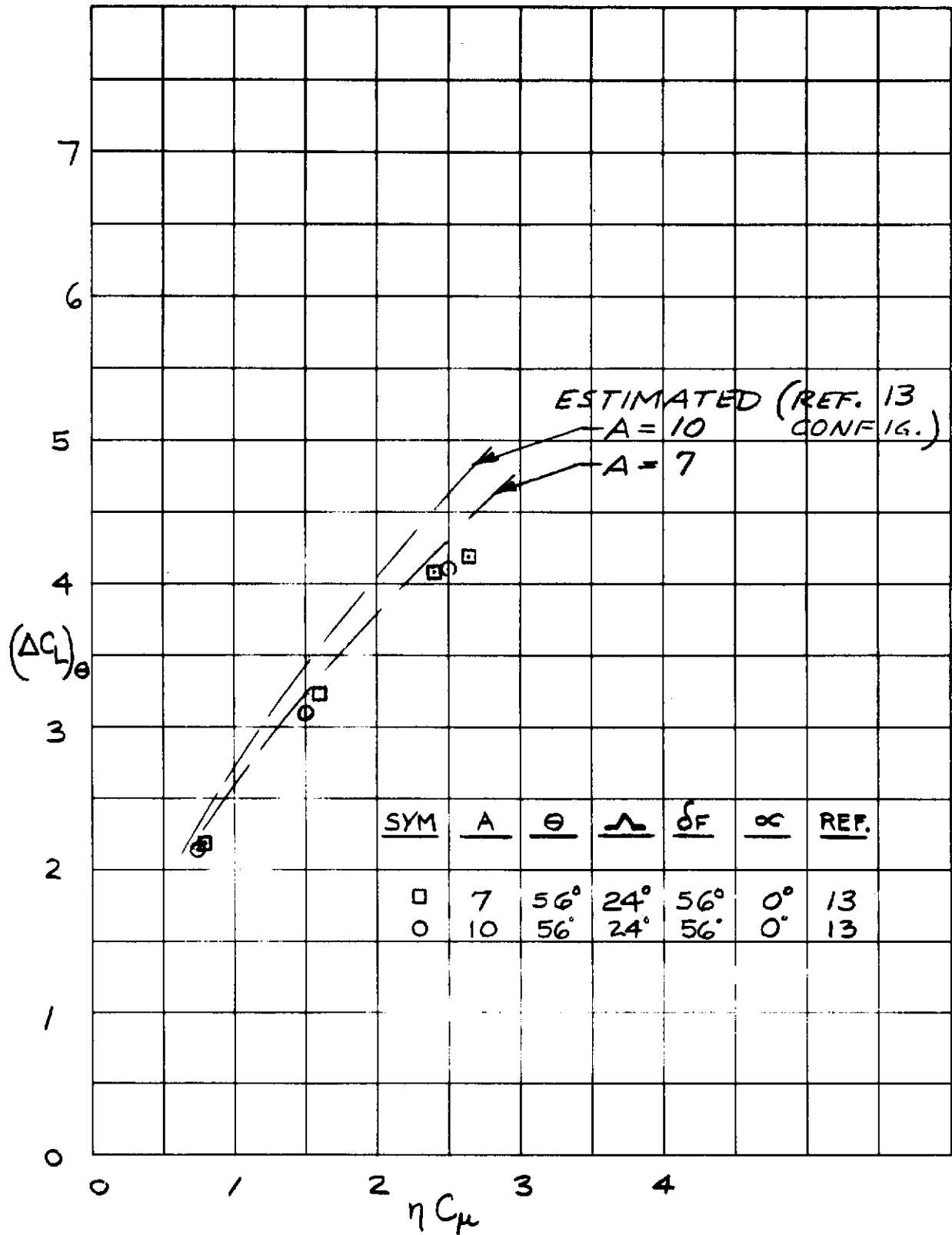


Figure 24. Effects of Aspect Ratio on Lift Due to Power

3.8 EFFECTS OF FLAP SPAN

Investigation of the effects of varying flap span on the lift augmentation due to flap blowing has shown that use of the effective wing area, S' , as defined in Section 3.1.3 adequately accounts for flap span variations. As discussed in Section 3.1.3, available pressure data from Reference 14 indicate that the circulation lift due to blowing on externally blown flaps extends over the entire span of the flaps, regardless of the spanwise placing of the engines. Analysis of the pressure data in Reference (14) shows that the carryover loading on the wing area outboard of the 75 percent span flap is about one-half of that on the flapped portion of the wing. This observed characteristic would obviously not hold for extreme variations from the test configurations, but it is believed to be a valid assumption for reasonable STOL configurations.

The effects of flap span are thus included in the lift calculation through the dependency of the effective area, S' , and the effective aspect ratio, on flap span. The correlation plots of lift at $\alpha = 0$, Figure 17, and $C_{L\alpha}$, Figure 19, show equally good correlation of the part-span data as that of the full-span data.

Two sets of data were available (References 13 and 14) where all model geometry except the flap span was held constant. These models were tested with both full span and 75 percent span flaps. Results of these tests are shown in Figure 25. It is seen that the test data follow the trend of the estimated variation of lift with flap span ratio, although the absolute level of the zero sweep data is underestimated.

Contrails

EST.	TEST	CASE* NO.	REF.	FLAP SPAN	A	$\Lambda_{c/4}$	C_M
—————	○	18	13	100%	7	24°	2.0
—————	○	148	13	75%	7	24°	2.0
-----	□	218	14	100%	7	0°	2.05
-----	□	228	14	75%	7	0°	2.05

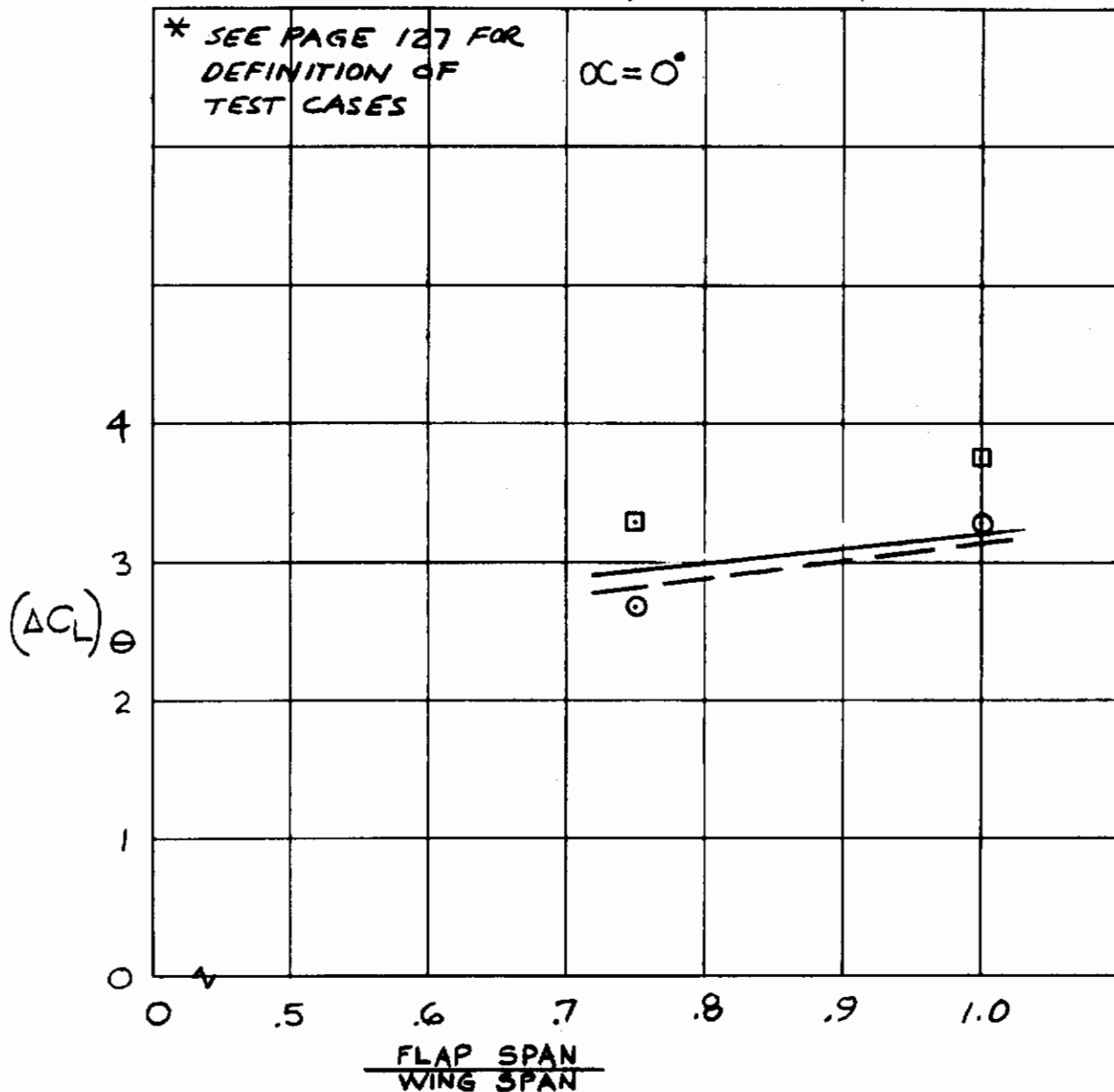


Figure 25. Correlation of Effects of Flap Span on Lift due to Power

3.9 EFFECTS OF WING SWEEP

In the present methods of estimation of lift augmentation due to flap blowing the effects of wing sweep appear only in the jet turning efficiency, η , as seen in Figures 7, 8, and 11. Figure 11 shows only a modest effect of sweep except for the zero sweep, double slotted flap case, which exhibits a markedly reduced efficiency. Referring to Figure 17 where estimated and experimental values of zero incidence lift are compared it is seen that the lift data for the unswept wing with double slotted flaps are generally underestimated.

It is possible that the turning efficiency data for the zero sweep wing which were taken from References 8 and 14, reflect some experimental technique which is not consistent with the other tests. Further tests of other models with low wing sweep values should be made to investigate the turning efficiency of double-slotted flapped wings at low sweep angles.

Tests were conducted in Reference 13 where only the wing sweep of the model was varied; flap deflection, nacelle geometry, and blowing coefficient were held constant. Results of these tests are shown in Figure 26 for sweep angles of 9° to 30° . The close agreement of estimated lift increments with the experimental data indicates that the prediction methods adequately account for sweep effects.

Contrails

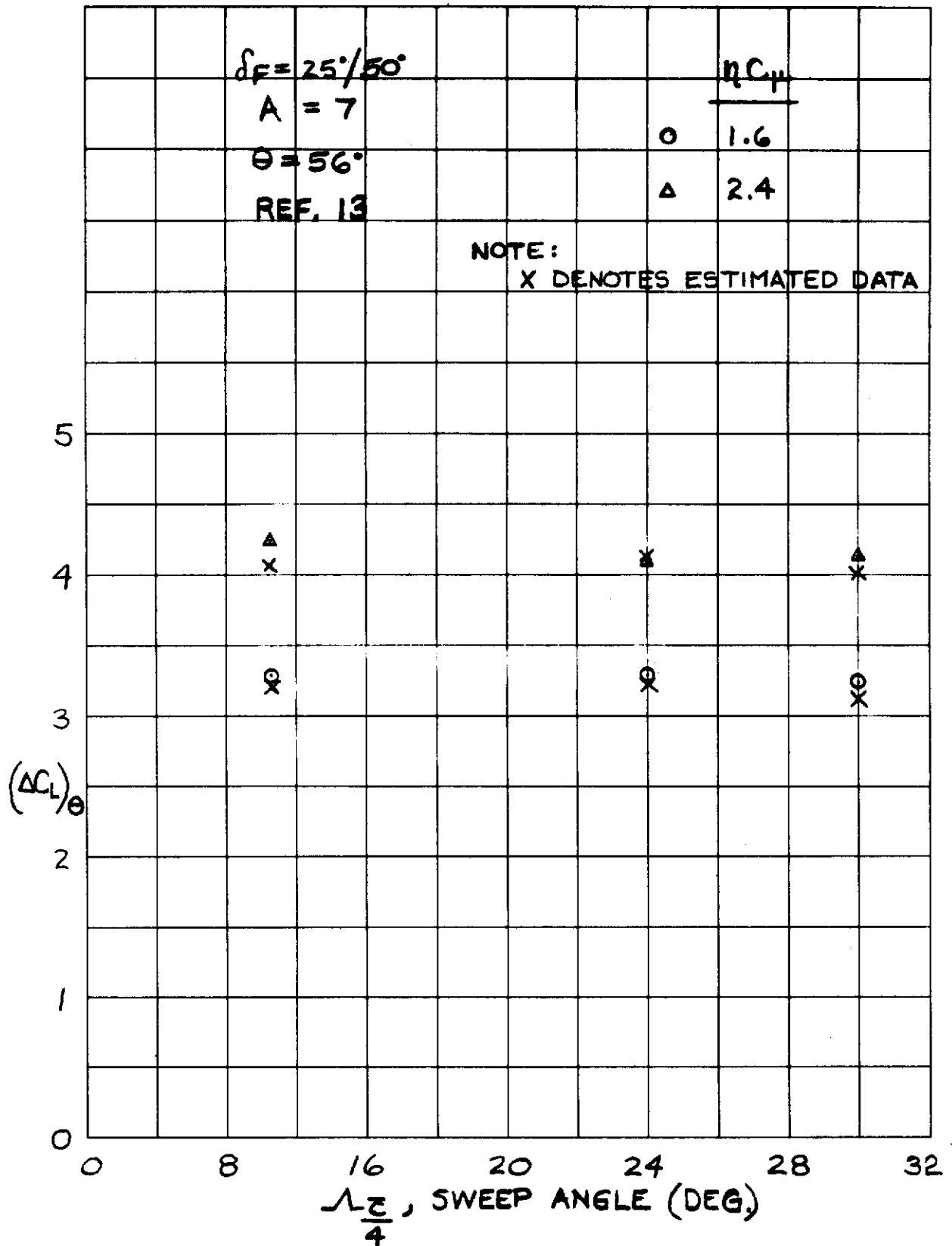


Figure 26. Correlation of Effects of Wing Sweep on Lift Due to Power

3.10 EFFECTS OF FLAP CONFIGURATION

The methods of prediction of lift increment due to power indicate a small benefit of triple slotted flaps over double slotted flaps due to better turning effectiveness (see Figure 13). A comparison with experimental data from Reference (13), shown in Figure 27, shows that the predicted variation with flap angle is correct, but the differences due to double versus triple slotted flaps are no greater than the experimental scatter of the data. It is also observed that flap separation starts at flap angles above about 65 degrees for these tests at $C_{L0} = 2$.

These results are in agreement with other data from Reference (6). There, single, double, and triple slotted flaps were investigated with a model having a straight wing. The various flap geometries are shown in Figure 28. The power-off lifts for these geometries are presented in Figure 29 for $\alpha = 0$, showing a large improvement in lift in going from one gap to multi-gapped flap geometries. The large improvement above the single gap is probably due to a lessening of flow separation. Power effects from external blowing are presented in Figure 30 for the same flap geometries, using a blowing coefficient of $C_{L0} = 1.0$. The single slotted flap shows the largest lift increment which probably results from an elimination of the flow separation that might exist without the blowing. However, little difference is found between the double and triple slotted flap. Figure 31 shows the sum of the freestream lift and the increment due to power, i.e., the total lift. It is seen that the differences in total lift between double and triple slotted flaps are minor.

Also it should be noted that the comparison of the number of gaps is carried out at constant flap chord extensions. However, in case a simultaneous increase of flap chord is achieved together with a larger number of gaps, an increase of turning angle may be obtained because of a larger impingement parameter.

The prediction methods have no provision for flap gap variations. Test data from References (6) and (13) show that an optimum gap is 3 percent to 3.5 percent of wing chord (see Figure 32). It is assumed that any EBF design would utilize a near optimum gap in order to derive the maximum lift capability from the flap system, since there are no apparent reasons to use other gap dimensions.

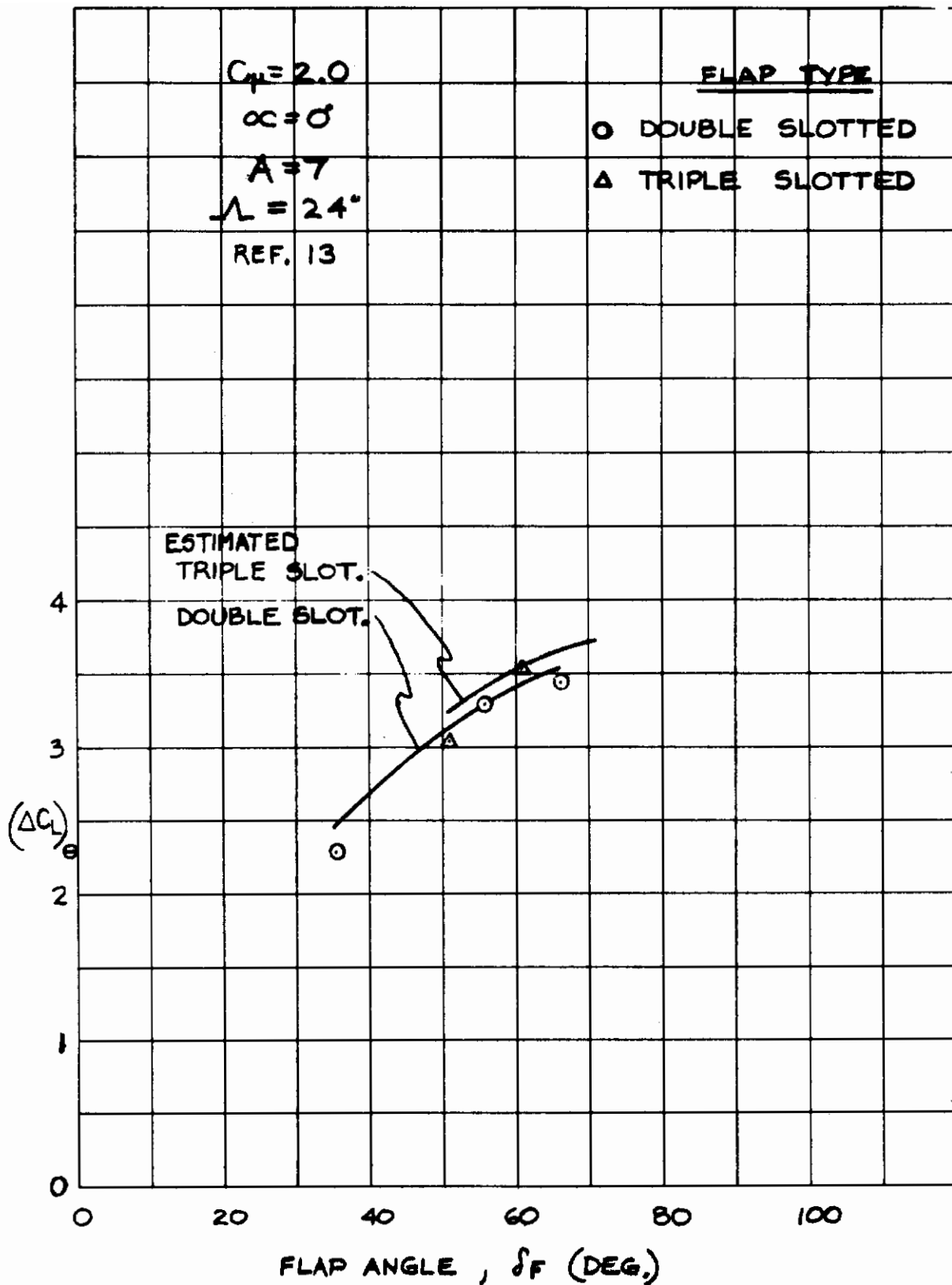


Figure 27. Effects of Flap Configuration on Lift Increment Due to Power

Contrails

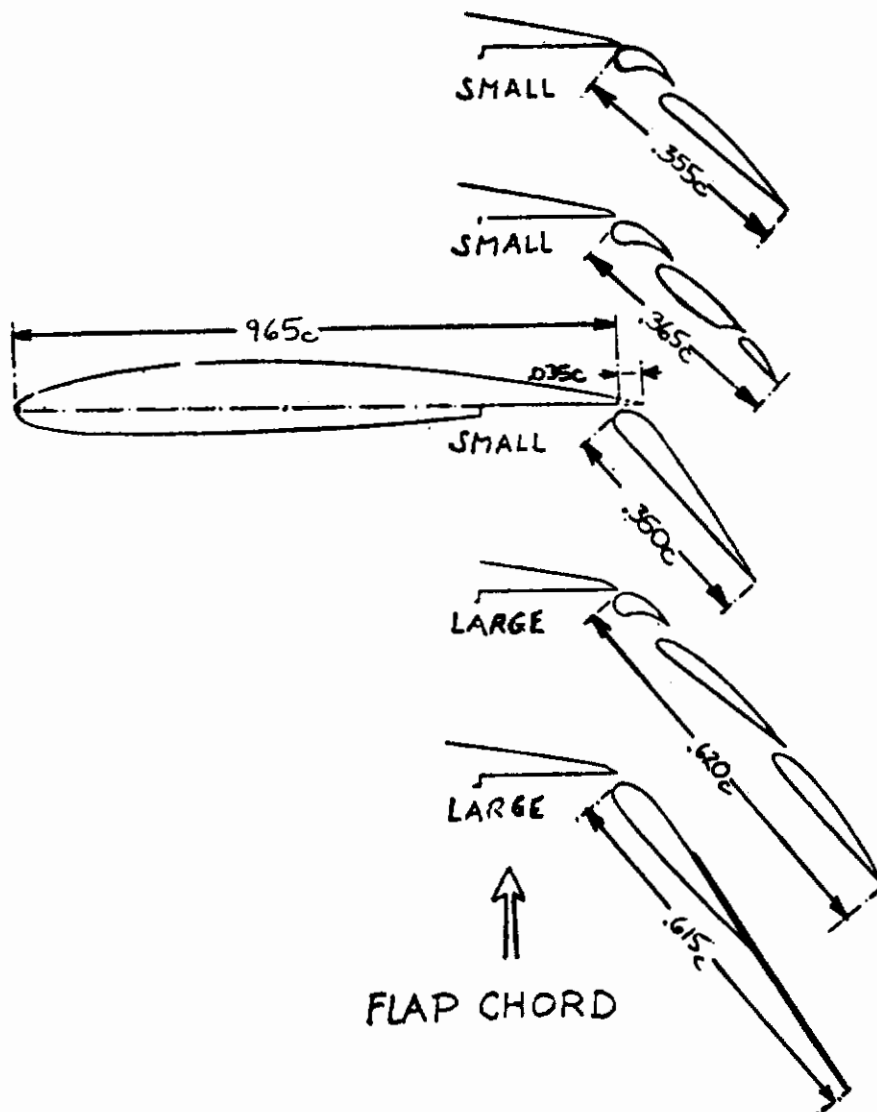


Figure 28. Flap Details for Comparison of Flap Chord Effects

REF. 6

$\alpha = 0^\circ$

---	▽	FLAP	N ^o OF
---	◇	CHORD	GAPS
---	▽	SMALL	THREE
---	◇	SMALL	TWO
---	□	SMALL	ONE
---	△	LARGE	THREE
---	○	LARGE	ONE

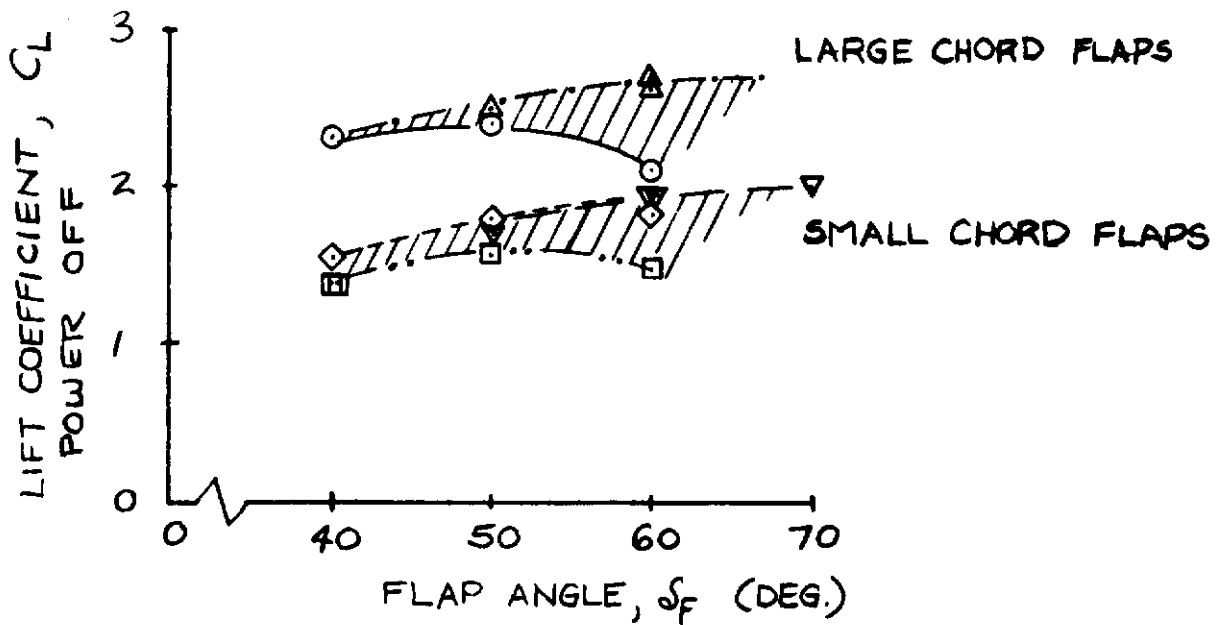


Figure 29. Effect of Flap Configuration on Lift - Power Off

Contrails

$$C_{\mu} = 1.0$$

$$\alpha = 0^{\circ}$$

$$\delta_N = 25^{\circ}$$

FLAP CHORD	N ^o OF GAPS
▽	SMALL THREE
◇	SMALL TWO
□	SMALL ONE
△	LARGE THREE
○	LARGE ONE

REF. 6.

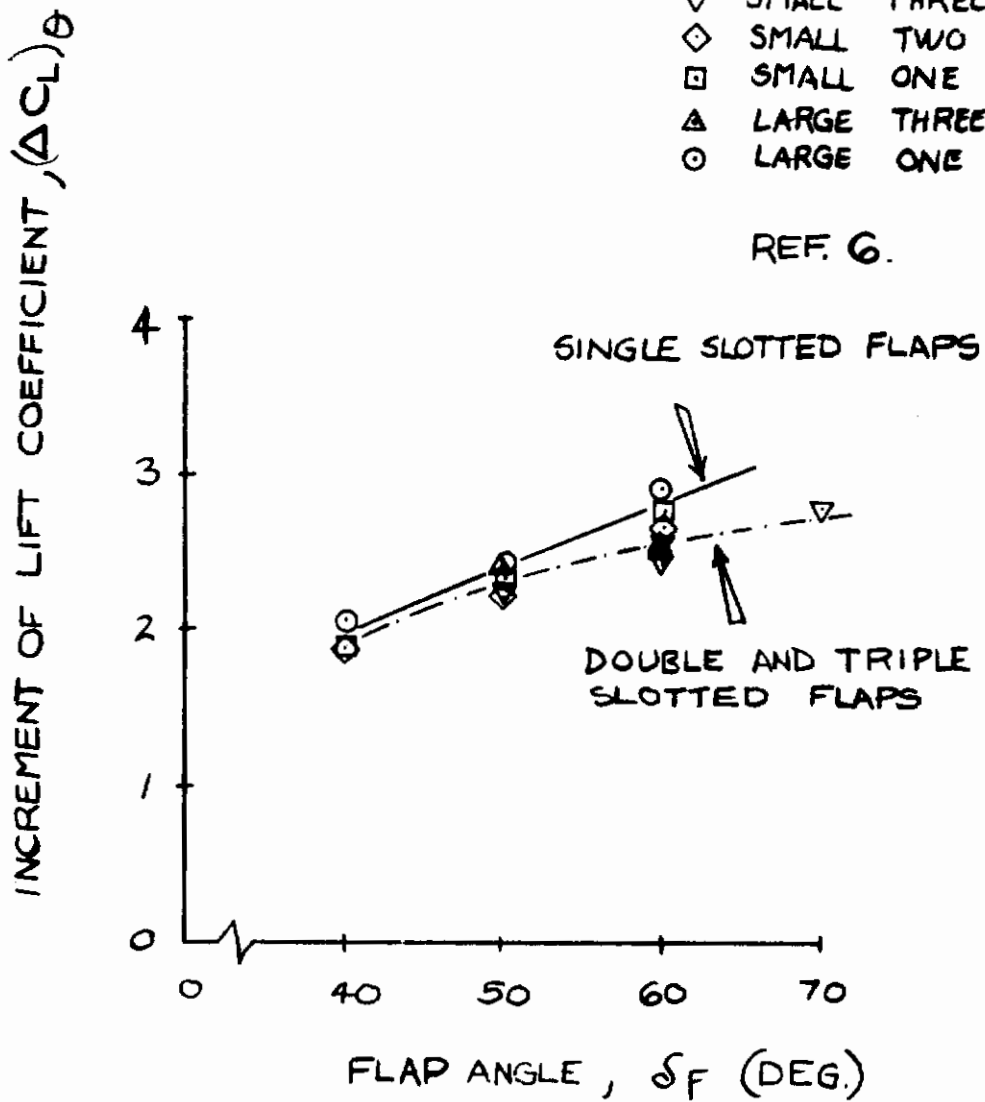


Figure 30. Effect of Flap Configuration on Lift Due to Power

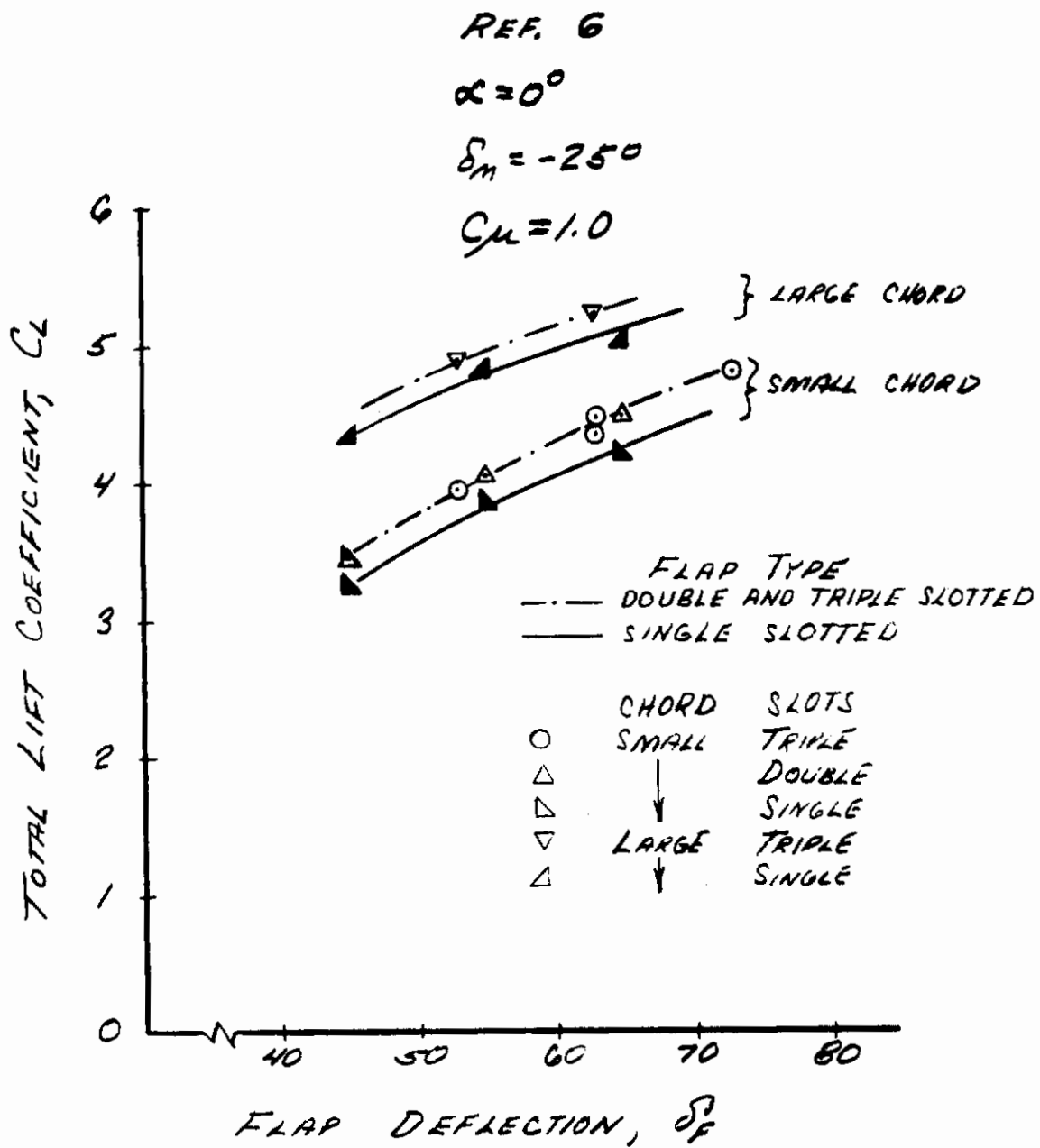


Figure 31. Effect of Flap Configuration on Total Lift Coefficient

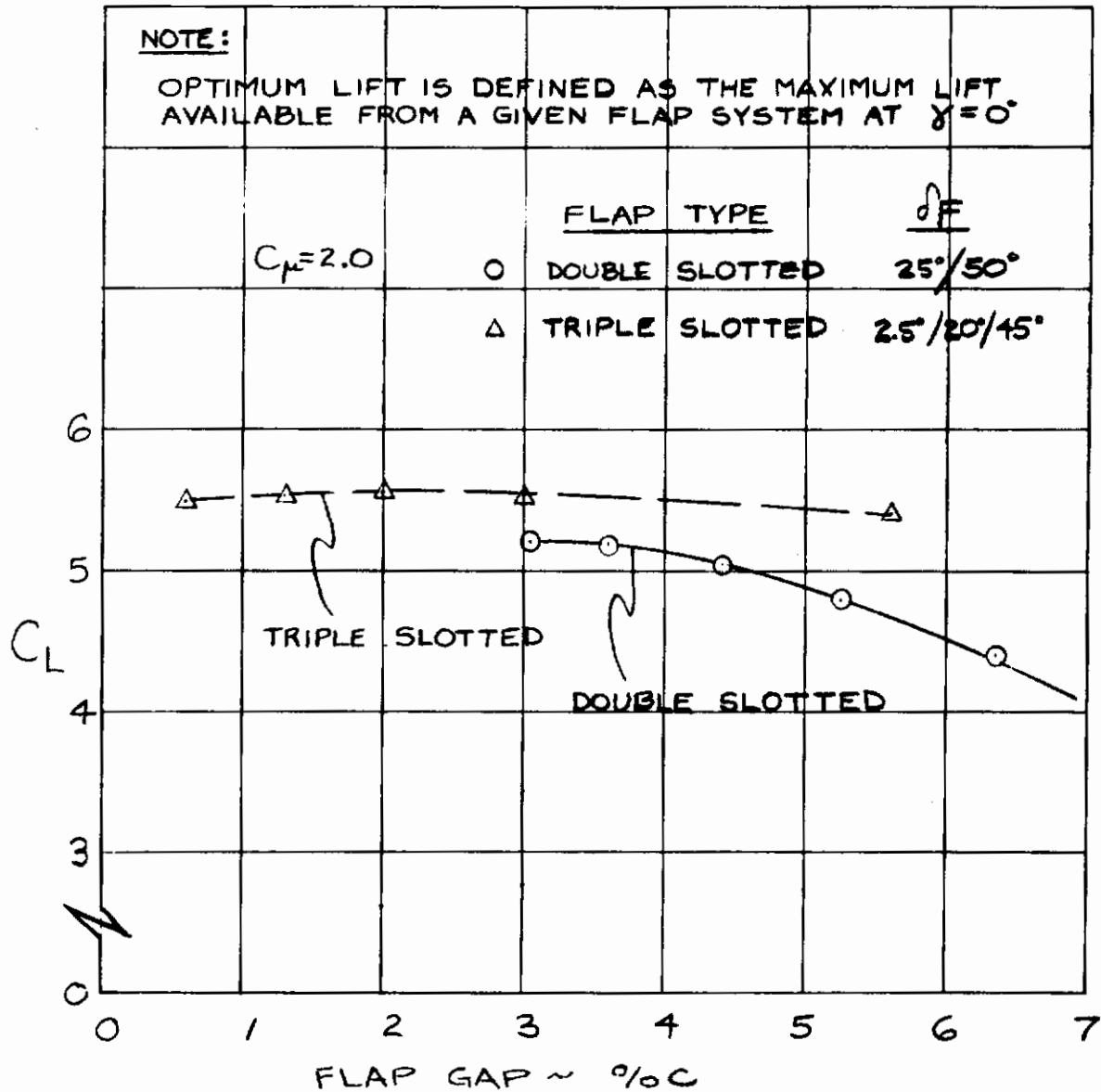


Figure 32. Effect of Flap Gap on Optimum Lift

3.11 EFFECTS OF LEADING EDGE DEVICES

The primary effect of the leading edge device is to increase $C_{L_{MAX}}$ by delaying leading edge stall to higher angles of attack. In application to an externally blown flap, test data indicate that the increment in $C_{L_{MAX}}$ due to the leading edge device is developed in the power-off condition, and no further increase in $C_{L_{MAX}}$ due to the leading edge device is realized for the power-on case.

In the present methods, the effects of the leading edge device are estimated for the power-off case by DATCOM or other suitable methods. Power effects are then added as described in Sections 3.2 through 3.5.

Tests were made in Reference 13 of systematic variations of Krueger flap span from 100 percent span to 40 percent span. Figure 33 presents the lift increment due to flap blowing at zero incidence, and shows no effect of Krueger flap span. Figure 34 shows the effect of leading edge flap span on $C_{L_{MAX}}$ for the power-off and power-on cases. It is seen here that the estimated power effects on $C_{L_{MAX}}$, which assume no effect of the leading edge device, are in good agreement with the experimental data at all values of the leading edge flap span. The increment of $C_{L_{MAX}}$ due to power is shown in Figure 35 for two values of blowing coefficient.

Contrails

$$\int F = 25/50^\circ$$

$$\alpha = 0^\circ$$

$$C_{\mu} = 2.0$$

REF. 13

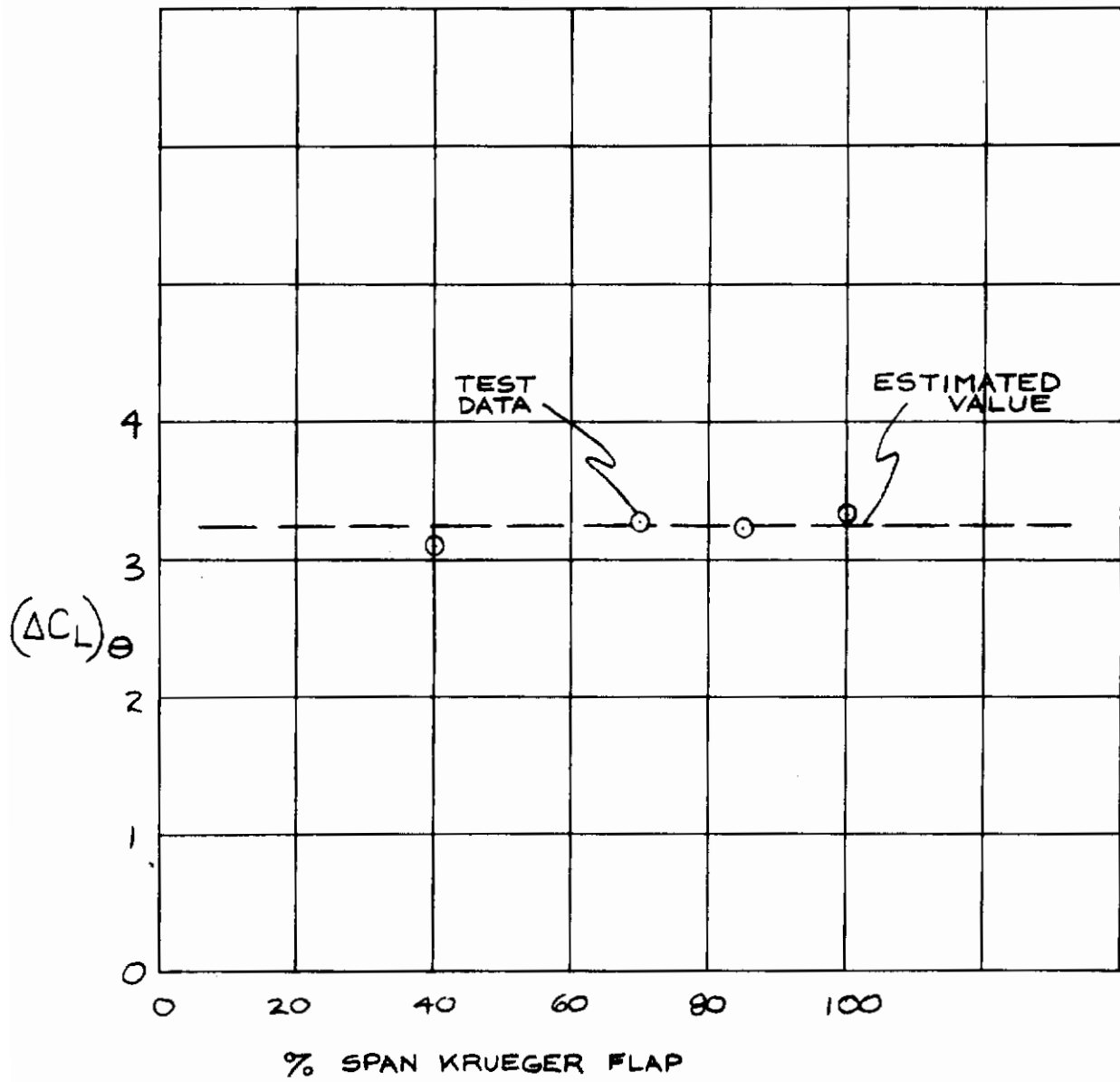


Figure 33. Effect of Leading Edge Flap Span on Lift due to Power

○ $C_{\mu}=0.0$

□ $C_{\mu}=2.0$

REF. 13

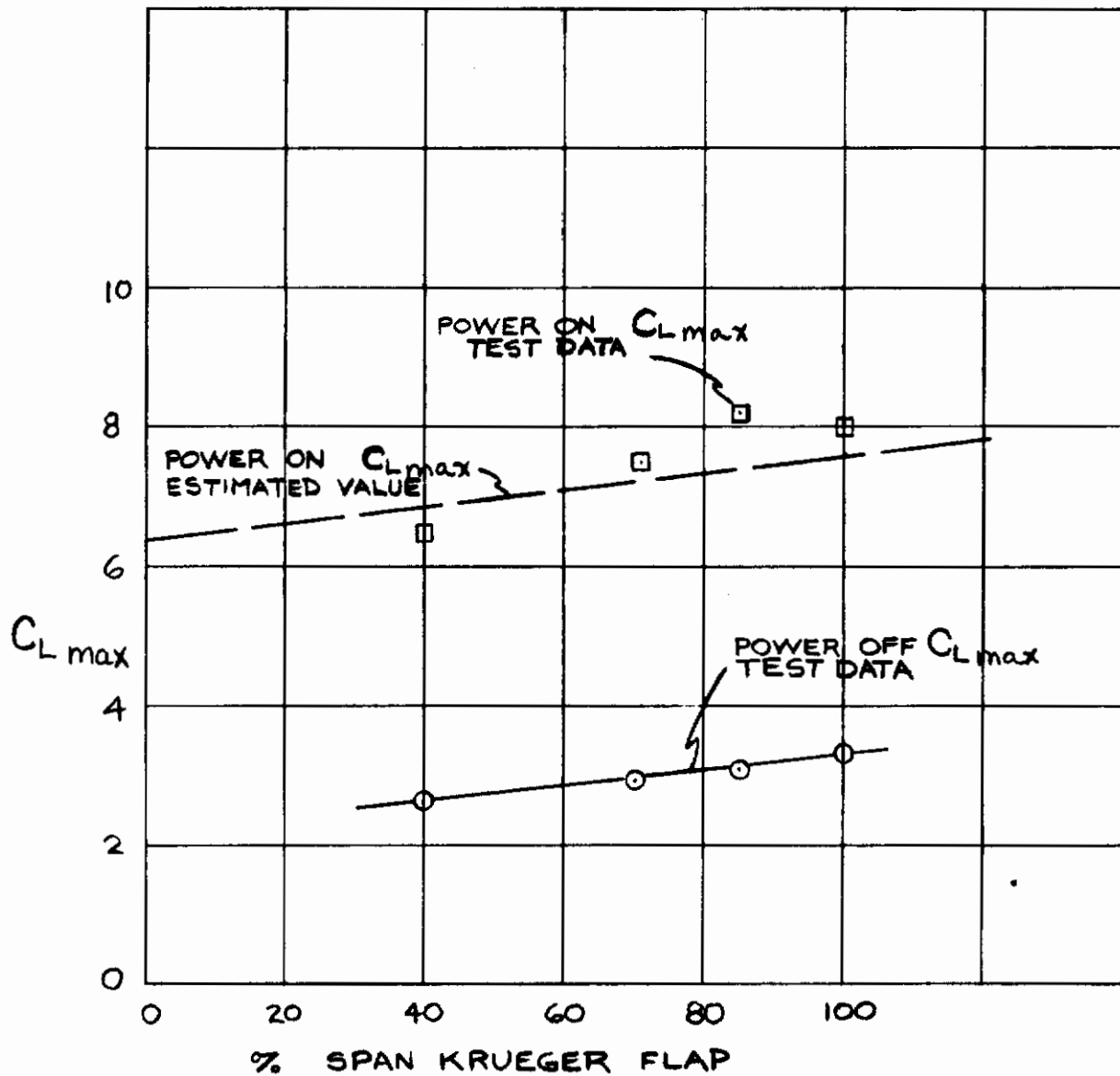


Figure 34. Effect of Leading Edge Flap Span on C_{Lmax}

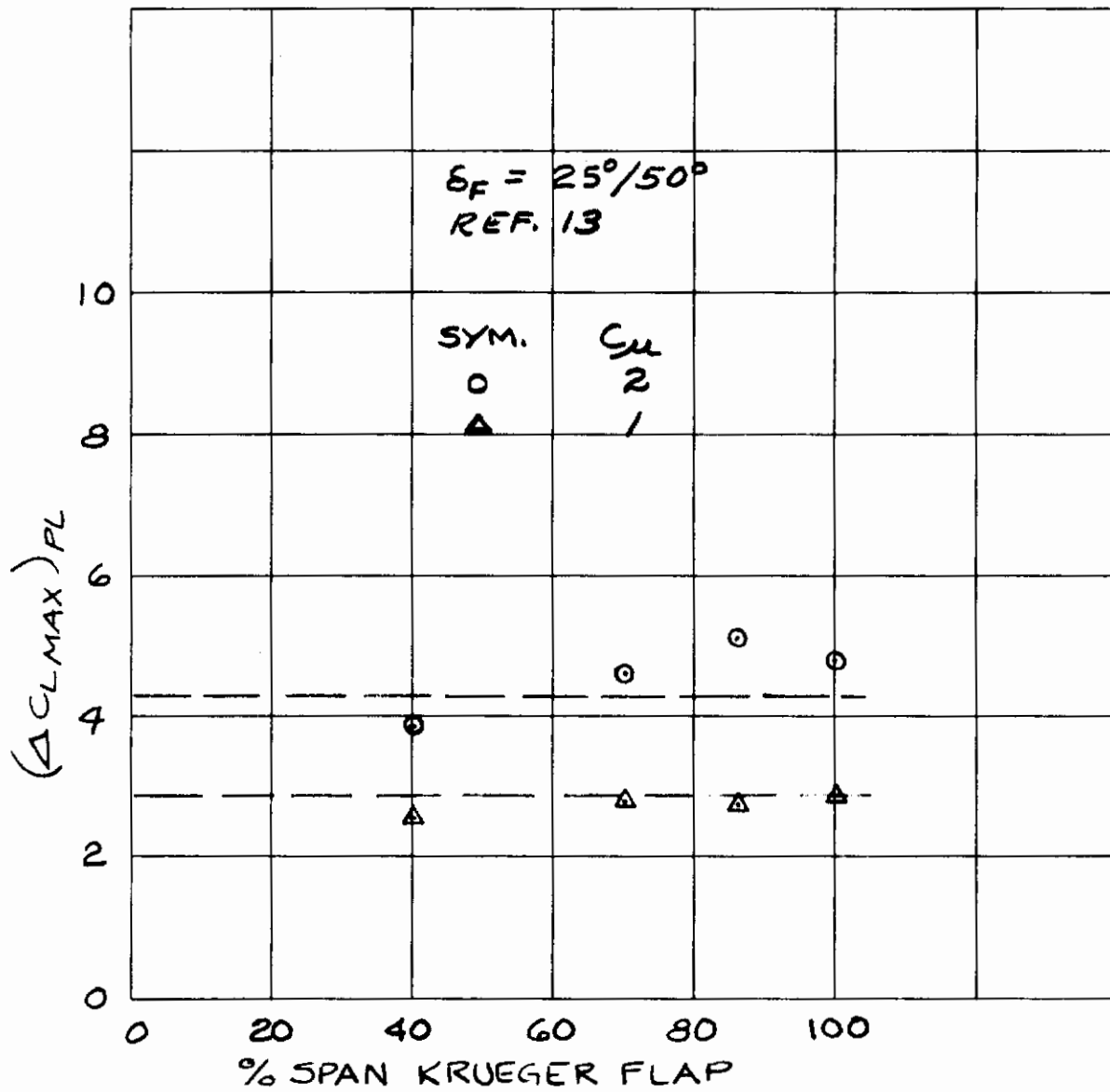


Figure 35. Effect of Leading Edge Flap Span on ($\Delta C_{L_{max}}$) Due to Power

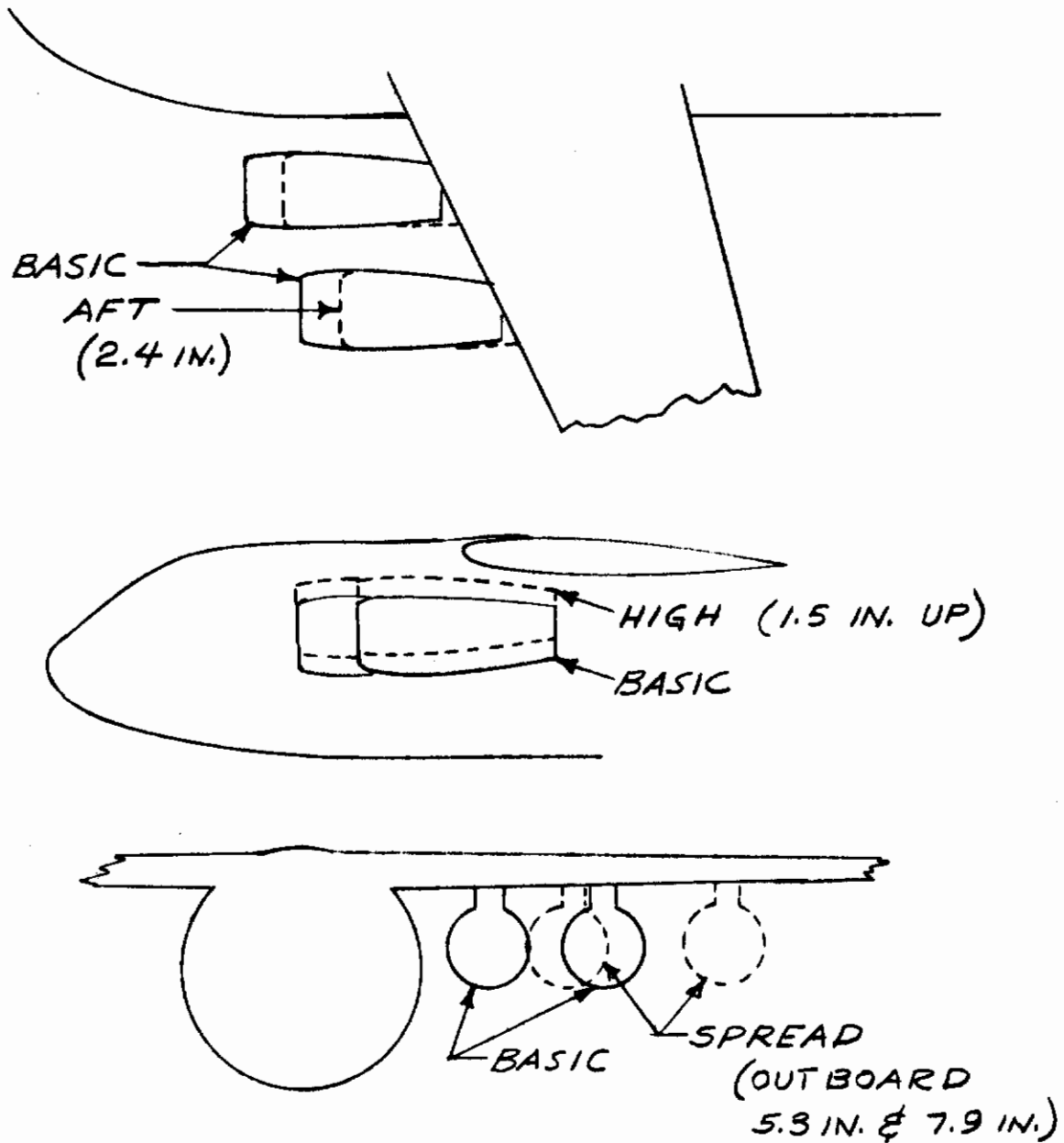


Figure 36. Alternate Nacelle Positions Tested in Reference 13

3.12 EFFECTS OF NACELLE LOCATION AND ENGINE ORIENTATION

The methods of estimation developed in this report account for the effects of nacelle location and engine orientation through the use of the "impingement ratio," Z_F/R , and the inclusion of direct force terms due to thrust axis incidence. Test results of a systematic variation of nacelle position (Figure 36) and nozzle deflection angle conducted in the wind tunnel tests of this program, substantiate these methods.

Test data are shown in Figure 37 of lift increment due to power versus engine nozzle angle for various nacelle locations. It is seen that the high nacelle location has better performance, and the aft nacelle location has poorer performance than the basic nacelle location. Also, there is no apparent benefit in spreading the engines spanwise any farther than the basic arrangement. These data show the very potent effects of deflecting the nozzle upward into the flaps. The nozzle angle effect is about the same for all nacelle locations.

These same data when shown as a function of the impingement ratio in Figure 38, tend to collapse about a single curve with the exception of the aft nacelle location data, which is about 10 percent below the other data. Static calibration data of the aft location were not taken, but it is believed that the aft location might produce a higher drag force which would result in a lower turning efficiency, thus explaining the reduced lifting effectiveness. It is concluded that the prediction methods adequately account for effects of nacelle location and thrust incidence, although they do not account for the penalty incurred by moving the nozzle closer to the flaps. Here again, it should be a design objective to locate the nozzle at or near the wing leading edge.

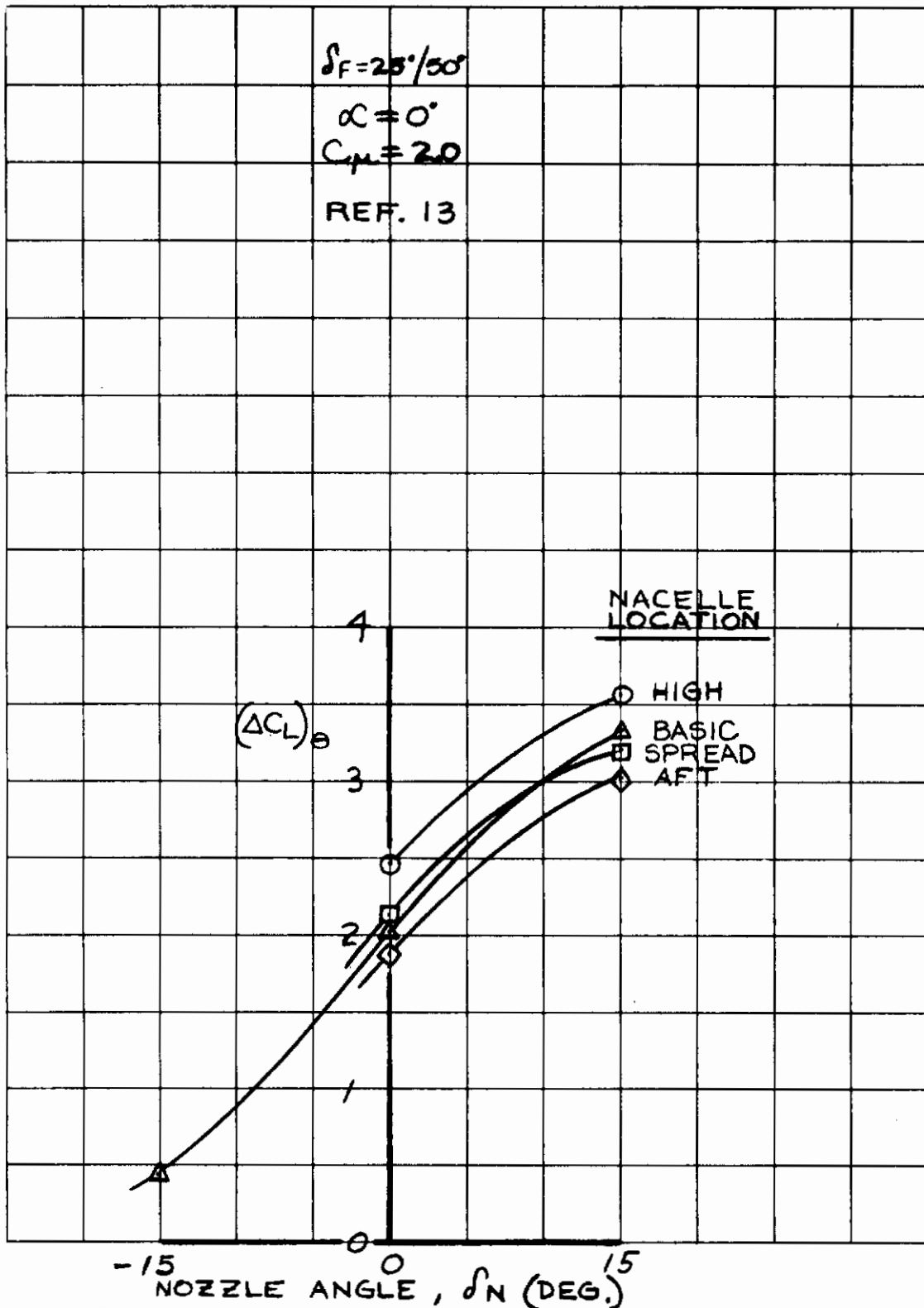


Figure 37. Effects of Nacelle Location and Nozzle Deflection on Lift Due to Power - Versus δ_N

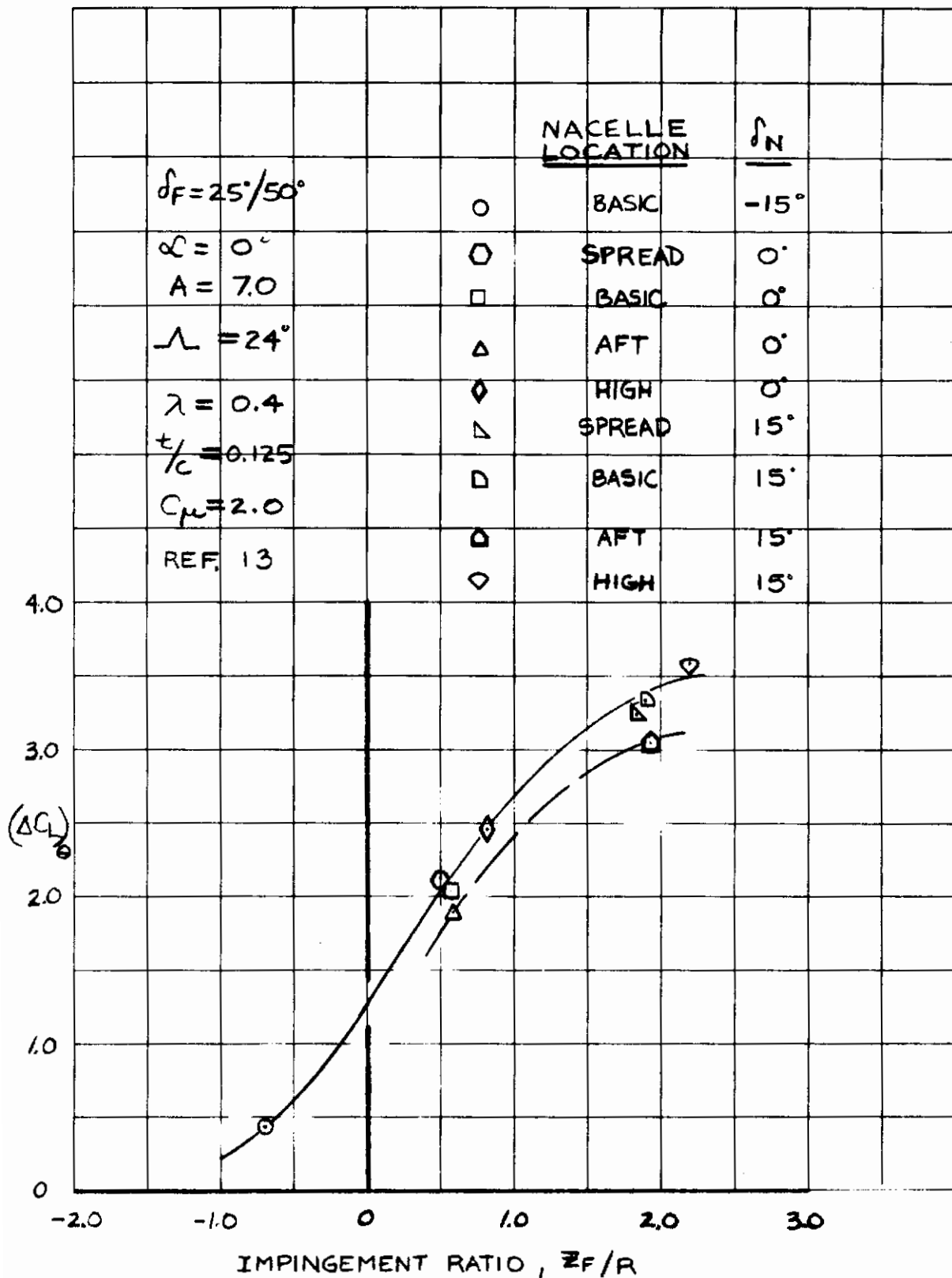


Figure 38. Effects of Nacelle Location and Nozzle Deflection on Lift due to Power

3.13 EFFECTS OF ASYMMETRIC THRUST

Experimental results of test simulating the loss of thrust on one engine of a four-engine airplane is shown on Figure 39. It is seen that the loss in lift due to one-fourth reduction in $7C$ is very nearly equal to one-fourth of the total lift. Since the powered lift increment is not linear with C_{μ} , the loss of lift due to an engine failure is not equivalent to the reduction in lift that would result from the reduction of C_{μ} by 25 percent uniformly on all engines.

The loss of lift due to an engine failure with the thrust held constant on the remaining engines, can then be estimated by:

$$(\Delta C_L)_{\text{engine failure}} = \frac{1}{N} (\Delta C_L)_{\text{p.L. all engines}} \quad 3.26$$

where N is the total number of engines on the airplane.

The test data presented in Figure 39 show that the loss of an inboard engine results in slightly less lift loss than the loss of an outboard engine. This might be due to the outboard engine affecting a larger portion of the wing than the inboard engine. This effect is negligibly small.

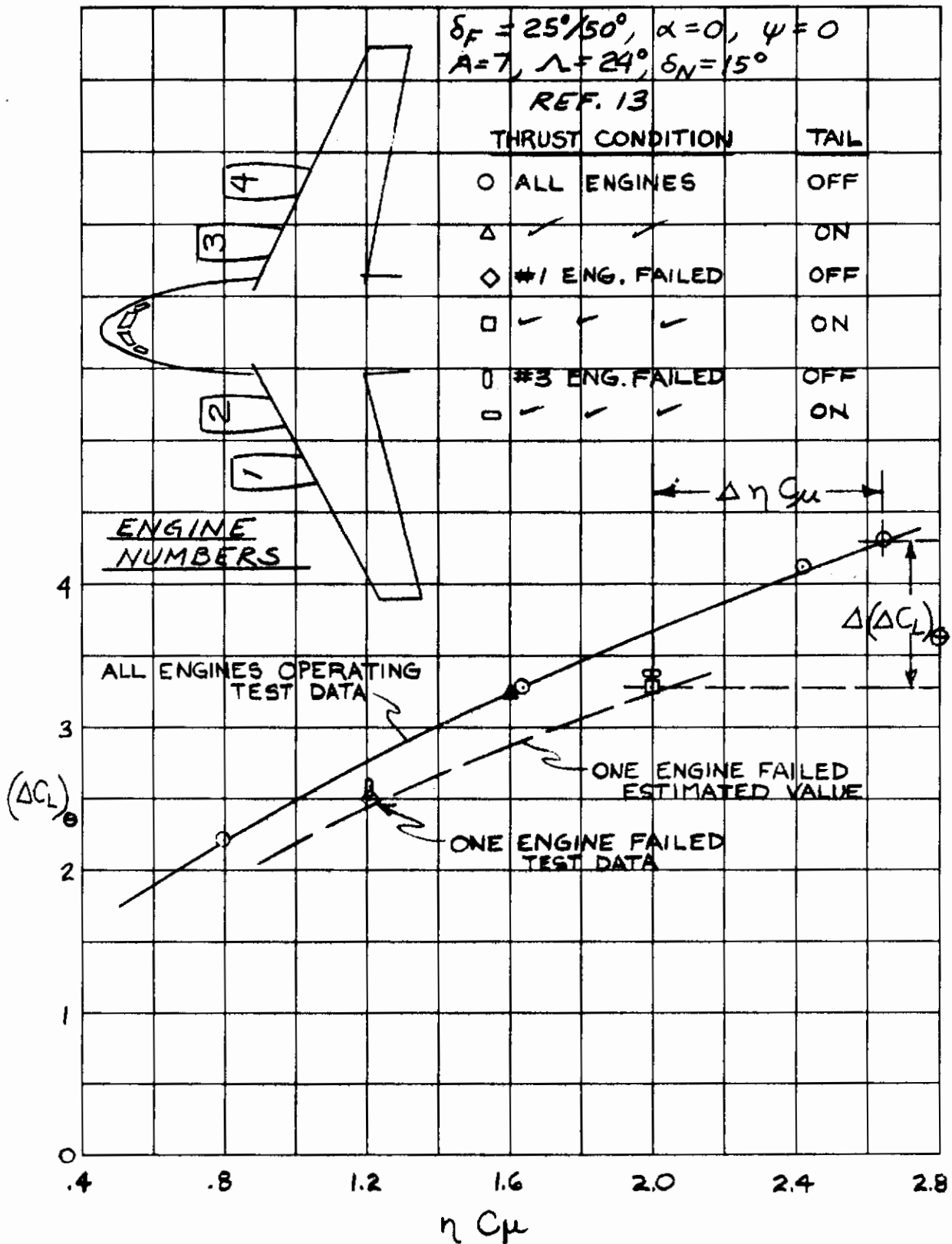


Figure 39. Effect of Asymmetric Thrust on Powered Lift Increment

Contrails

Section IV

DRAG

Defining drag as the total force in the wind direction, including engine thrust, the total drag coefficient is:

$$C_D = C_{Df} + C_{Di} - \eta C_{\mu} \cos(\theta + \alpha) + \Delta C_{DR} \quad 4.1$$

where C_{Df} is the power off minimum drag minus $(C_L \text{ at min. drag})^2 / \pi A$;
 C_{Di} is the induced drag due to lift (see Section 4.1); and ΔC_{DR} is ram drag.

The drag increment C_{Df} is estimated by conventional methods or obtained from unpowered wind tunnel model data, and is defined by:

$$C_{Df} = C_{Dmin} - \frac{(C_L @ C_{Dmin})^2}{\pi A} \quad 4.2$$

The ram drag component is:

$$\Delta C_{DR} = \frac{W_a V}{2 g \rho} \quad 4.3$$

where W_a = weight rate of flow of air through engine inlets, lb/sec.,
obtained from engine data

V = freestream velocity, fps

4.1 DRAG DUE TO LIFT

The drag due to lift for a jet flap wing of finite aspect ratio has been derived in Reference 11 as:

$$C_{D_i} = C_L^2 / (\pi A + 2 C_\mu),$$

where C_L is the total lift coefficient including the jet reaction term. Attempted correlations of this expression with wind tunnel test data of externally blown flap models have produced negative results. However, good correlations have been obtained by using the unpowered form of the induced drag expression, and removing the jet reaction force from the total lift:

$$C_{D_i} = [C_L - \eta C_\mu \sin(\theta + \alpha)]^2 / \pi A \quad 4.4$$

Experimental data representing various configurations and several different aspect ratios have been plotted in the form of

$$[C_L - \eta C_\mu \sin(\theta + \alpha)]^2 \text{ versus } [C_D + \eta C_\mu \cos(\theta + \alpha) - \Delta C_{D_R}]$$

in Figure 40. Ram drag and uncertainty in the values of η and θ (see Section 4.2) cause some dispersion of the data, but for one set of conditions held constant the slope is consistent with the assumed value of $1/\pi A$.

A summary of estimated induced drag compared to induced drag derived from test data by removing the drag at zero lift, ram drag, and thrust reaction, is shown in Figure 41. The agreement is reasonably good.

Contrails

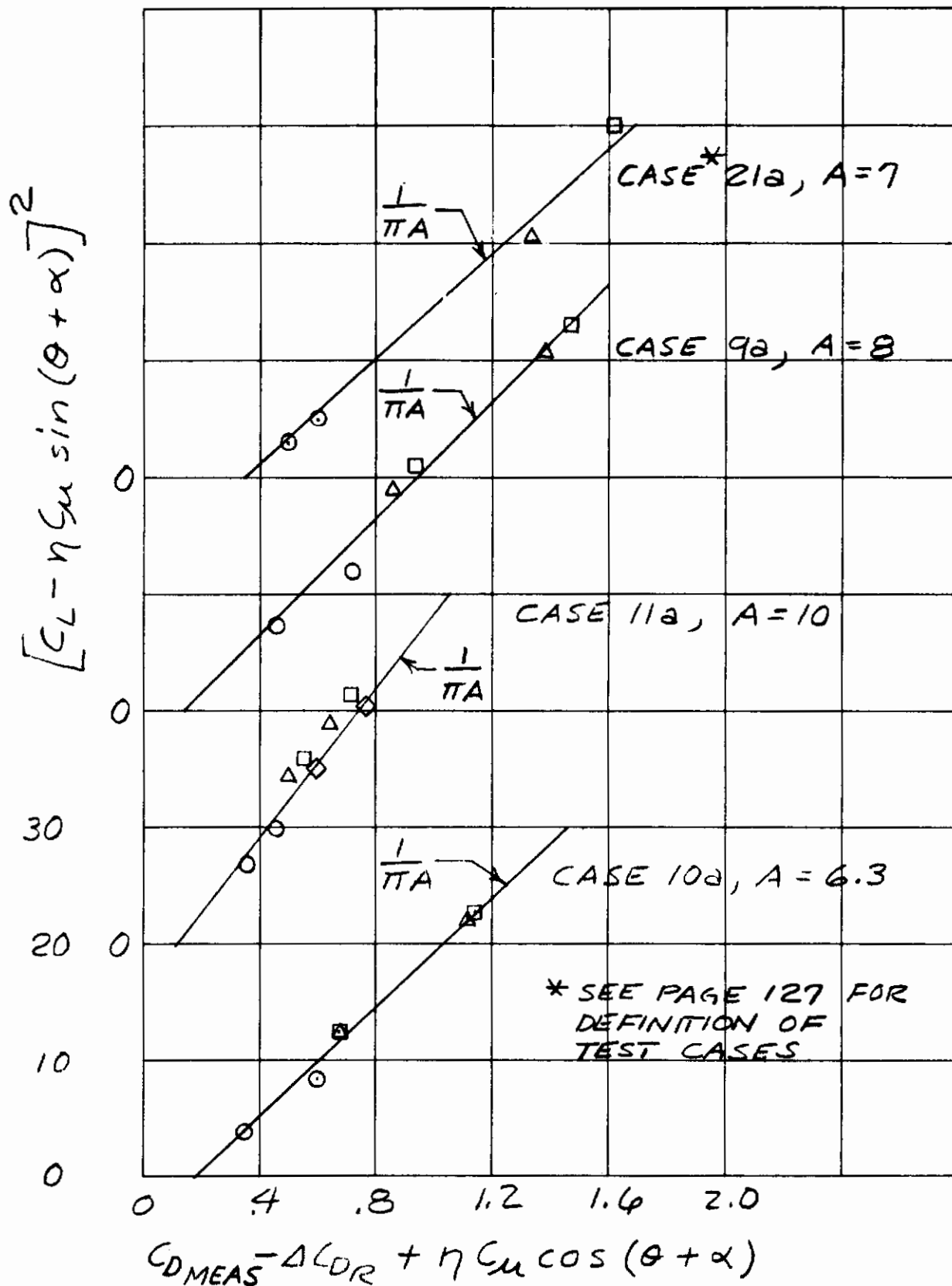


Figure 40a. Correlation of Induced Drag Data

Contrails

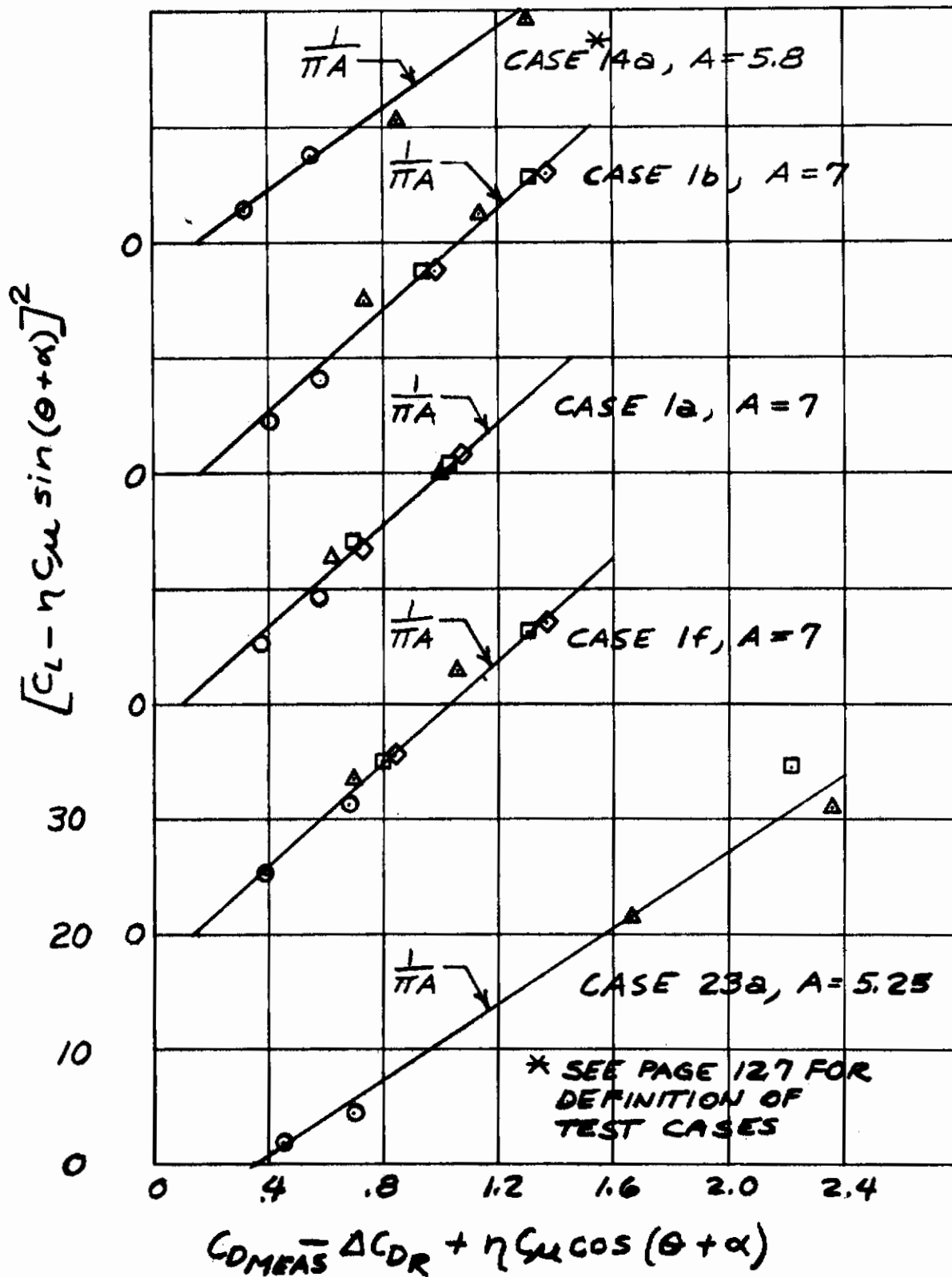


Figure 40b. Correlation of Induced Drag Data

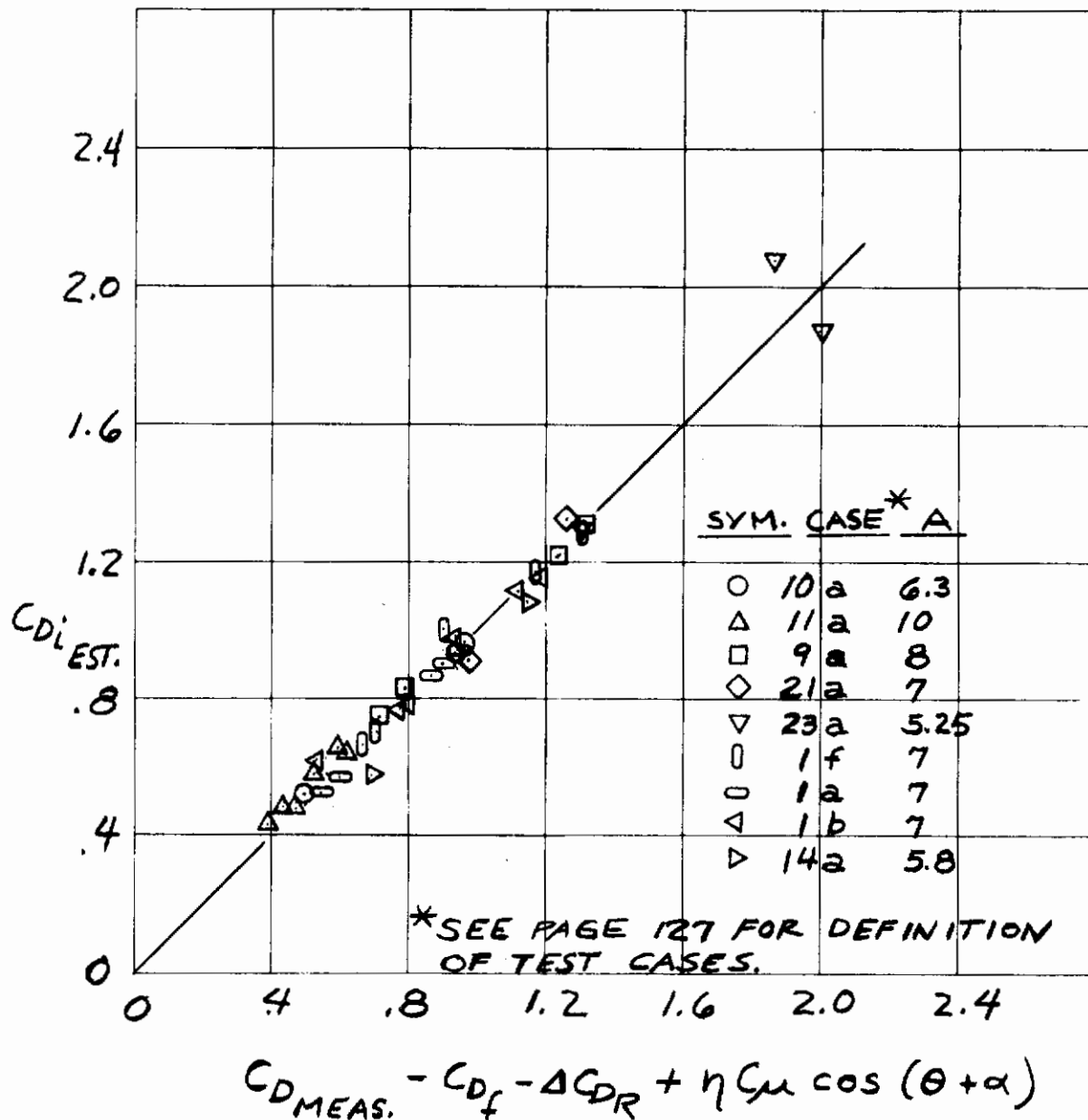


Figure 41. Summary of Induced Drag Data

4.2 THRUST REACTION FORCE

The thrust reaction term, $\eta C_{\mu} \cos (\theta + \alpha)$, is determined from static values of η and θ as discussed in Section II. In estimating the total drag force, this is the component most difficult to define accurately. Both η and θ are subject to variable details of the airplane and flap configuration, and methods are given only for estimating performance of a "well-designed" system. In attempting correlations with wind tunnel test data, good agreement depends on availability of good static calibration results for η and θ .

The deviation of experimental values of the jet turning efficiency from the design curves of Figure 11 are summarized for the various types of flaps and wing sweeps in Figure 42. Most of the experimental points fall within a $\Delta \eta$ of $\pm .10$. The sensitivity of estimated drag with the parameter η , $\Delta C_D / \Delta \eta$, varies from about 0.5 in the range of C_L 's of 4 to 5, to about 2.0 at high lift coefficients. So, the experimental scatter in η could result in deviations in the estimated drag coefficient of $\pm .05$ at nominal lift coefficients and ± 0.2 at high lift coefficients.

Contrails

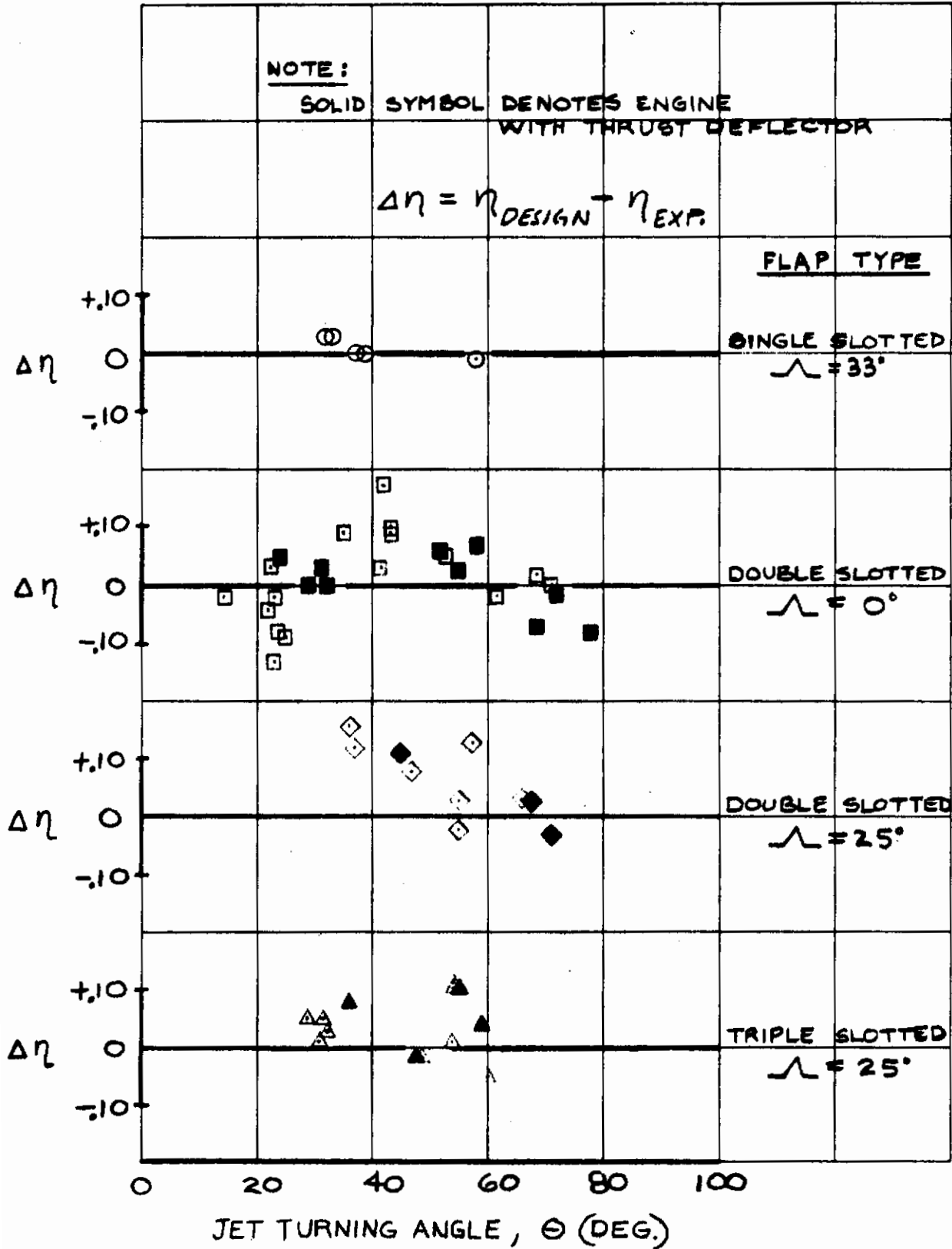


Figure 42. Uncertainty of Jet Turning Efficiency Parameter, η

Contrails

Section V

PITCHING MOMENT

A theoretical development of the pitching moment of a two-dimensional wing with a blown flap has been made by Spence in Reference (17). These methods assume uniform spanwise distributed blowing at the wing trailing edge or knee of the flap so they do not simulate the three dimensional externally blown flap sufficiently for direct application. However, the framework of the theoretical development can be used to guide an empirical approach to solution of the problem.

The method recommended here for estimation of the pitching moment characteristics was developed from consideration of pressure distribution data of externally blown flap tests from References (13) and (14). Typical chordwise and spanwise distributions from Reference (14) are reproduced here in Figures 43 and 44.

From these pressure and loading distribution data it has been concluded that the pitching moments due to an externally blown flap can be predicted by treating the three major components - the thrust reaction, circulation lift at zero incidence, and lift due to angle of attack - individually. The pressure data indicate the following characteristics which have been applied in the present prediction methods.

1. Thrust Reaction Term

The lift component of the thrust reaction, $\eta C_{\mu} \sin \theta$, acts primarily on the flap with no noticeable carry-over forward of the flap. Spanwise, this force is centered about the thrust centerline, as illustrated in Figure 44.

2. Circulation Lift at Zero Incidence

In the chordwise direction this force is quite uniformly distributed, so the center of pressure would fall very close to mid-chord. This is in agreement with two-dimensional jet flap theory which predicts a .5c location of the center of pressure of the induced lift at zero incidence. The spanwise loading distribution of the circulation lift is also quite uniform even when the blowing is concentrated inboard, so the spanwise c.p. of this load can be assumed to be at the MAC of the wing. Data with partial span flaps show a carry-over on the panel outboard of the flaps that averages about half of the unit loading of the flapped portion of the wing.

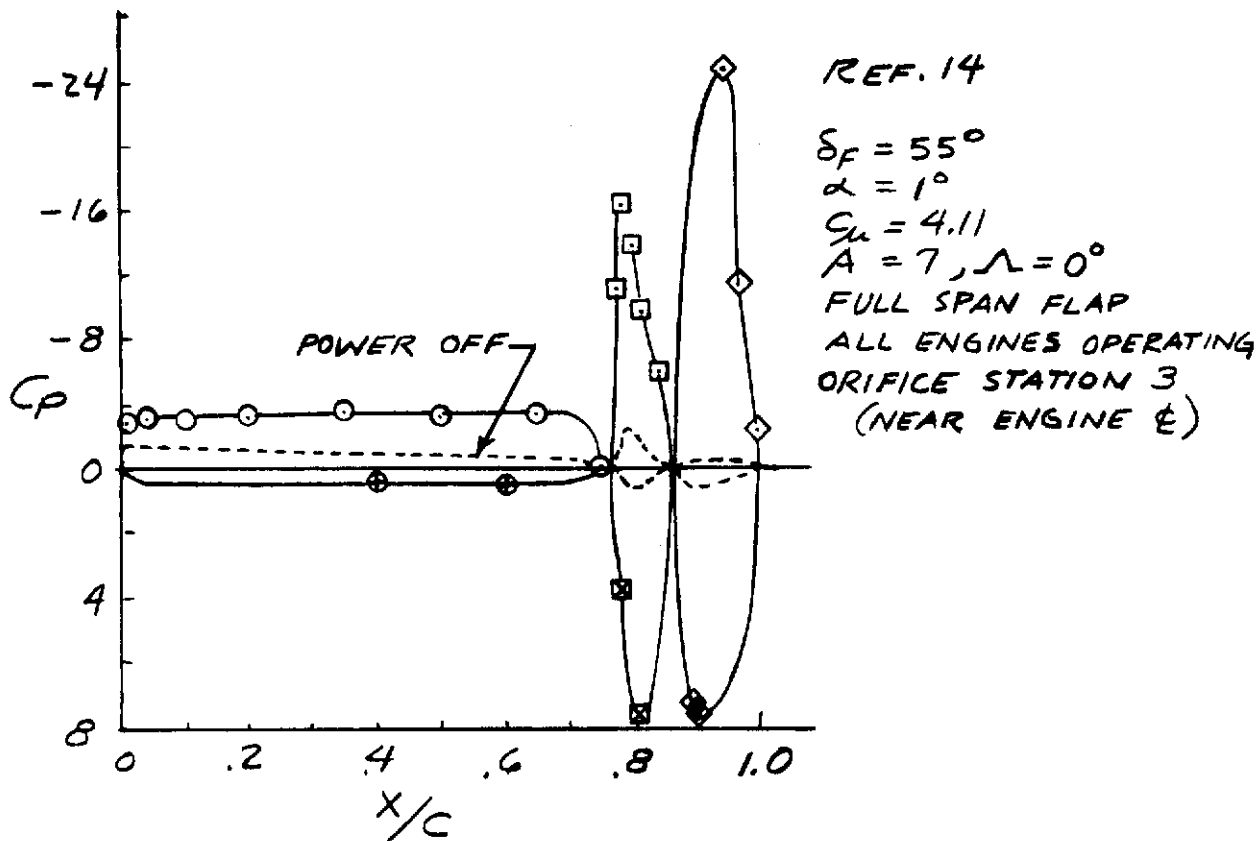


Figure 43. Chordwise Pressure Distribution of an Externally Blown Flap

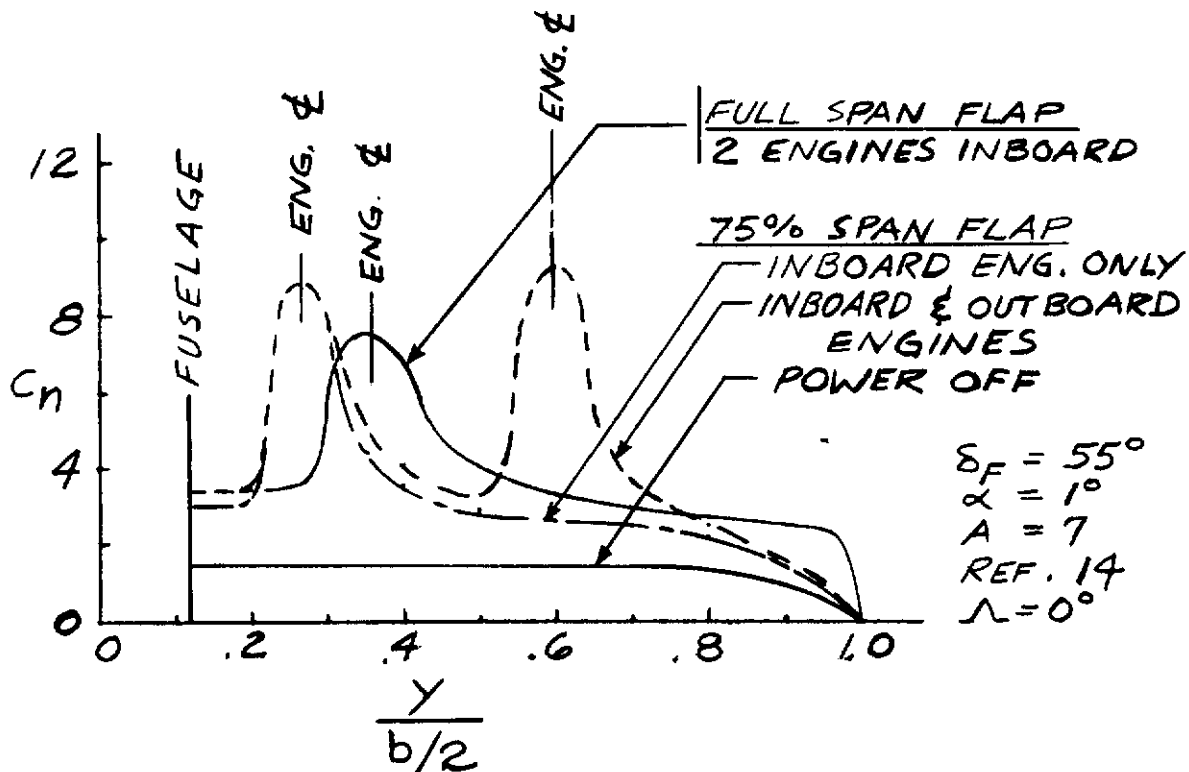


Figure 44. Spanwise Loading Distribution of an Externally Blown Flap

3. Lift Due to Angle of Attack

The additional load due to angle of attack has a conventional distribution, peaking near the leading edge, with a c.p. near the quarter chord. This loading is also uniformly distributed spanwise, so the MAC of the wing can be assumed to be the spanwise location of the c.p.

The tail-off pitching moment characteristics are estimated by adding the powered lift effects to the power off characteristics which are estimated by conventional methods, or are available from unpowered wind tunnel model tests. As discussed above, the total tail-off pitching moment is developed by summing the effects of the several moment inputs:

$$C_m = (C_m)_B + (\Delta C_m)_R + (\Delta C_m)_\Gamma + (\Delta C_m)_\alpha + (\Delta C_m)_{RD} \quad 5.1$$

where $(C_m)_B$ = basic power-off moment coefficient, variable with angle of attack, with flaps extended

$(\Delta C_m)_R$ = moment coefficient due to thrust reaction

$(\Delta C_m)_\Gamma$ = moment coefficient due to circulation lift at zero incidence

$(\Delta C_m)_\alpha$ = moment coefficient due to power effects on additional lift at angle of attack

$(\Delta C_m)_{RD}$ = moment coefficient due to ram drag.

Each of these pitching moment increments will be discussed in the following sections.

5.1 THRUST REACTION MOMENT

By definition, the thrust reaction force, F_R , acts at an angle to the reference plane of $\theta = \tan^{-1} (F_N/F_A)$, where F_N is the normal force component of F_R , and F_A is the axial force component. At forward speed these force components are defined by the coefficients: ηC_u , $\eta C_u \sin \theta$ and $\eta C_u \cos \theta$. Now, according to our analogy to the jet flap, this jet reaction force represents the momentum in the jet sheet leaving the trailing edge of the flap system at the angle θ . Therefore, the moment of this force can be found by extending the force vector from the trailing edge of the flap at angle θ , and determining its moment arm about the moment reference center.

Contrails

The spanwise location of the thrust reaction force, ηC_{μ} , is taken to be at the engine centerline; or, in the case of a four-engine installation, midway between the two engines on one wing. Now to determine the length of the moment arm it is probably more convenient to work with the normal and axial thrust reaction components. By extending the vector, ηC_{μ} , from the flap trailing edge at angle θ , the chordwise location of the intersection of this vector with the reference plane (the horizontal plane through the moment reference center) can be found (see figure 45). Then the pitching moment about the moment reference center due to the thrust reaction force is equal to the normal force component, $\eta C_{\mu} \sin \theta$, acting at the distance from the moment reference center to the intersection of the thrust reaction force with the reference plane. The axial force component has no moment arm in this system. So, taking moments about the wing leading edge at the location of the engine centerline:

$$(\Delta C_m)_{R_{L.E.}} = -\eta C_{\mu} \sin \theta \left(\frac{C_R}{c'} \right) \left(\frac{c'}{\bar{c}} \right) \quad 5.2$$

where C_R = chordwise distance of intersection of thrust reaction vector and the reference plane from the wing leading edge

c' = length of wing chord at engine centerline

\bar{c} = MAC of wing.

These parameters are illustrated in Figure 45 for two possible locations of the moment reference center. This pitching moment can be transferred to the moment reference center by conventional methods:

$$(\Delta C_m)_{R_{REF.}} = -\eta C_{\mu} \sin \theta \left[\left(\frac{C_R}{c'} \right) \left(\frac{c'}{\bar{c}} \right) - \left(\frac{x_{REF} - x_{L.E.C'}}{\bar{c}} \right) \right] \quad 5.3$$

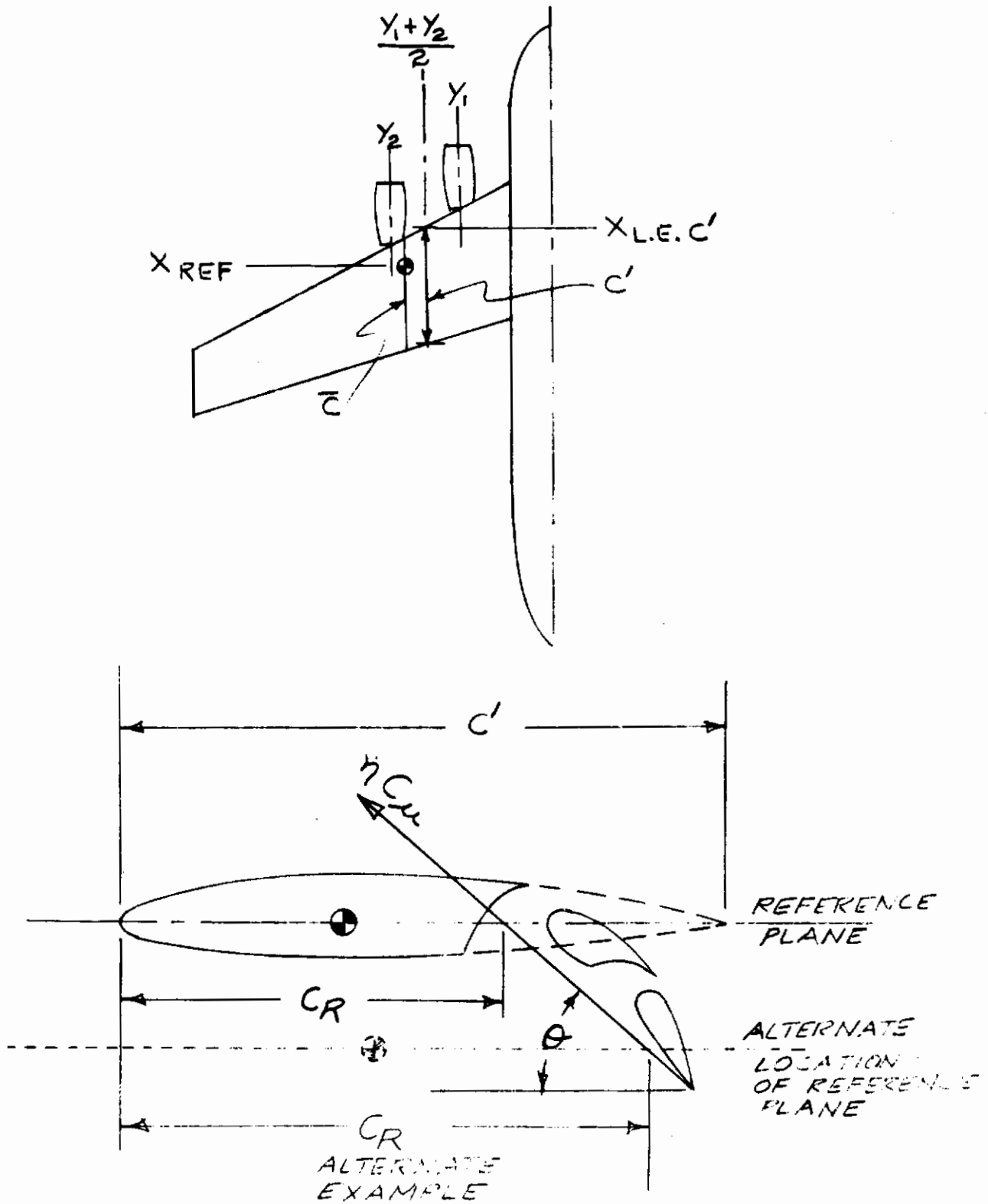


Figure 45. Definition of Thrust Reaction Moment Arm

5.2 MOMENT DUE TO CIRCULATION LIFT AT ZERO INCIDENCE

As discussed above the circulation lift at zero incidence can be assumed to act at the mid chord of the MAC of the affected portion of the wing. An alternate approach is to define the center of pressure of the circulation lift due to power to be equal to the center of pressure of the power-off, zero incidence, flaps down lift. Rather extensive investigations of experimental results of various configurations have shown this correlation. This approach should give better accuracy, especially if unpowered wind tunnel model data are available. The pitching moment increment of the circulation lift at zero incidence about the moment reference center is then:

$$(\Delta C_m)_{REF} = (\Delta C_L)_\Gamma \frac{(C_m)_{B_0}}{(C_L)_B} \quad 5.4$$

where $(C_m)_{B_0}$ = pitching moment coefficient about moment reference center, power off, flaps down, $\alpha = 0$

$(C_L)_B$ = lift coefficient, power off, flaps down, $\alpha = 0$

$(\Delta C_L)_\Gamma$ = circulation lift at zero incidence as defined in Section 3.2.

5.3 PITCHING MOMENT DUE TO ANGLE OF ATTACK

The center of pressure of the additional lift due to angle of attack for a two-dimensional jet flap has been derived by Spence in Reference (10). His results can be approximated by the relation:

$$\frac{x_{c.p.}}{\bar{c}} \approx .25 - .01 \eta C_{\mu} \quad 5.5$$

so the center of pressure of the angle of attack term is very near the quarter chord. Experimental data confirm that the additional lift acts essentially at the quarter chord. The recommended procedure for estimating the incremental pitching moment due to angle of attack effects is, then:

$$(\Delta C_m)_{\alpha_{L.E.}} = - \left[(\Delta C_L)_{\alpha} - (\Delta C_L)_{\alpha_{PO}} \right] \left[\left(\frac{x_{c.p.}}{\bar{c}_F} \right) \left(\frac{\bar{c}_F}{\bar{c}} \right) \right] \quad 5.6$$

where: $(\Delta C_L)_{\alpha}$ = lift increment due to angle of attack, defined in Section 3.3

$$(\Delta C_L)_{\alpha_{PO}} = \text{lift increment due to angle of attack, power-off} \\ \approx 2 \pi F \alpha (1 + \frac{1}{2}c) = \frac{2\pi \alpha (1 + \frac{1}{2}c) A}{57.3 (A + 2)}$$

$$\frac{x_{cp}}{\bar{c}_F} \approx .25 - .01 \eta C_{\mu}$$

\bar{c}_F = MAC of affected wing area as defined in Section 3.1.

This moment increment can be transferred to the moment reference center by conventional methods:

$$(\Delta C_m)_{\alpha_{REF}} = - \left[(\Delta C_L)_{\alpha} - (\Delta C_L)_{\alpha_{PO}} \right] \left[\left(\frac{x_{c.p.}}{\bar{c}_F} \right) \left(\frac{\bar{c}_F}{\bar{c}} \right) - \left(\frac{x_{REF} - x_{LE}\bar{c}}{\bar{c}} \right) \right] \quad 5.7$$

5.4 RAM DRAG MOMENT

The pitching moment of the ram drag about the moment reference center is:

$$(\Delta C_m)_{RD} = - (\Delta C_D)_R \frac{\Delta l_R}{c} \quad 5.8$$

where $(\Delta C_D)_R$ = ram drag, defined in Section 4.

Δl_R = moment arm of engine inlet axis about moment reference center, positive when engine is below reference plane. In the stability axis system this dimension is variable with angle of attack.

5.5 TOTAL PITCHING MOMENT

The total pitching moment coefficient about the moment reference center is, then, the sum of the above increments:

$$\begin{aligned}
 C_{M_{REF}} = & (C_m)_B - \eta L_u \sin \theta \left[\left(\frac{C_R}{C'} \right) \left(\frac{C'}{\bar{c}} \right) - \left(\frac{x_{REF} - x_{L.E.C'}}{\bar{c}} \right) \right] \\
 & + (\Delta C_L)_P \frac{(C_m)_{B_0}}{(C_L)_B} \\
 & - \left[(\Delta C_L)_\alpha - (\Delta C_L)_{\alpha_{P.O.}} \right] \left[\frac{x_{C.P.}(\bar{c}_F)}{\bar{c}_F} \left(\frac{\bar{c}_F}{\bar{c}} \right) - \left(\frac{x_{REF} - x_{L.E.}\bar{c}_F}{\bar{c}} \right) \right] \\
 & - (\Delta C_D)_R \frac{\Delta l_R}{\bar{c}}
 \end{aligned}
 \tag{5.9}$$

Correlations with experimental data using these methods have been made for several varied configurations with the results being shown in Figure 46. In general the agreement is very good, falling within + 10 percent. Those data showing the largest deviation are due to overestimation of the lift increment due to blowing. Again, this noticeable discrepancy in lift estimation is primarily due to the aspect ratio effects.

Contrails

<u>SYM</u>	<u>CASE</u> *	<u>SYM</u>	<u>CASE</u>	<u>SYM</u>	<u>CASE</u>
○	1a	◁	9a	△	25a
△	1b	▷	10a	◃	23a
□	1d	⊙	11a	x	24a
◇	1f	∅	21a	+	91a (U.S.B)
▽	14a	=	22a	γ	71a

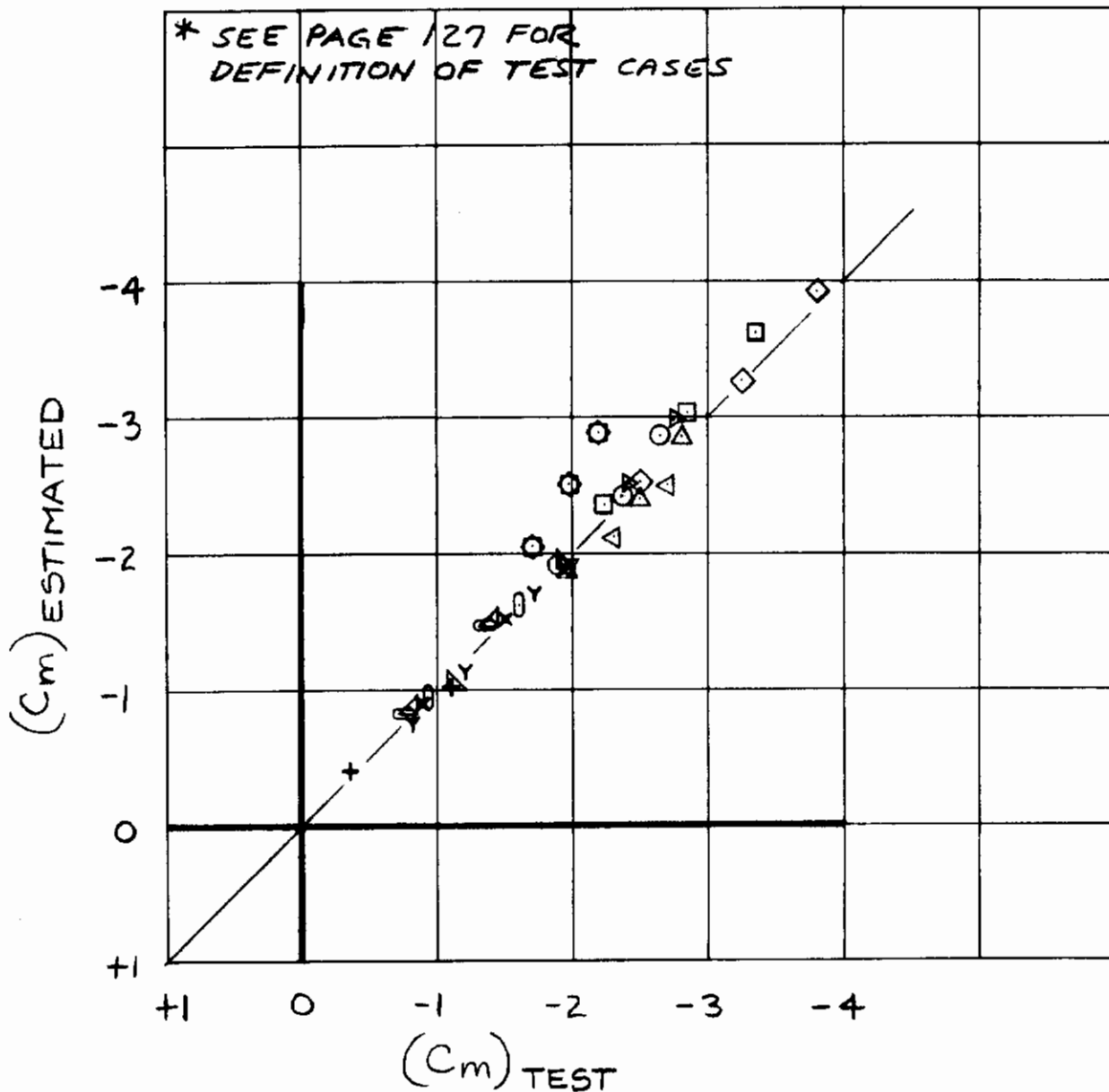


Figure 46. Correlation of Pitching Moment Coefficient Data

5.6 EFFECT OF LEADING EDGE DEVICES

The effect of wing leading edge blowing on the center of pressure location of the power effects at $\alpha = 0$ was analyzed and found to be negligible, see Figure 47.

Also, the effect of Krueger flaps and leading edge droop was found to be negligible, see Figure 48.

REF. 5

BASIC LEADING EDGE

TRIPLE SLOTTED FLAPS

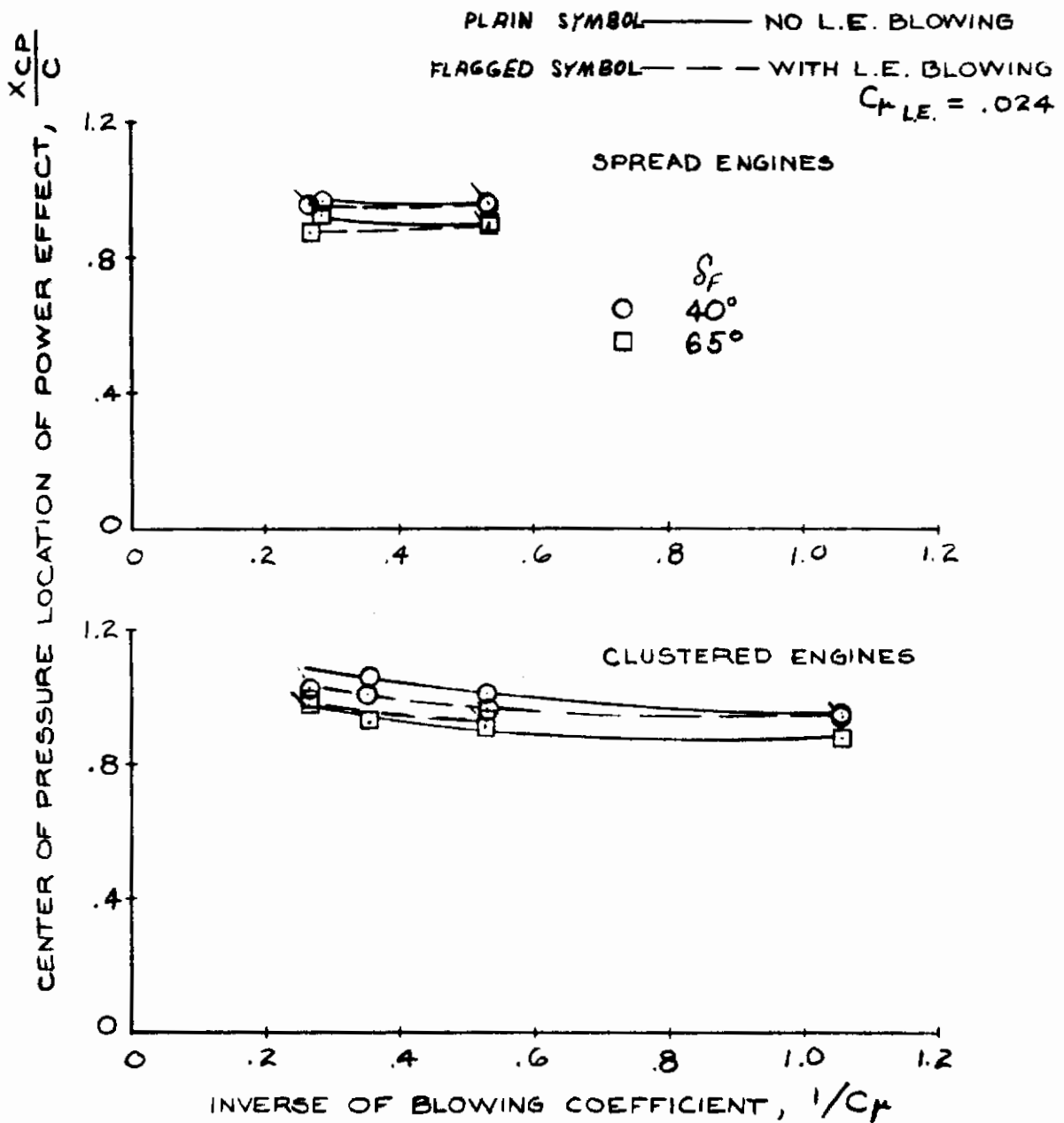


Figure 47. Effect of Leading Edge Blowing on Center of Pressure Location of Power Effect

SPREAD ENGINE CONFIGURATION

REF. 5

TRIPLE SLOTTED FLAPS

$$\delta_f = 60^\circ$$

$$C_{\mu, LE} = 0$$

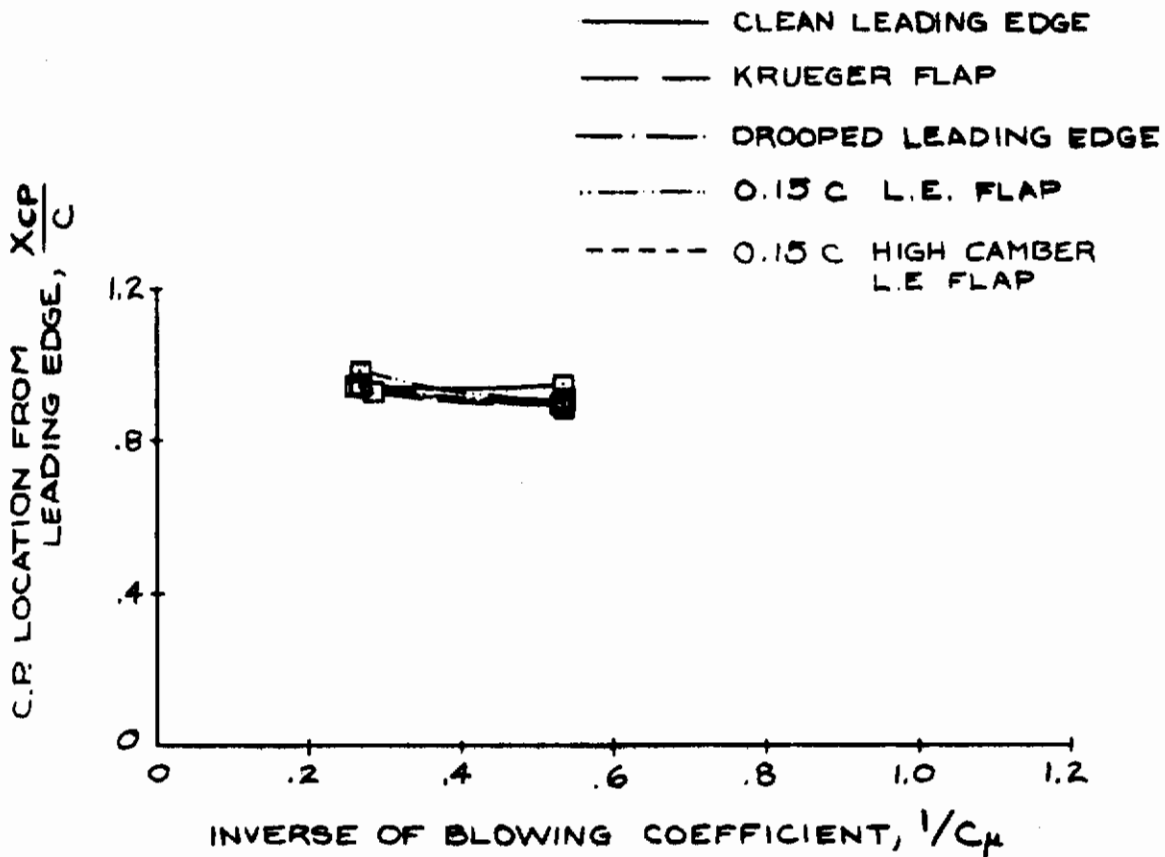


Figure 48. Effect of Leading Edge Configuration Variation on Center of Pressure Location of Power Effect

Contrails

Section VI

TAIL ENVIRONMENT EFFECTS

The tail environment characteristics are presented in this section as the downwash angle at zero angle of attack and the change of downwash angle with lift due to power. Next the downwash factor ($1 - d\epsilon/d\alpha$) is discussed. In particular various configuration effects have been examined. A limited amount of data on the dynamic pressure environment at the airplane tail is presented herein.

6.1 DOWNWASH AT ZERO INCIDENCE

The method of Ross, Reference (18), for estimation of the downwash behind jet-flapped wings was evaluated for application to the externally blown flap. Although reasonable agreement of the theory with test results was found for small jet deflection angles, the theory significantly underestimated the downwash for larger jet deflection angles. This was contributed in Reference (12) to overestimation of the deflection of the jet wake due to jet angle, and due to roll-up of the vortex sheet, which is not accounted for in the theory. A further discrepancy in this theoretical treatment is the assumption of elliptical spanwise loading distribution which can be substantially violated with EBF configurations.

Since the linearized theory did not give satisfactory results in the region of interest, an empirical approach to providing means of estimating the downwash was taken. The limited amount of test data available for externally blown flaps were generalized and are presented in Figure 49 showing the relation of downwash angle at zero angle of attack with lift coefficient, tail height, and tail length. In this form the effects of flap deflection angle and blowing coefficient are reflected in the lift coefficient, so any independent effect of these variables on downwash angle is not defined. Other limitations of these data are that they are for the aspect ratio range of 7 to 8.

The aspect ratio effect on downwash angle, which might be expected to be a function of C_L/A or $C_L A / (\pi A + 2C_{mu})$ (from jet flap theory), could be incorporated in this type of data presentation if sufficient experimental data were available for development and substantiation of such a factor. Unfortunately, experimental data to investigate this relationship with aspect ratio were not available.

The faired curves of Figure 49 have been superimposed on test data from References (2), (4), and (13) in Figures 50 through 53 at the appropriate tail heights and tail lengths to illustrate the degree of experimental data variation.

Contrails

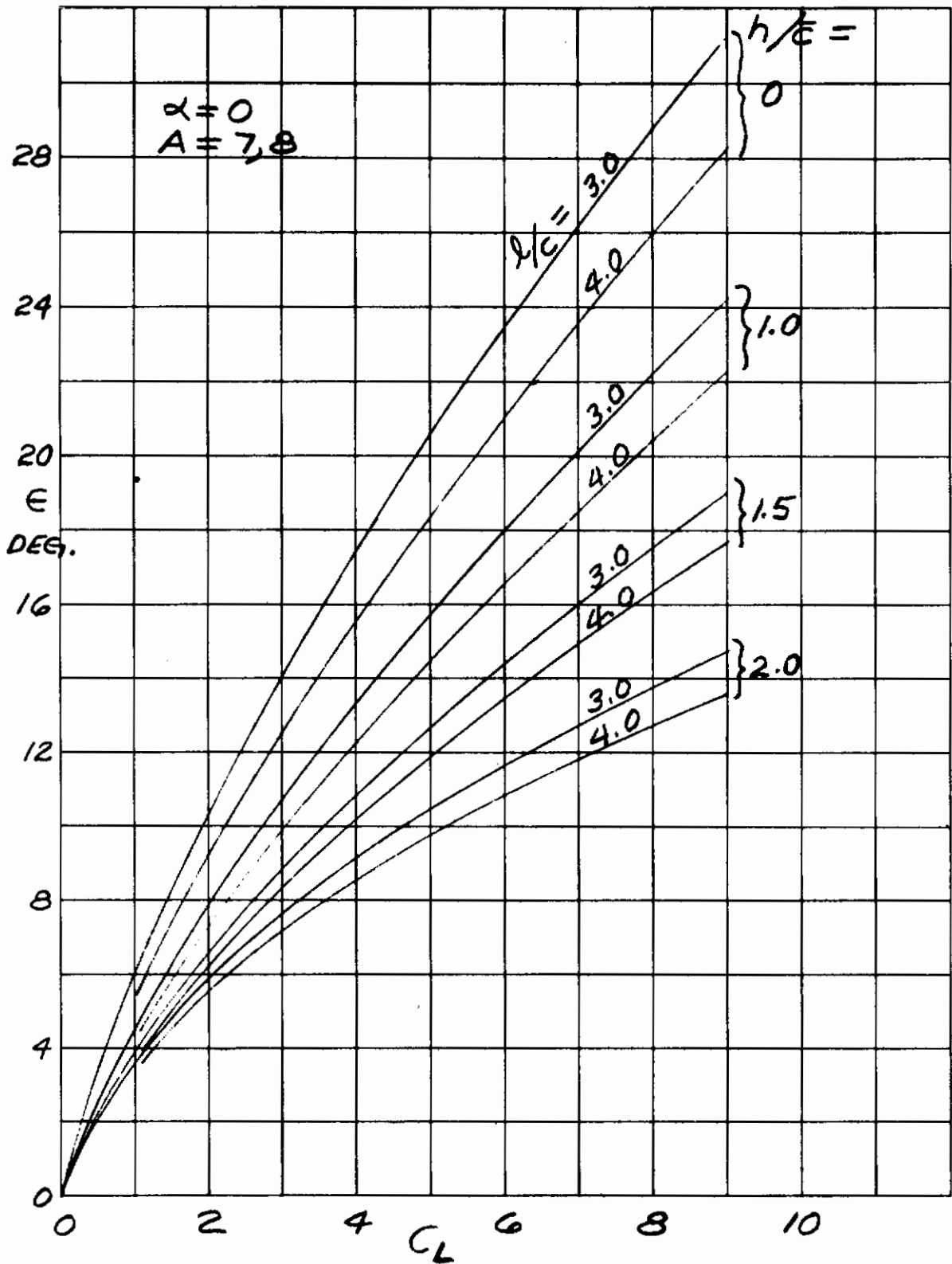


Figure 49. Downwash Angle at Zero Incidence, Summary Curves

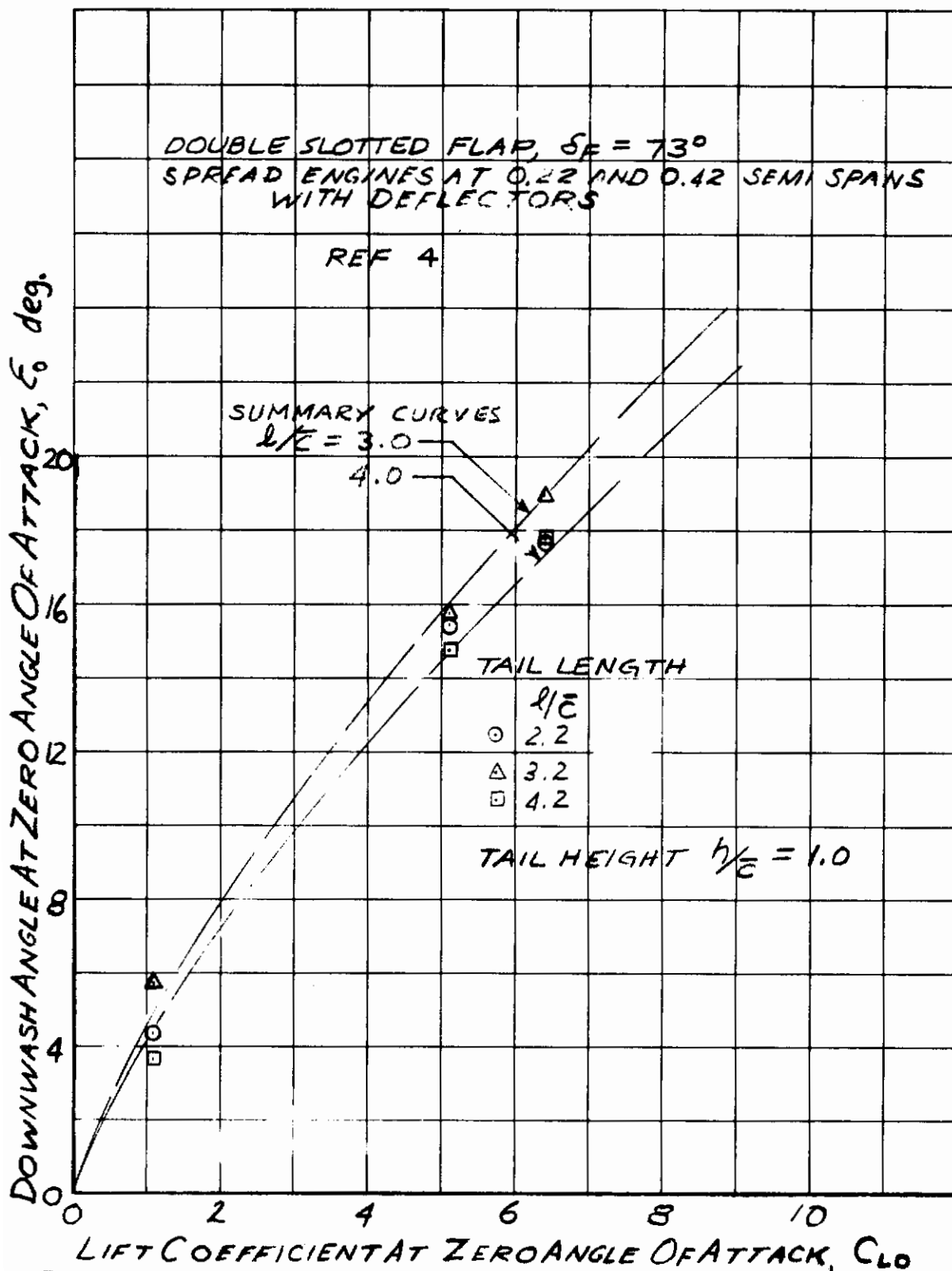


Figure 50. Effect of Tail Length on Downwash Variation With Lift Change Due to Power

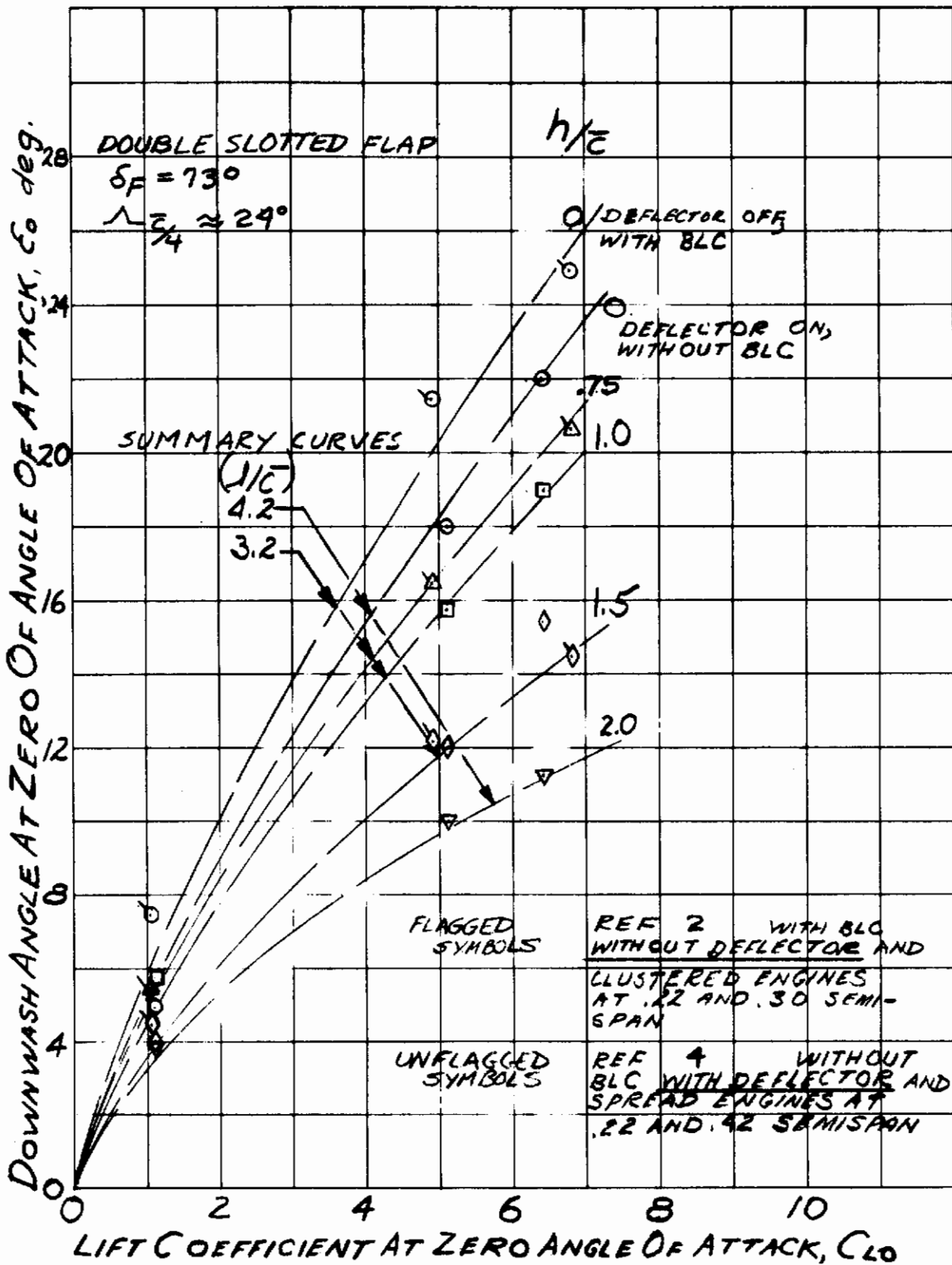


Figure 51. Effect of Tail Height and Engine Deflectors on Downwash Variation With Lift Due to Power at Zero Angle of Attack

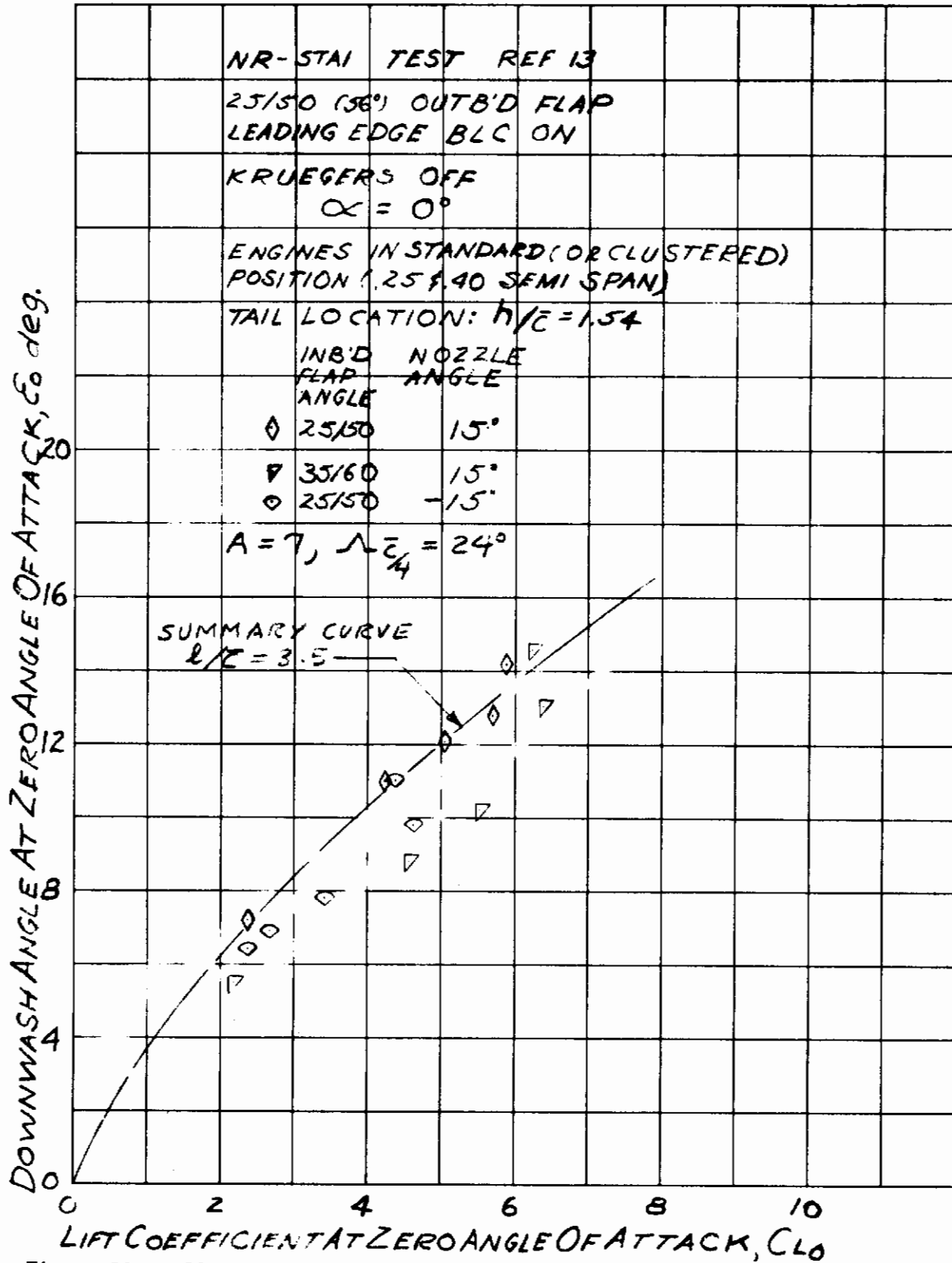


Figure 52. Effect of Flap and Nozzle Angles on Downwash Variation With Lift Change Due to Power

Contrails

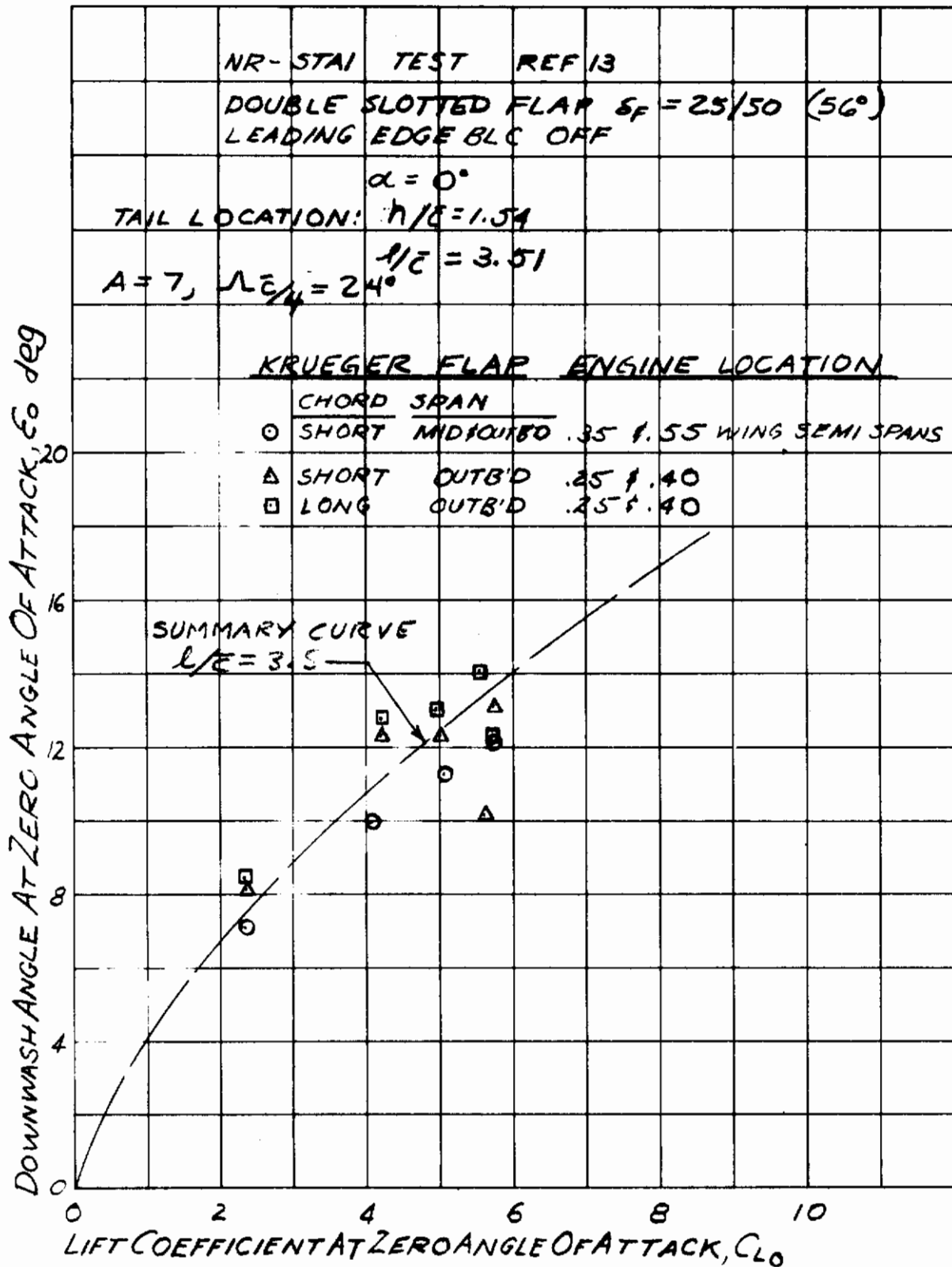


Figure 53. Effect of Spanwise Engine Location and Leading Edge Devices on Downwash Variation With Lift Change Due to Power

6.2 DOWNWASH FACTOR

Within the limitations of the parameters discussed above the downwash angle and the downwash factor $(1 - \partial \epsilon / \partial \alpha)$ can be estimated by the following procedure:

$$\epsilon = \epsilon_0 + \frac{\partial \epsilon}{\partial \alpha} \Delta \alpha \quad 6.1$$

where ϵ_0 is the downwash angle at zero incidence, given by Figure 50.

To find $\partial \epsilon / \partial \alpha$ it was assumed that from a given baseline downwash angle corresponding to a certain lift coefficient, blowing coefficient and tail location, the downwash angle changes with angle of attack as C_L and tail height change with angle of attack. Expressing the change in downwash angle as:

$$\Delta \epsilon = \frac{\partial \epsilon}{\partial C_L} \Delta C_L + \frac{\partial \epsilon}{\partial Z} \Delta Z \quad 6.2$$

and holding S_{ul} constant and varying only angle of attack,

$$\frac{\Delta \epsilon}{\Delta \alpha} = \frac{\partial \epsilon}{\partial C_L} \frac{\Delta C_L}{\Delta \alpha} + \frac{\partial \epsilon}{\partial Z} \frac{\Delta Z}{\Delta \alpha}$$

Then for small changes in α :

$$\frac{\partial \epsilon}{\partial \alpha} = \frac{\partial \epsilon}{\partial C_L} \frac{\partial C_L}{\partial \alpha} + \frac{\partial \epsilon}{\partial Z} \frac{\partial Z}{\partial \alpha} \quad 6.3$$

where $\partial C_L / \partial \alpha$ is the power-on lift curve slope as defined in Section 3.3, and $\partial Z / \partial \alpha$ is equal to the tail length l/c (where Z is in units of chord length).

The slopes, $\partial \epsilon / \partial C_L$ and $\partial \epsilon / \partial Z$, have been derived from the plot of Figure 49 and shown versus C_L in Figure 54. It should be noted that these values are in degrees, whereas $\partial C_L / \partial \alpha$ and $\partial Z / \partial \alpha$ are per radian. Accounting for these differences in units, the expression for $\partial \epsilon / \partial \alpha$ is:

$$\frac{\partial \epsilon}{\partial \alpha} = \frac{1}{57.3} \left[\frac{\partial \epsilon}{\partial C_L} C_{L\alpha} + \frac{\partial \epsilon}{\partial Z} l/c \right] \quad 6.4$$

A plot of the downwash factor calculated by this expression for a tail length of 3.5 and using typical values of $C_{L\alpha}$ is shown in Figure 55. Comparisons with experimental results from References (2), (4), (5), and (13) are shown in Figure 56. The average correlation is fairly good although some unaccounted configuration effects are apparent.

6.3 CONFIGURATION EFFECTS

The major configuration effect on downwash angle is the tail height as shown in the data of Figure 51. Tail length has a much lesser effect as seen in Figure 50. The data in Figure 52 indicate a small reduction in downwash angle when increasing the flap deflection from 50 degrees to 60 degrees. Also shown in this figure is the effect of rotating the engine exhaust nozzles from 15 degrees up to 15 degrees down; again, only a small reduction in downwash angle is observed. The effects of leading edge flap span and chord, and the effect of engine spacing is shown in Figure 53. The increased span leading edge flap with spread engines shows a small reduction in downwash angle. Unfortunately the individual effects of these two factors cannot be separated in the present data.

The most significant effects on the downwash factor ($1 - \partial \epsilon / \partial \alpha$), other than tail height appear to be due to leading edge treatment. Figures 56(e) through (h) show rather large, unpredictable, effects of leading edge blowing, producing different effects with different locations of the outboard engines. The effects of leading edge flap span and chord on the downwash factor is illustrated in Figure 56(a). At the lower lift coefficients, reduction of leading edge flap span and chord appear to improve the downwash factor. At higher lift coefficients no noticeable effect is observed.

The effects of flap deflection angle, shown in Figure 56(c) indicate no observable effect on the downwash factor in increasing flap deflection angle from 50 to 60 degrees.

The erratic behavior of the data at the higher lift coefficients observed in Figures 56(h) and 56(i), is evidently due to the spanwise location of the outboard engine. Both sets of data are from the same model with the engines in the "spread" configuration. Moving the outboard engine further inboard, or application of leading edge blowing, appears to improve the downwash factor to values compatible with the other configurations. Other data with spread engines from Reference (13), Figures 56(b), is quite comparable to that of Reference (5) with leading edge blowing, Figure 56(e).

The effects of varying tail length from $l/c = 2.2$ to 4.2 as shown in Figure 56(i), are negligible, which is in agreement with the methods of estimation.

Contrails

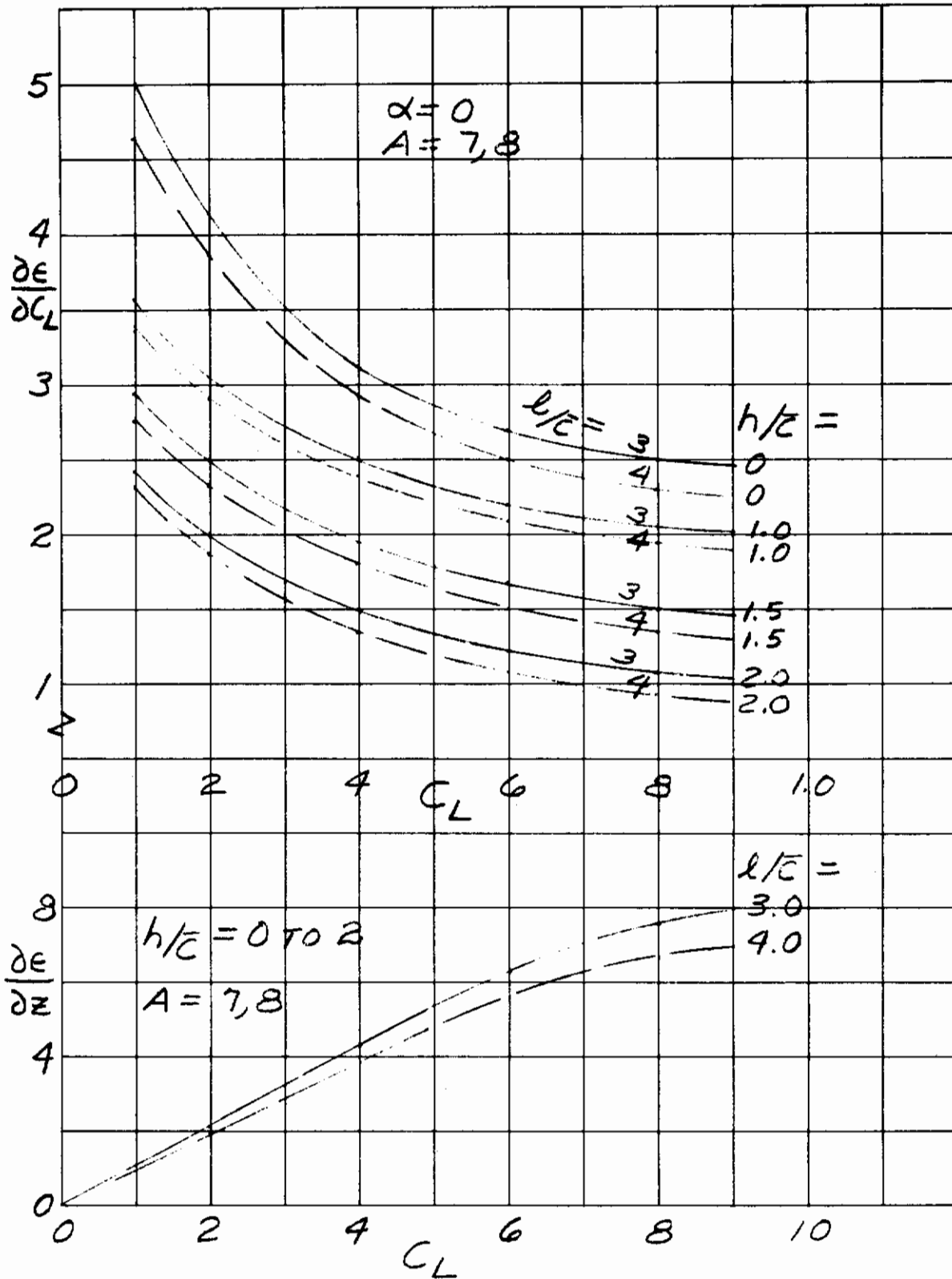


Figure 54. Gradient of Downwash Angle with Lift Coefficient and Tail Height

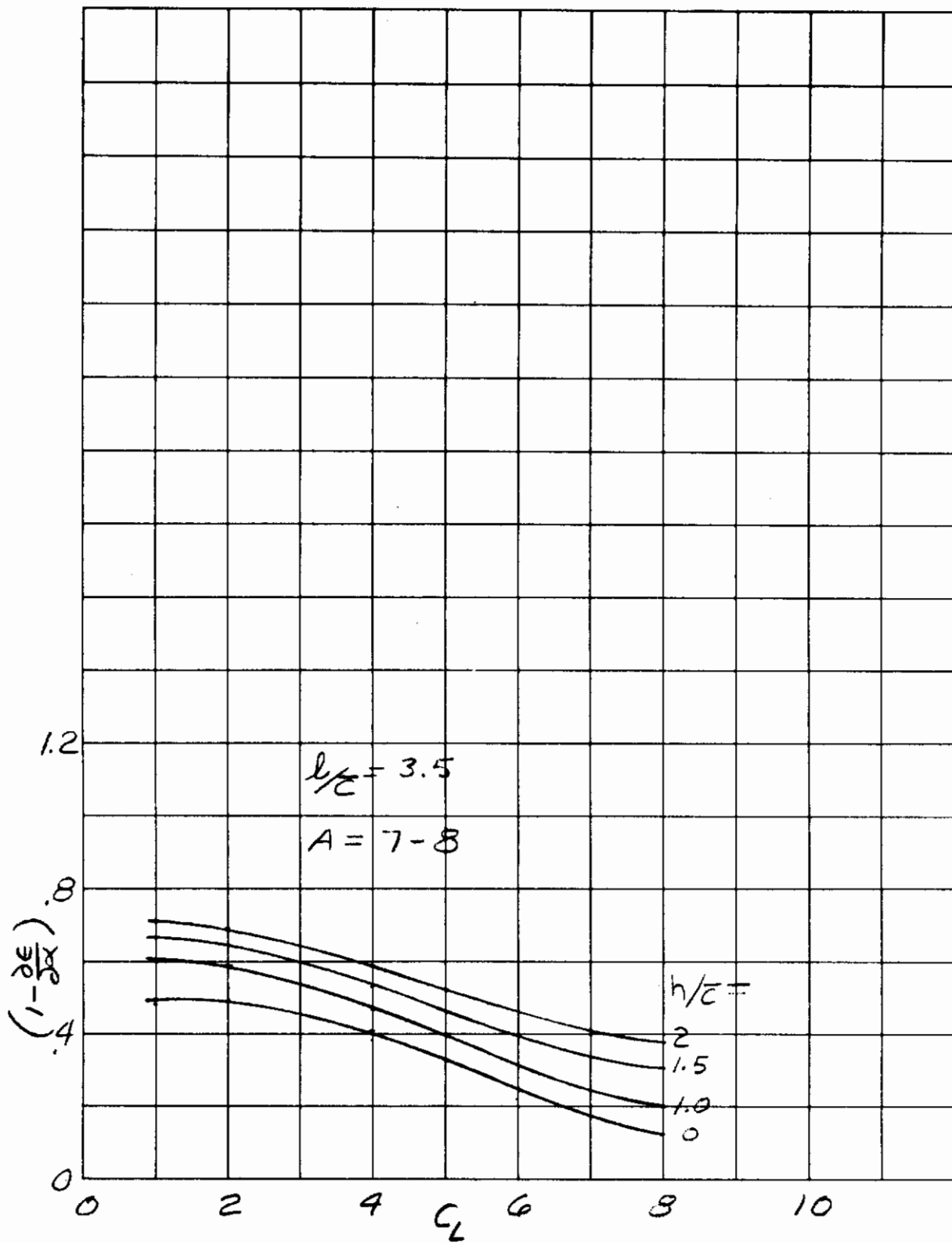


Figure 55. Sample Estimated Downwash Factor

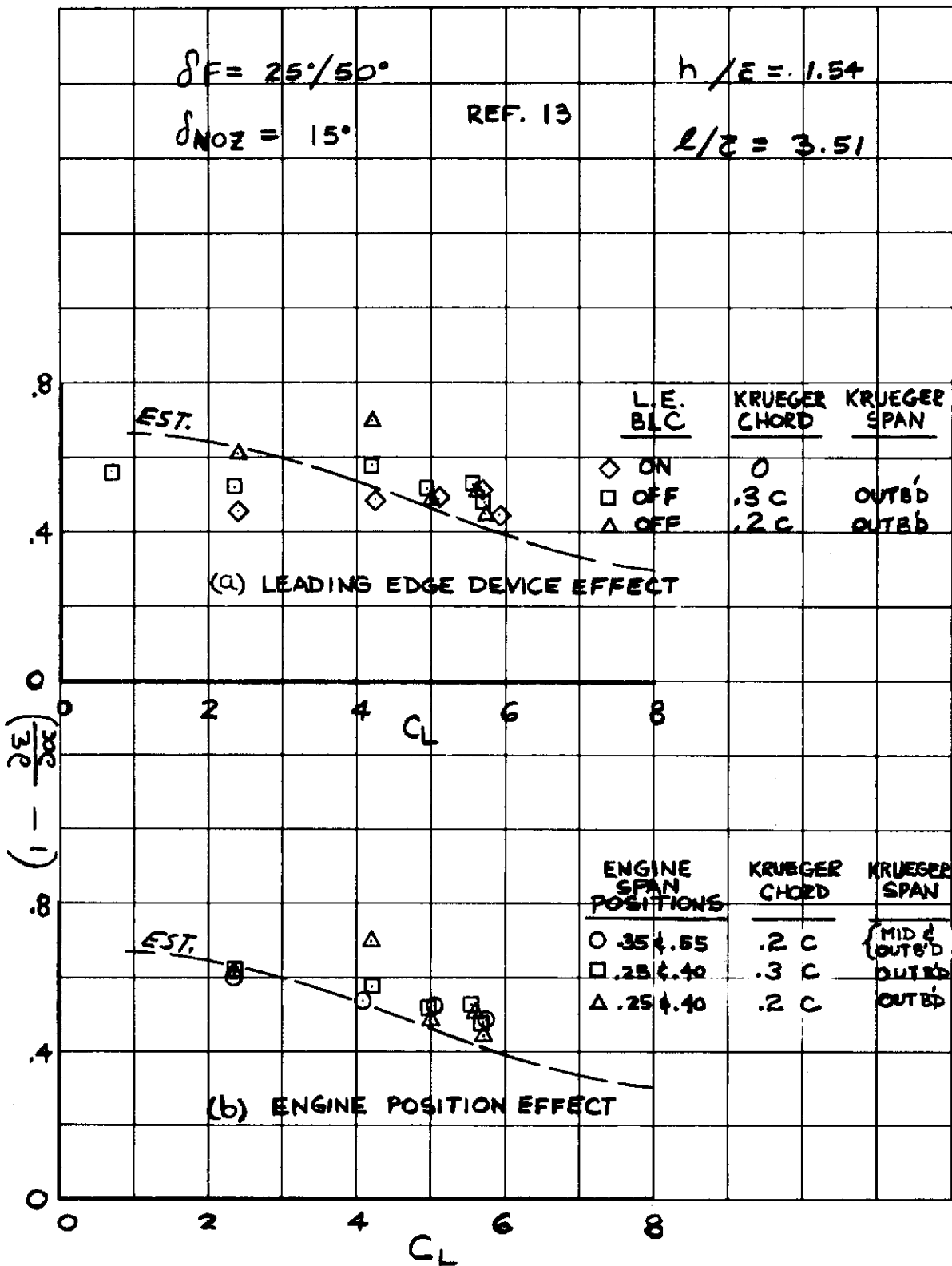


Figure 56. Experimental Downwash Factor Data

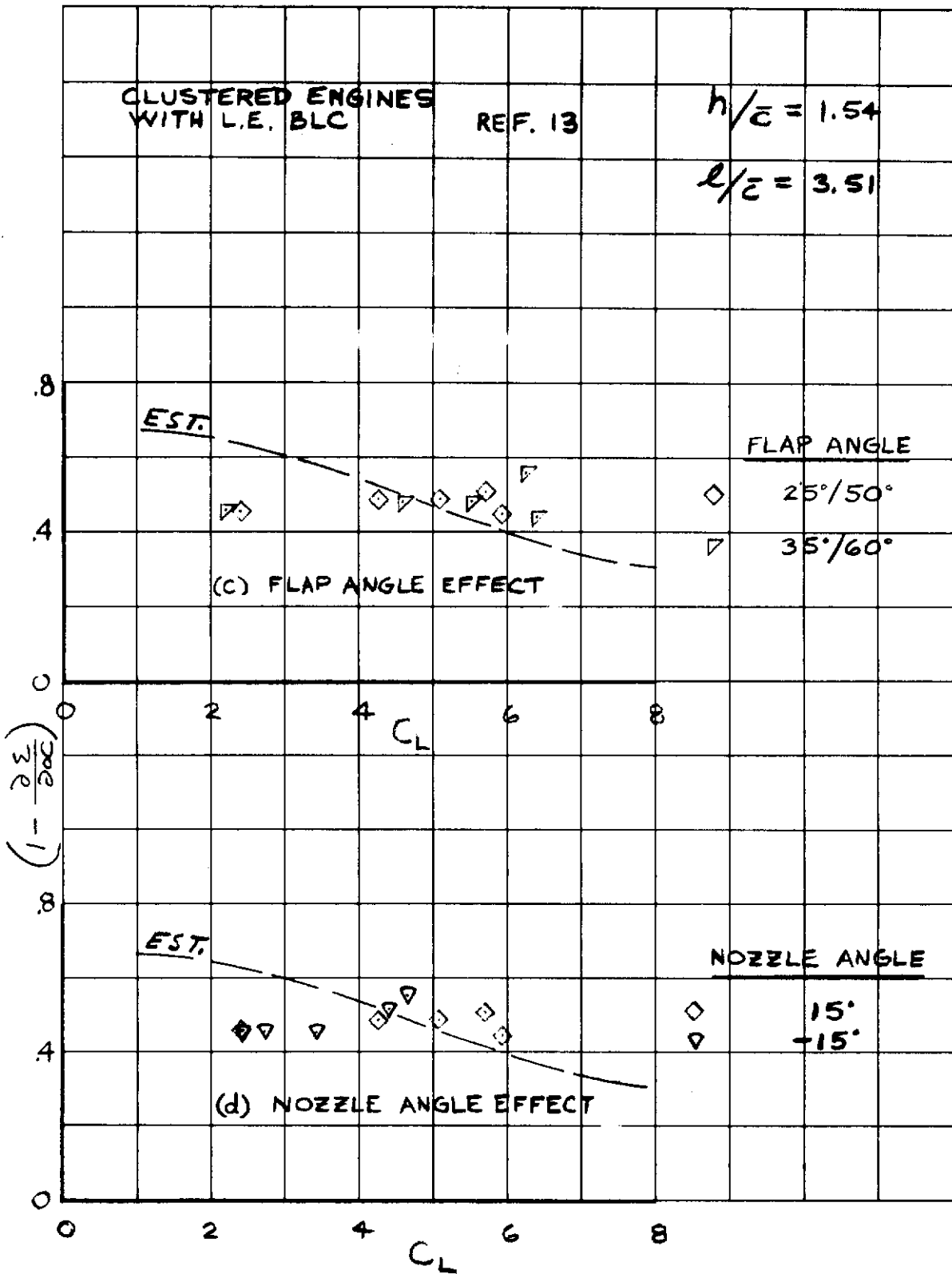
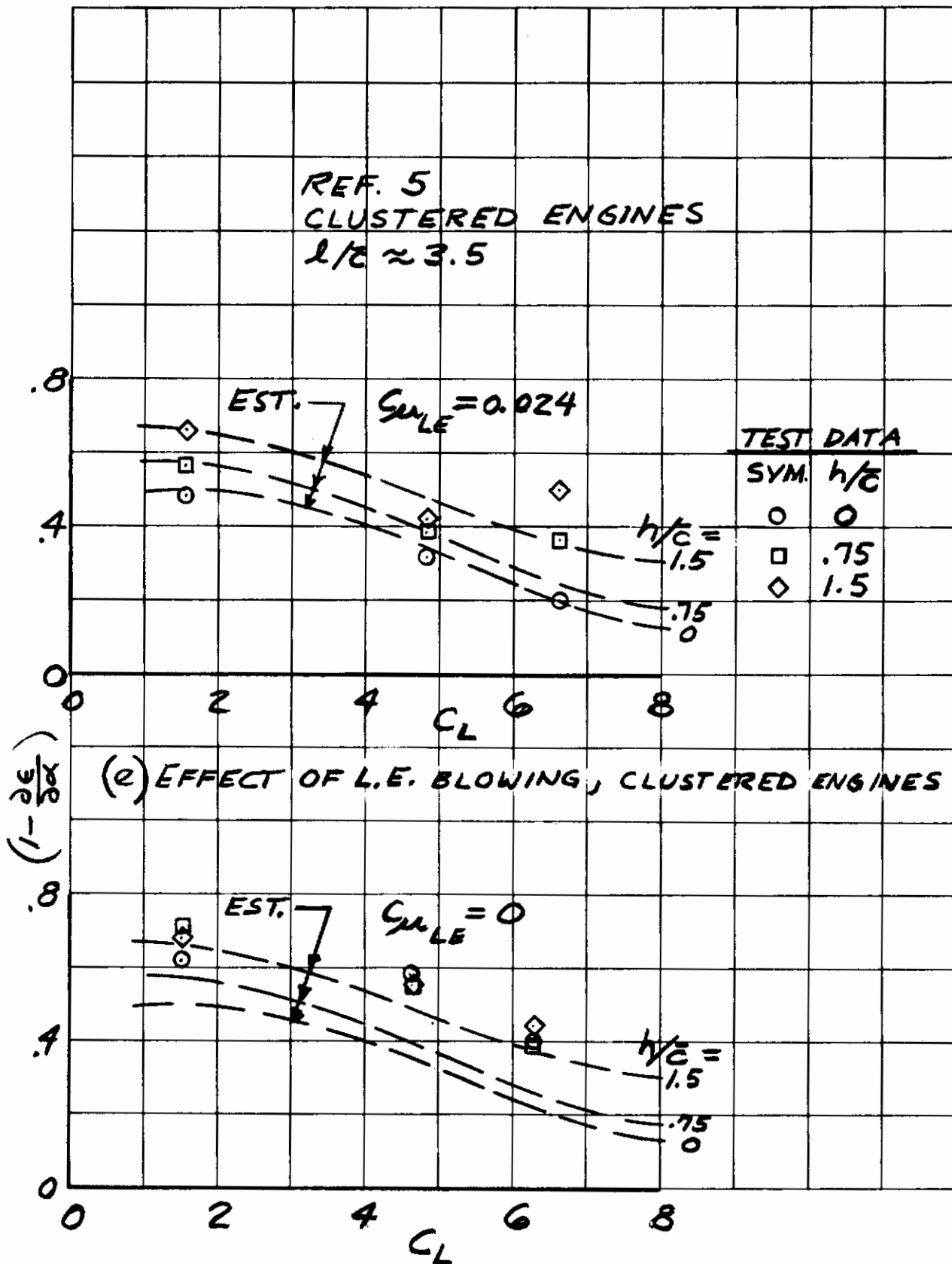
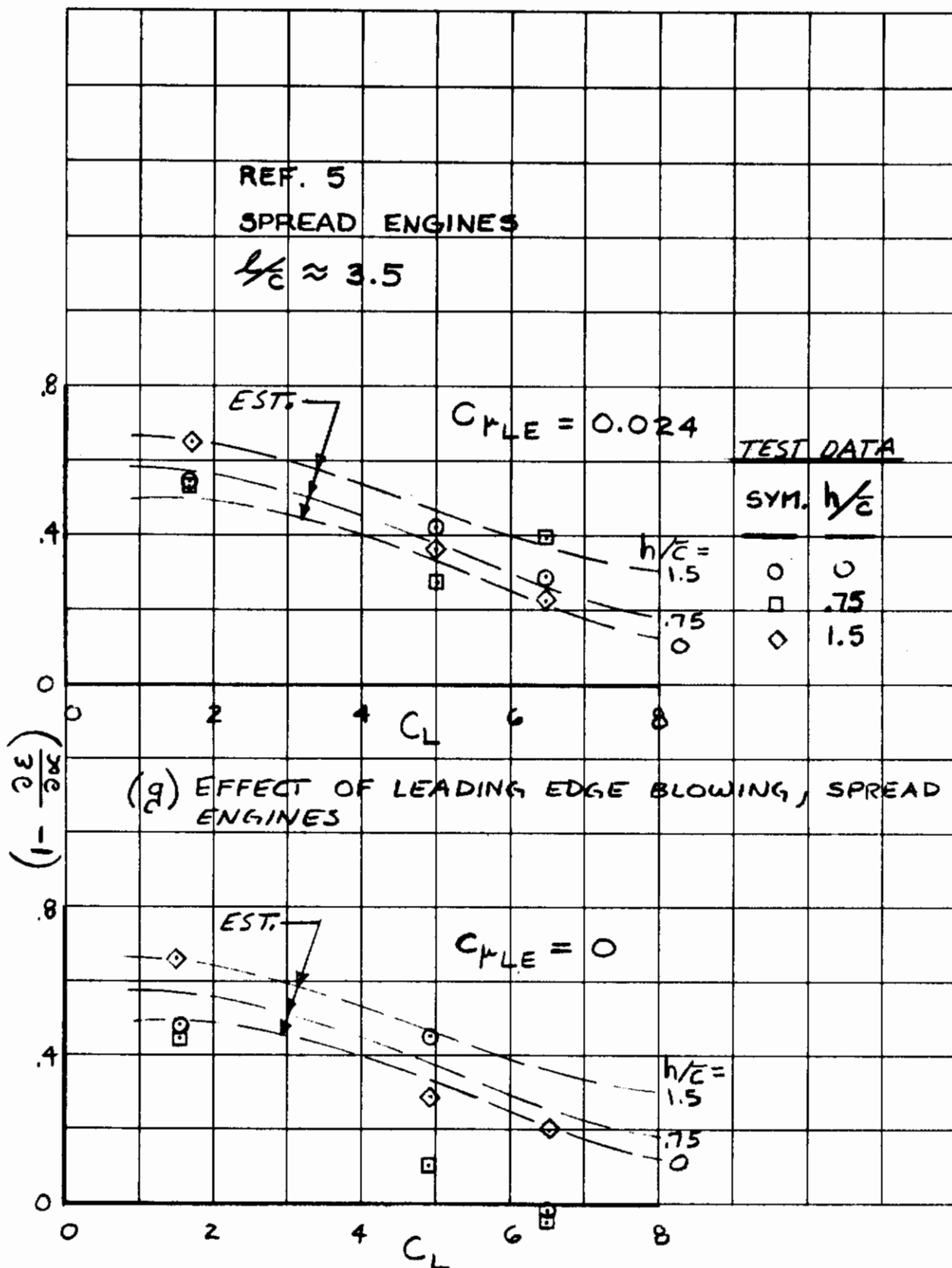


Figure 56. Experimental Downwash Factor Data (Continued)



(f) EFFECT OF L.E. BLOWING, CLUSTERED ENGINES

Figure 56. Experimental Downwash Factor Data (Continued)



(h) EFFECT OF LEADING EDGE BLOWING, SPREAD ENGINES

Figure 56. Experimental Downwash Factor Data (Continued)

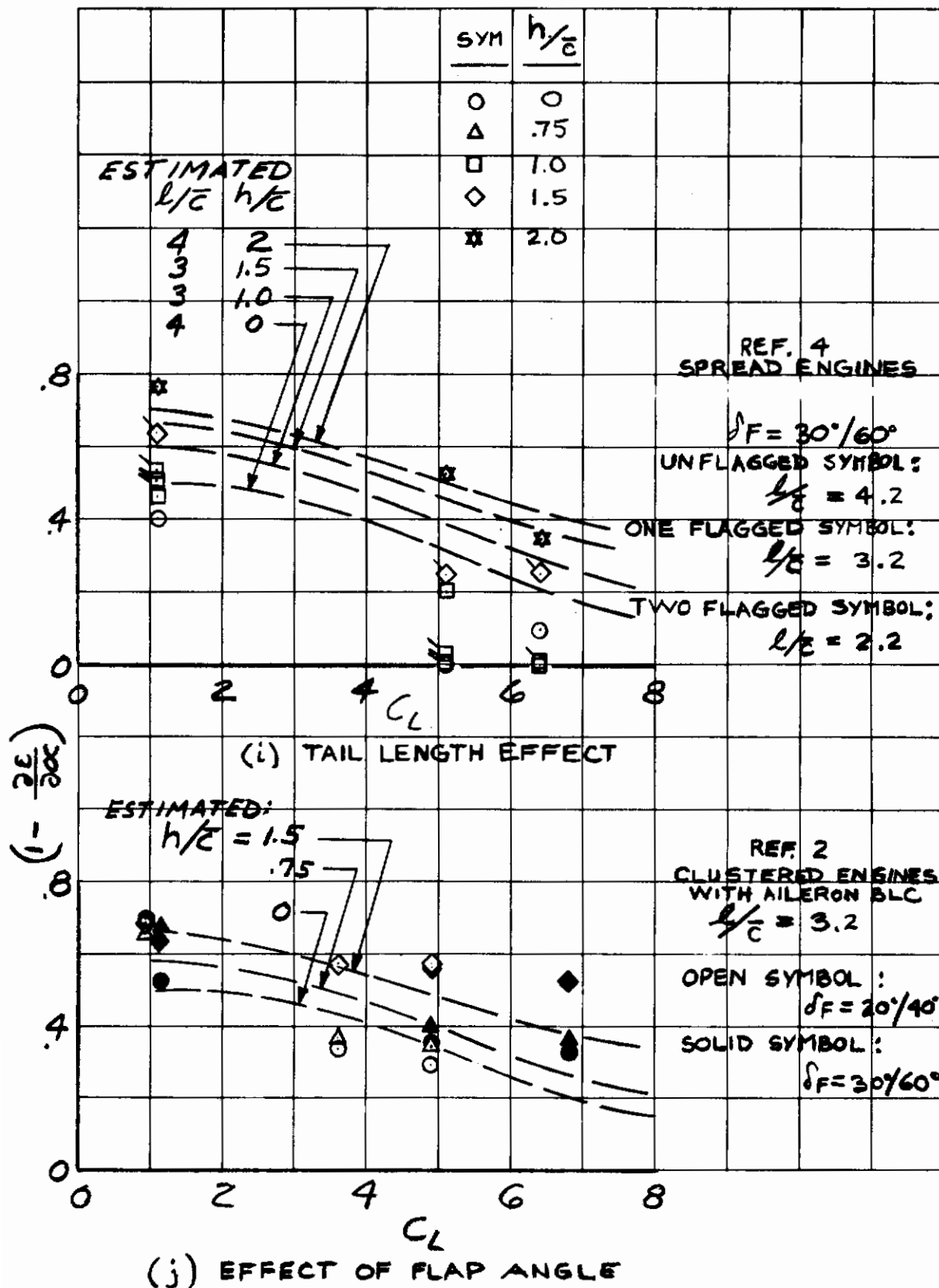


Figure 56. Experimental Downwash Factor Data (Concluded)

Contrails

The methods of estimation of the downwash angle and the downwash factor given here are believed to be adequate for typical EBF STOL configurations which utilize a leading edge device, large span flaps, and aspect ratio of 7 to 8. The most important configuration variable not accounted for here is the aspect ratio of the wing, or of the flapped portion of the wing. Additional data should be obtained of this variable and analyzed in the context of the approach used here for prediction methods.

6.4 TAIL DYNAMIC PRESSURE

The dynamic pressure ratio at the tail was obtained from Reference (2) and has been presented, verbatim, at the top of Figure 57. The dynamic pressure increase coefficient ($\Delta q/(T/S)$) may readily be determined from:

$$\frac{\Delta q}{(T/S)} = \left(\frac{q_{TAIL}}{q} - 1 \right) / C_{\mu} \quad 6.5$$

The dynamic pressure increase coefficient in this case was a linear function of the gross thrust or blowing coefficient, C_{μ} .

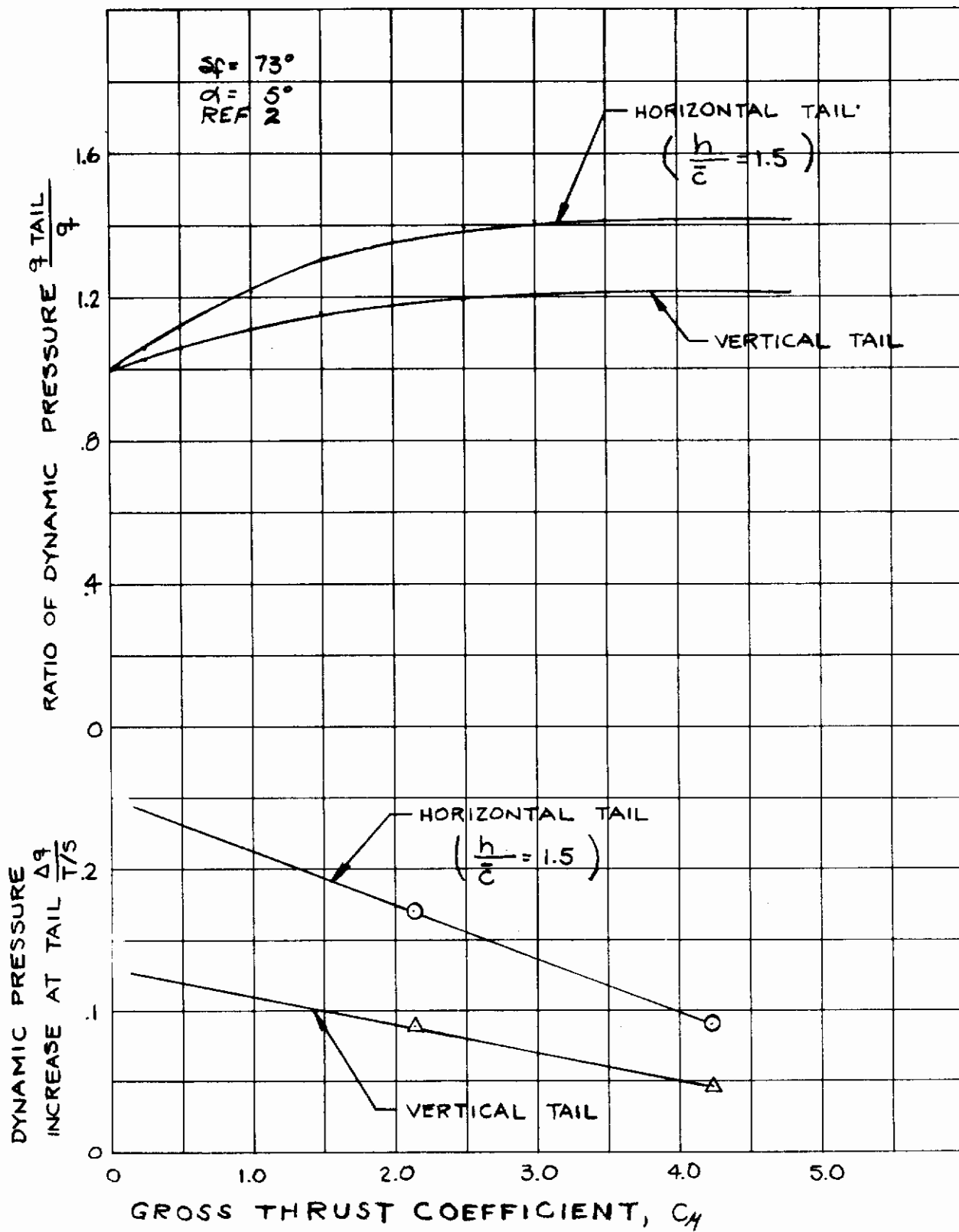


Figure 57. Tail Dynamic Pressure Characteristics

Section VII

ASYMMETRIC POWER EFFECTS ON LATERAL CHARACTERISTICS

7.1 ROLLING MOMENT DUE TO ENGINE FAILURE

The rolling moment due to engine failure is determined from the lift change due to the failure times a moment arm:

$$C_{l_{EF}} = \Delta C_{L_{EF}} \cdot \frac{1}{2} \left(\frac{y}{b/2} \right)_{EF} \quad 7.1$$

Herein, the subscript EF denotes "engine failure", while Y denotes the lateral distance of the center of pressure of the forces due to engine failure.

The lateral distance can be taken as being equal to the lateral location of the centerline of the exhaust nozzle of the failed engine. Correlations of several test results, Figure 58, show some variation of this, both inboard and outboard; however, since the variation is reasonable over a large range of configurations it is recommended that the engine centerline be used as the c.p. of the failed engine forces. In the method presented hereafter the lateral c.p. location is assumed to be independent of α_c .

The lift change due to engine failure can be computed below the stall angle of attack from

$$\left(\Delta C_L \right)_{EF} = \left(\Delta C_L \right)_{NOP} - \left(\Delta C_L \right)_{OEO} = \frac{1}{N} \left(\Delta C_L \right)_{PL} \quad 7.2$$

as defined in Section 3, where N is total number of engines and $(\Delta C_L)_{PL}$ is the lift increment due to powered lift with all engines operating.

The maximum change in lift at an angle of attack beyond stall can be substantially larger, as illustrated in Figure 59. The magnitude depends very much on the effect of power on the stall angle of attack, and probably also on the wing sweep angle. Data for 24-degree swept back wings and clustered engines are presented in Figure 60.

A comparison of test data with computations of the rolling moment due to engine failure, using the above described method, is given in Figures 61 and 62. It is seen that the method is useful for the prediction of the rolling moment versus angle of attack.

Contrails

FLAP ANGLE	α	
○ 20/40 (53°)	0°	} REF 4 OPEN SYMBOLS
△ 25/50 (63°)	↓	
□ 30/60 (73°)	0°	} " 2 HALF FILED SYMBOLS
▽ 25/50 (58°)	↓	
▽	4°	} REF 13 NR STAI TEST
△	8°	

NO FLAG = OUTBOARD ENGINE FAILED
 FLAG = INBOARD ENGINE FAILED

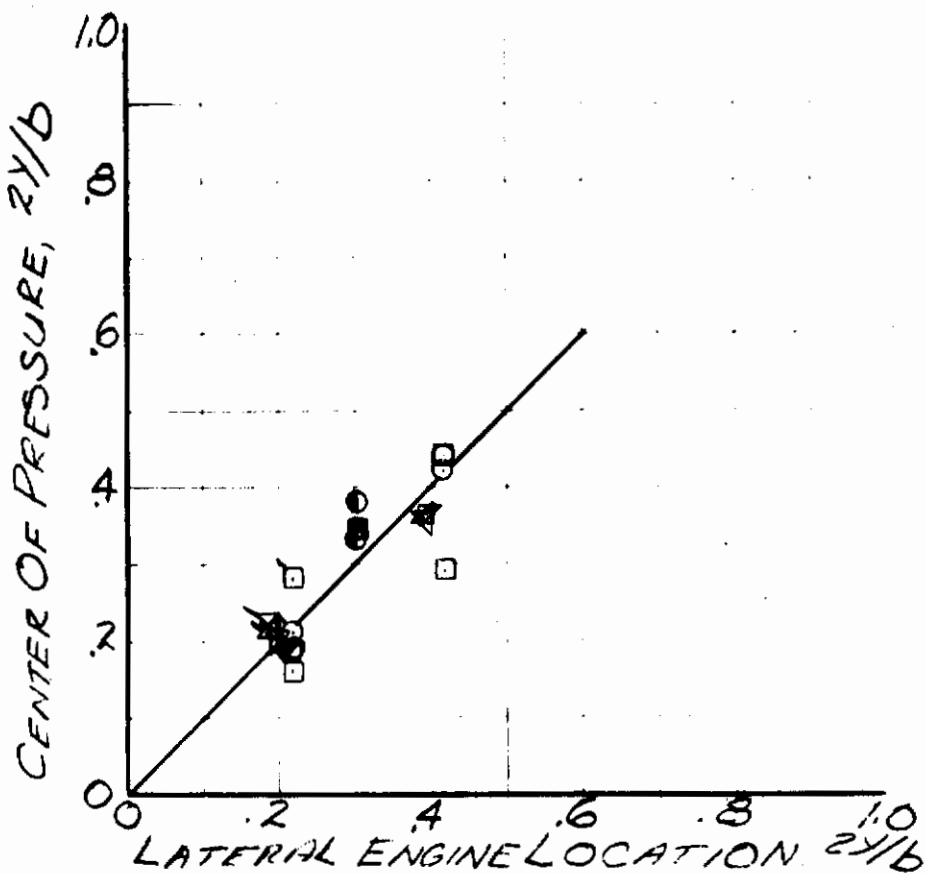


Figure 58. Lateral Center of Pressure For Span Loading Due to Power With One Engine Not Operating

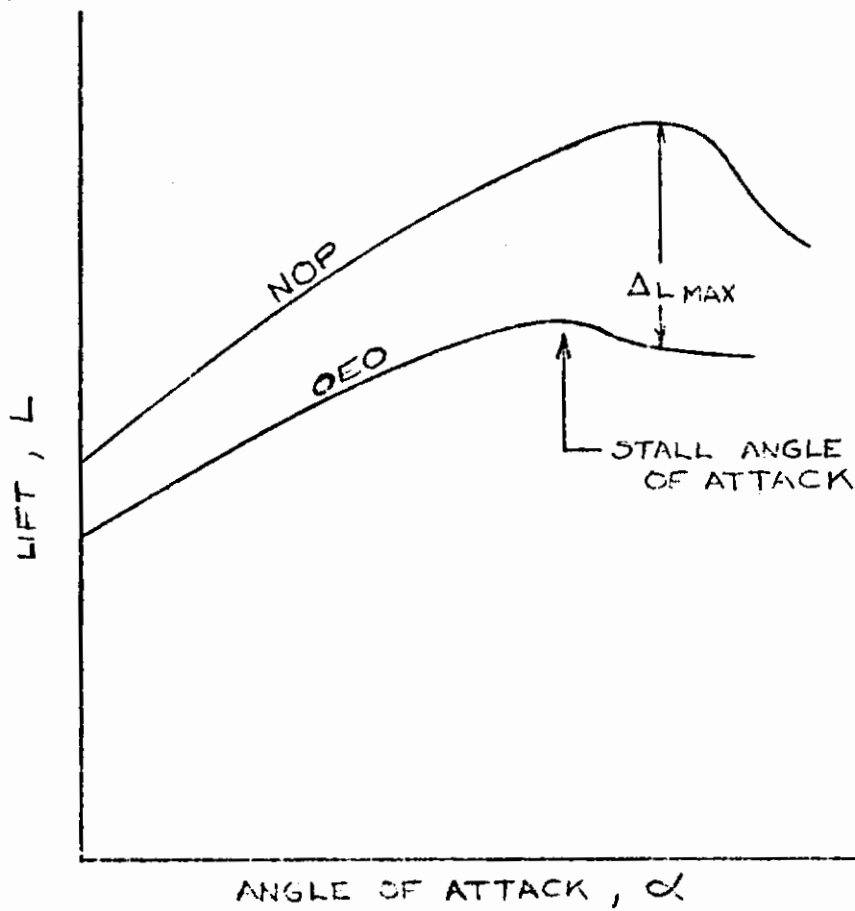


Figure 59. Maximum Lift Loss Due to One Engine Out

$$\Delta C/L = 24^\circ$$

- | | |
|---|-----------------|
| | REF |
| ○ | 13 NR STAI TEST |
| ◇ | 2 |
| △ | 2 |

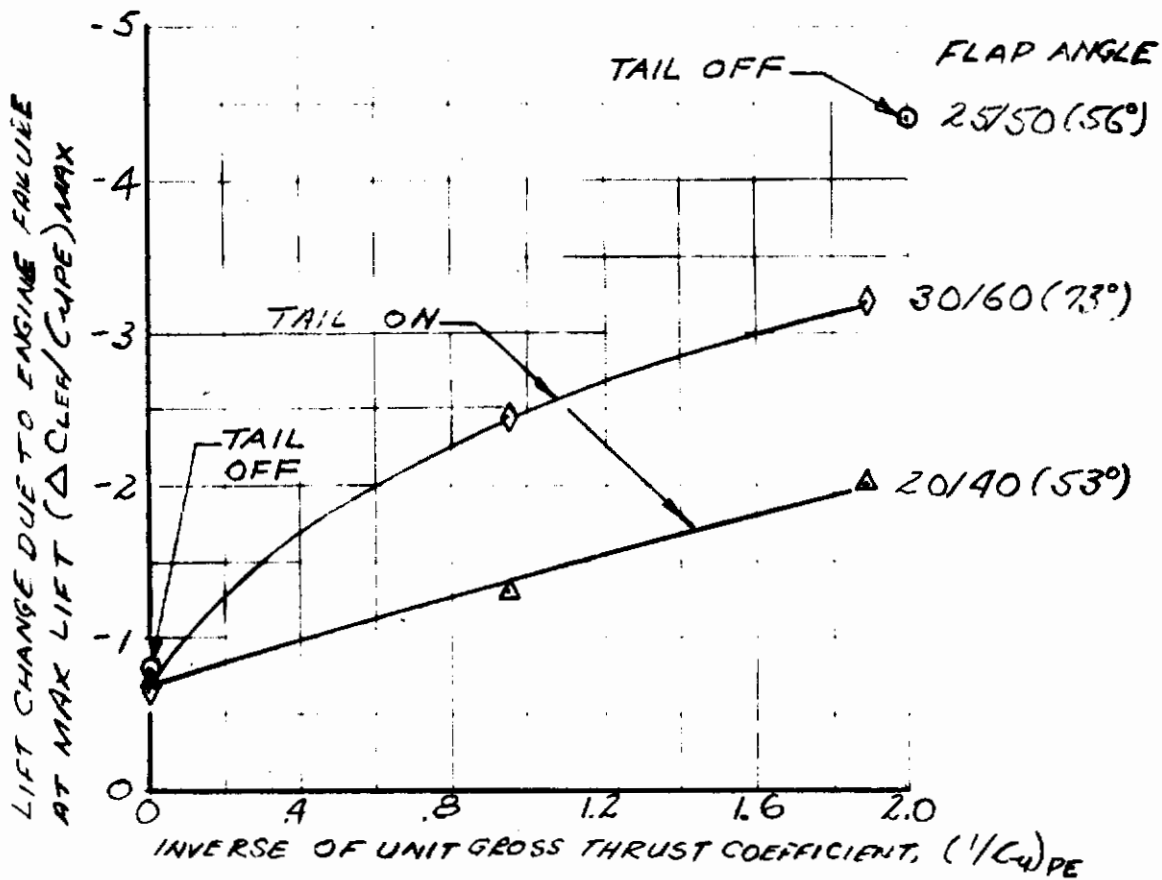


Figure 60. Engine Failure Effect on Maximum Lift

Contrails

REF 13

C_{M} PER ENGINE = 0.5

FLAP ANGLE	INOPERATIVE ENGINE	TAIL
◇ 25/50 (56°)	OUTBOARD	OFF
△	INBOARD	"
◊	OUTBOARD	ON

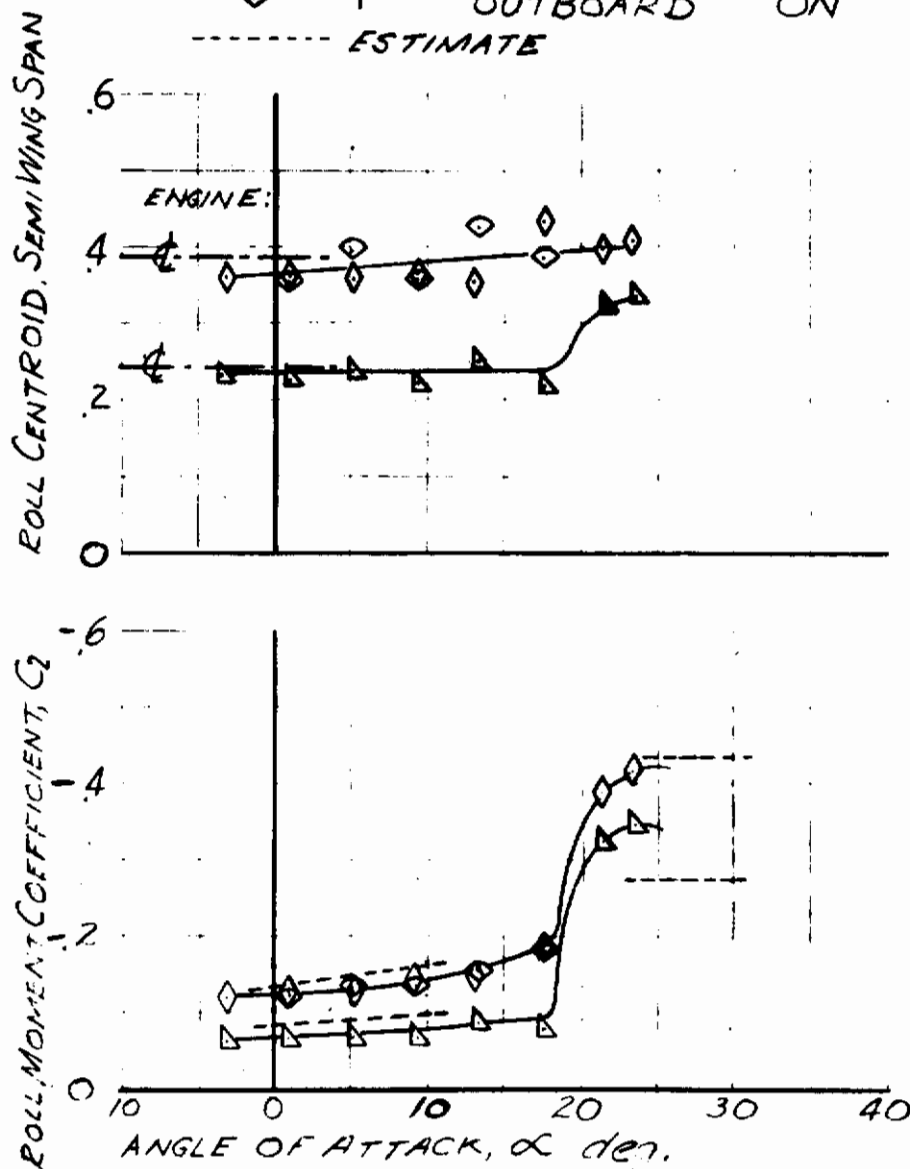


Figure 61. Roll Characteristics With Left Engine Inoperative

Contrails

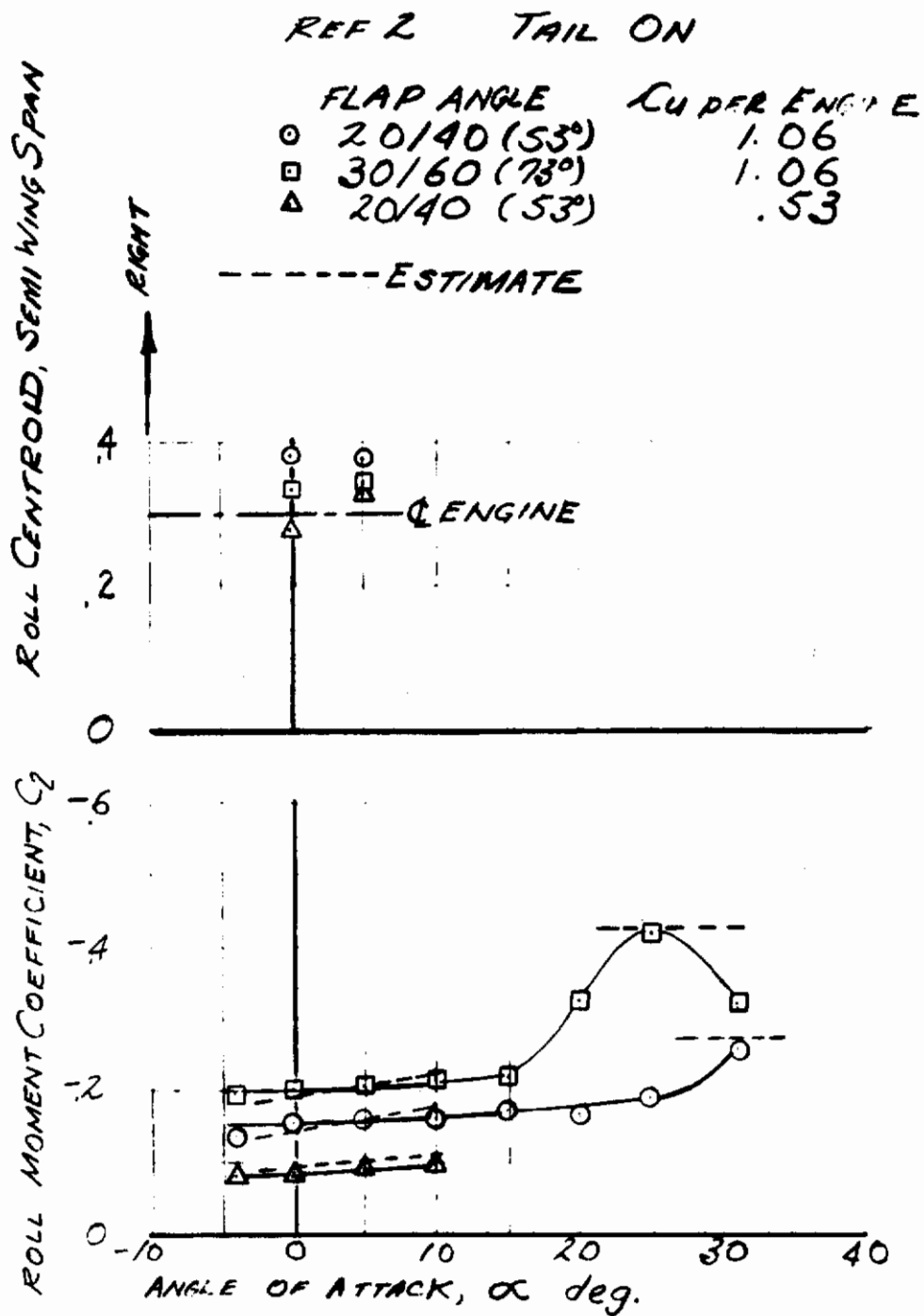


Figure 62. Roll Characteristics With Left Outboard Engine Inoperative

7.2 YAWING MOMENT DUE TO ENGINE FAILURE

An attempt was made to use a similar technique to predict the yawing moment with asymmetric power by replacing the normal force, used for the rolling moment predictions, with the axial force or drag increase due to engine failure. The results show that the centroid of the outboard failed engine is near the engine centerline, but the centroid of the inboard failed engine is far outboard (see Figure 63). It is also observed that the center of pressure, or yaw centroid, moved outboard when the tail was added to the configuration; apparently the failure of an engine is inducing a strong cross-flow which has a greater reaction on the fuselage in the case of an inboard engine failure, than for that of an outboard engine failure.

An investigation of the sidewash induced by the asymmetric vortex system resulting from a failed engine might yield a method for predicting the engine-out directional characteristics.

Contrails

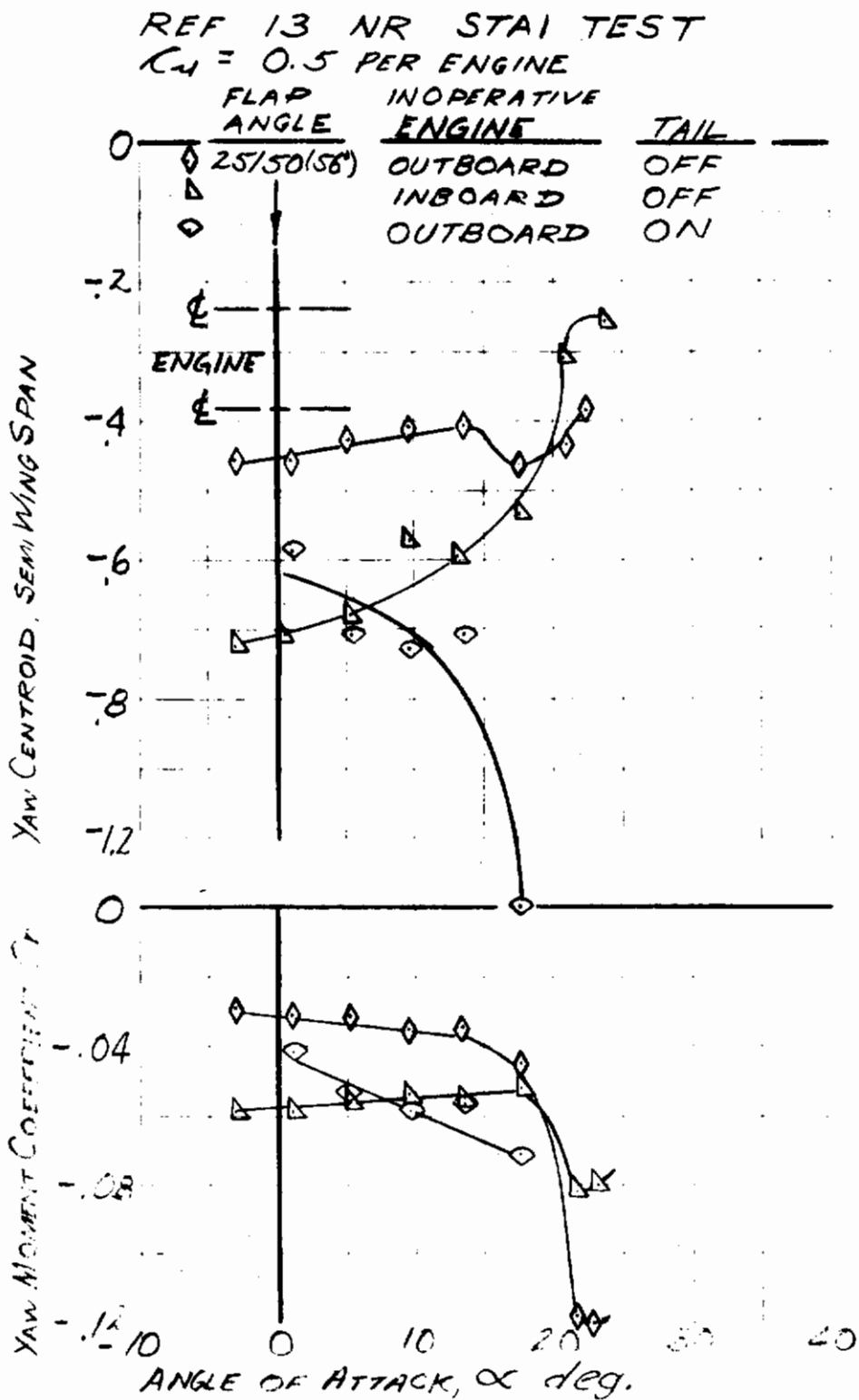


Figure 63. Yaw Characteristics With Left Engine Inoperative

Section VIII

POWER EFFECTS ON AERODYNAMIC DERIVATIVES

8.1 LONGITUDINAL DERIVATIVES

8.1.1. CHANGE IN FORWARD VELOCITY DERIVATIVES

C_{x_u} , C_{z_u} , C_{m_u} - These derivatives arise from three sources; Mach number effect, aeroelastic effects, and thrust or power effects. The first two of these sources are very small in the STOL flight region and may be neglected. The thrust or power effects, of concern in this section, however, can become quite important in some configurations and should be investigated in detail, as their effect is seen in both the period and damping of the phugoid oscillation.

In general, major contributions from power can be broken into three categories:

1. Direct effects
2. Inlet effects
3. Induced flow effects.

Both direct and inlet effects are readily handled once the engine characteristics are known through normal analysis. An example of a typical direct effect is, at low speeds when the net thrust varies greatly with velocity, noticeable C_{m_u} effects can occur if the thrust vector is highly offset from the center of gravity. The velocity-power effects from the inlet are usually negligible, as the resulting forces generated are basically a function of inflow angle, but power effects may arise here for other derivatives such as, $C_{m_{\dot{\omega}}}$, C_{m_q} , $C_{\dot{\omega}_p}$, and C_{m_r} . In all cases caution should be used in dynamic analysis bookkeeping to avoid a double entry of power effects when thrust coefficient terms are included.

Induced flow effects are more difficult to assess. A successful prediction method, if test data on similar vehicles are available, is to plot a nondimensionalized contributor against the inverse of the blowing coefficient as illustrated in Figure 64. Since all the factors in the power-speed relationship, $1/C_{\mu_{PE}} = qS/T_{PE}$, are known and q is a function of velocity, a graphical differentiation when corrected by the appropriate constants will yield the desired change in forward velocity derivation due to induced flow power effects for that component. The total derivative is naturally the summation of all such contributing components.

8.1.2 CHANGE IN ANGLE OF ATTACK DERIVATIVES

$C_{x\alpha}$, $C_{z\alpha}$, $C_{m\alpha}$ - Power effects on these derivatives can be determined directly using prediction methods shown in Sections 3, 4, and 5. Of the contributing factors, $C_{L\alpha}$, $C_{D\alpha}$, and $C_{m\alpha}$, the first two normally exhibit a substantial positive increase, while the last ($C_{m\alpha}$) only a small, almost negligible positive amount.

8.1.3 RATE OF PITCH DERIVATIVES

C_{xq} - This derivative results basically from the increase in horizontal tail drag due to pitching about the center of gravity. Since it in itself is small and for first approximations set to zero, power effects are also assumed small and should be neglected.

C_{zq} , C_{mq} - The horizontal tail is again the main contributor to both of these derivatives. In STOL (low speed) flight it is basically the effect of the curved flight path which increases the horizontal's angle of attack producing a negative C_{zq} and C_{mq} (pitch damping). Correlation of prediction methods and test data is difficult since results are always combined with linear acceleration (&c) derivatives. It is reasonable to assume, however, that the theoretical horizontal tail contributions of;

$$\left[C_{zq} \right]_H \approx - \left[\frac{\partial C_L}{\partial \left(\frac{q_H}{2V_0} \right)} \right]_H = - \left[C_{Lq} \right]_H = -2 C_{L\alpha} \frac{q_H}{q} \frac{S_H}{S} \frac{l_H}{c} \quad 8.1$$

$$\left[C_{mq} \right]_H \approx - \left[C_{Lq} \right]_H \frac{l_H}{c} \quad 8.2$$

still hold and estimations can thus be made knowing the variation of $C_{L\alpha}$ or/and q_H/q with power.

8.1.4 LINEAR ACCELERATION DERIVATIVES

$C_{x\dot{\alpha}}$ - As in the rate of pitch case, resulting drag increases are usually neglected in this derivative since they are small in comparison with that of the total aircraft and power effects would thus be even a smaller contribution.

Contrails

$C_{z\dot{\alpha}}$, $C_{m\dot{\alpha}}$ - Predictions similar to those in the rate of pitch derivatives can be made for the theoretical horizontal tail contribution. The potential for error in estimating these derivatives is increased due to the additional $\partial E/\partial \alpha$ variation with power factor

$$\left[C_{z\dot{\alpha}} \right]_H \approx - \left[C_{L\dot{\alpha}} \right]_H \frac{\partial E}{\partial \alpha} \quad 8.3$$

$$\left[C_{m\dot{\alpha}} \right]_H \approx - \left[C_{L\dot{\alpha}} \right]_H \frac{l_H}{\bar{c}} \frac{\partial E}{\partial \alpha} \quad 8.4$$

8.1.5 LONGITUDINAL CONTROL DERIVATIVES

$C_{x\delta_e}$ - This frequently neglected derivative is of little significance in longitudinal calculations. The power effects on it are of even less significance and should therefore also be neglected.

$C_{z\delta_e}$, $C_{m\delta_e}$ - Power effects on these derivatives are readily determined knowing the variation of horizontal tail effectiveness with power through:

$$C_{z\delta_e} = - C_{L\alpha_H} \frac{q_H}{q} \frac{S_H}{S} \frac{\partial \alpha_H}{\partial \delta_e} \quad 8.5$$

$$C_{m\delta_e} = \frac{l_e}{\bar{c}} C_{z\delta_e} \quad 8.6$$

8.2 POWER EFFECT ON LATERAL-DIRECTIONAL DERIVATIVES

8.2.1 CHANGE IN SIDESLIP DERIVATIVES

$C_{Y\beta}$ - The major portion of the total derivative comes from both the vertical tail and fuselage, in an approximately even magnitude, for the vehicles investigated. As normally the case, an almost negligible contribution comes from the wing; flaps up or down. Power effects on this derivative are small. The increase (a larger negative value) is attributed to the increased flow generated by the engines and can be approximated by the velocity ratio at the vertical tail.

$$C_{Y\beta} \approx (C_{Y\beta})_{\text{POWER OFF}} \frac{q_t}{q_\infty} \quad 8.7$$

Large variations and even sign changes in this derivative can occur at low sideslip angles due to the vortex formed at the fuselage-wing-leading edge flap junction sweeping across the vertical tail. Caution should be exercised in interpreting test data with minimal points near the axis ($\beta \pm 4^\circ$) or other angles formed by extending similar discontinuities through the vertical tail.

$C_{l\beta}$ - With the main contribution of this derivative coming from the wing, variations due to power appear to be dependent on engine placement. Configurations with clustered engines or those causing a definite bulge in the wing lift distribution (with a trough across the fuselage) tend to produce negligible power effects, occasionally even decreasing the dihedral effect (positive $\Delta C_{l\beta}$ pwr). However, vehicles with spread engines that tend to increase the lift distribution elliptically with power application exhibit the expected increase in dihedral effect. Standard handbook methods, such as DATCOM, which relate $(C_{l\beta})_{WING}$ to lift coefficient, taking into account the proper sweep and aspect ratio factors, seem adequate for preliminary predictions.

$C_{n\beta}$ - Contrary to non-STOL, unblown flap configurations where this derivative is primarily the balance between the large fuselage and vertical tail contributions, the wing is the predominant factor with power application. The power effects on the vertical tail contribution may be neglected for first order approximations or increased by the q_t/q_∞ ratio if desired. Theoretical prediction methods for the power effects on the wing contribution to $C_{n\beta}$ need further investigation. Fair correlation has been obtained by modifying the expression from DATCOM for power-off $(C_{n\beta})_{WING}$ by the factor $(1+C_\mu)^{1/2}$. The power-off term from DATCOM is:

$$\frac{(\Delta C_{n\beta})_{WING}}{C_L^2} = \frac{1}{57.3} \left[\frac{1}{4\pi A} - \frac{\tan \Lambda}{\pi A(A - 4 \cos \Lambda)} \left(\cos \Lambda - \frac{A}{2} - \frac{A^2}{8 \cos \Lambda} + 6 \frac{\bar{x}}{c} \frac{\sin \Lambda}{A} \right) \right] \quad 8.8$$

where \bar{x} is the distance from the moment reference (usually c.g.) to wing a.c., positive aft.

Another area which requires further investigation is the variation of yawing moment with asymmetric power. While only minor effects on $C_{n\beta}$ have been noted, a large sidewash appears to exist with inboard engine failure due to change in the pressure field aft of the wing. This causes the inboard engine out case to be critical in yaw and may pose several design problems.

8.2.2 RATE OF ROLL DERIVATIVES

C_{Yp} - This derivative is of very little significance in lateral-directional dynamics and is frequently neglected in calculations. The small, garbled (sometimes negative, sometimes positive) power effect seen in available test data tends to corroborate data shown in Figure 7.1.2.1-3a of DATCOM. Assuming the major power effects are contributed by the wing, this figure indicates that for aspect ratios, sweeps, and taper ratios typical of STOL configurations the C_{Yp}/C_L ratio is very close to zero and could very well be either positive or negative depending on the specific configuration.

$C_{\dot{p}}$ - This derivative, quite important in lateral dynamics in roll damping, stems basically from the wing and is thus highly effected by power especially at high angles of attack as indicated by test data. While the theoretical analysis given by Thomas and Ross, in Reference (19), shows the damping-in-roll to increase linearly with C_j and be independent of angle of attack, a good analogy exists with the blown flap. It is suggested that the methods of this report be used for preliminary designs if similar configuration test data are unavailable.

C_{np} - The major power effect contribution to this derivative arises from the wing. It is negative and directly proportional to the lift coefficient. The secondary contribution from the vertical tail may be positive or negative depending on geometry and angle of attack. However, since its isolated contribution is greatly altered by the complex sidewash produced by the rolling wing and it is only the small change in this sidewash which is affected by power, prediction of this secondary contribution does not seem warranted.

Power effects on this derivative are fairly important due to the influence on dutch roll damping. High power settings have been seen to double the negative value of this derivative which is not desired since it represents a reduction in dutch roll damping. With present day stability augmentation systems normally providing a C_{np} feedback, it becomes more important to predict the power effects for the determination of gains and closed loop analysis.

C_{np} approximations can be obtained by first determining the power off derivative and then applying a $(C_L - \eta C_{\mu} \sin \theta)/C_{L P.O.}$ correction. The theoretical reversal shown in Reference (19) has not appeared in test data investigated.

8.2.3 RATE OF YAW DERIVATIVES

C_{Y_r} - Power effects on this relatively unimportant derivative are small and probably arise from augmentation of the sidewash produced through rotation at the vertical tail. As it is common practice to neglect this derivative in calculations, it is assumed that these minor power effects are of even less importance and may thus also be neglected.

C_{l_r} - Only very minor power effects have been noted in all test data surveyed, so it is concluded that power effects are negligible.

C_{n_r} - In general terms, power effects improve this derivative (provide larger negative values), which is the main contributor to dutch roll damping and hence an important factor. However, various attempted prediction methods have yielded only mediocre results. Since the vertical tail is by far the largest contributor to the total derivative, wing-fuselage-leading edge flap vortex interference effects are probably playing an important role. It is suggested that if similar configuration test data are unavailable, the unpowered C_{n_r} predictions be increased by the dynamic pressure ratio, q_c/q_∞ . The experimental data available show values of C_{n_r} at high power settings of 130 percent of the power-off value.

8.2.4 LATERAL ACCELERATION DERIVATIVES

C_{Y_β} , C_{l_β} , C_{n_β} - These derivatives are extremely difficult to estimate or extract from test data regardless of power effects. If for some particular reason these derivatives cannot be neglected and a method is available for power-off estimation, then the power effects can be assumed proportional to the dynamic pressure ratio, q_c/q_∞ , since these derivatives are a direct function of the sidewash time lag.

8.2.5 LATERAL-DIRECTIONAL CONTROL DERIVATIVES

It is necessary to evaluate each particular control system in its own realm. Since one engine-flap-aileron relationship will have a different lift distribution variation with power than another combination etc., a detailed discussion is not relevant. In general, power effects on conventional surfaces, those not directly impinged upon by engine thrust, are small when compared to large forces produced by these surfaces through double hinges and other means. Neglecting the power effects thus seems reasonable and conservative in preliminary design work.

Contrails

ASSUME: POINT 2 = q_0 S/T FOR U_0
 POINT 1 = $(q_0 - \Delta q)$ S/T
 POINT 3 = $(q_0 + \Delta q)$ S/T

THEN:

$$\left(\frac{\partial C_L}{\partial u}\right)_{\text{POWER}} = \left[\frac{(L/T)_3 - (L/T)_1}{(qS/T)_3 - (qS/T)_1} \right] \frac{1}{\frac{1}{2} U_0} = \frac{\Delta(L/T)}{\Delta(qS/T)} \frac{1}{14.5 \sqrt{q_0}}, \frac{1}{\text{fps}}$$

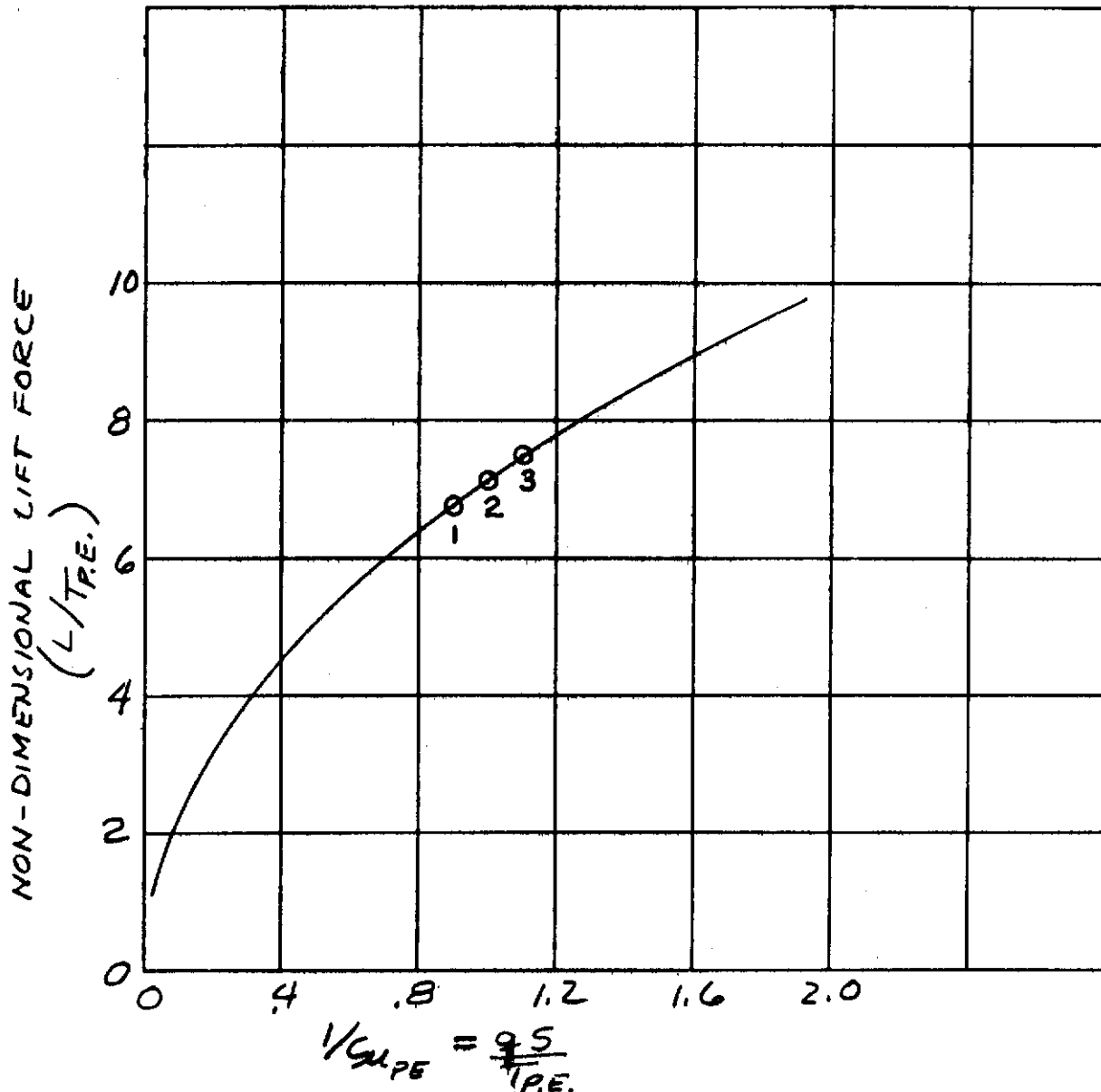


Figure 64. Sample Determination of Power Effects on Forward Velocity Derivatives

Contrails

Section IX

SAMPLE CALCULATIONS

A machine program, in Fortran IV, is given in the appendix for the calculation of lift, drag, and pitching moment, using the methods described in previous sections. The required input items and the output items are tabulated below.

INPUT	OUTPUT VS C_{μ} AND α
α	CL
C_{μ}	CLMAX
n	CD
θ	C_m
(CL)B	(Δ CL) θ
(C_m)B vs α	Δ CL/ Δ α
t/c	CDi
S'/S	(Δ CL) α
CDf	(Δ CL) r
A	(Δ Cm)RREF
δ_T	(Δ Cm) r REF
(Δ CD)R	(Δ Cm) α REF
(CLMAX)B	(Δ Cm)RD
(α_{MAX})B	ηC_{μ}
CR	α_{MAX}
$\frac{c}{x_{REF}-x_{LEc}}$	
CF	
$\frac{c}{x_{REF}-x_{LEc}}$	
CF	
$\frac{c}{x_{REF}-x_{LEc}}$	
Δl_R	

The results of three test cases are presented in Figure 65 comparing estimated versus test data. One case is from the current NR-STAI test, Reference (13), of a model with $A = 7$, $\Lambda = 24^\circ$, with full span flaps. The other case, selected to illustrate a wide variation in configurations, is from Reference (14) of a model with $A = 7$, $\Lambda = 0^\circ$, and 75 percent flap span. The third illustrates triple slotted flaps.

A sample calculation using manual methods is given below, using the same test case from Reference (13) as used in the sample machine calculation case.

A listing of test cases used in development and substantiation of these methods, identifying the source of the data, is shown in the table following this section.

SAMPLE CALCULATION

Geometric data:

$$A = 7$$

$$\Lambda_{.25\bar{c}} = 24^\circ$$

Type of flap = double slotted

Flap span = 100% wing span

$$S'/S = \lambda = .85$$

$$t/c = .125$$

$$\delta_T = 18^\circ$$

$$\delta_F = 56^\circ$$

$$Z_{F/R} > 1.0$$

$$\bar{c} = 15.5$$

$$x_{REF} - x_{LEc'} = 6.6$$

$$x_{REF} = .25\bar{c}$$

$$C_R = 14.6$$

$$x_{REF} - x_{LEc'_F} = 3.9$$

$$\bar{c}_F = 19.6$$

$$\Delta R = 4.7$$

Power-off wind tunnel data - or estimated power-off data:

$$(\alpha_{MAX})_B = 15^\circ$$

$$(C_L)_B = 2.25$$

$$(C_{LMAX})_B = 3.35$$

$$C_{Df} = .145$$

$(\Delta C_D)_R$ = neglected for wind tunnel data comparisons

$$(C_m)_B = -.95 \text{ at } \alpha = -5^\circ$$

$$- .95 \text{ at } \alpha = 0^\circ$$

$$- .86 \text{ at } \alpha = 10^\circ$$

Calculations:

$$\theta/\delta_F = 1.0 \text{ from Figure 6}$$

$$\theta = (\delta_F)(\theta/\delta_F) = 56^\circ$$

$$\eta = .76 \text{ from Figure 11}$$

$$\eta C_\mu$$

$$\eta C'_\mu = \eta C_\mu (S/S')$$

F, from Figure 13 at $\eta C'_\mu$

V, from Figure 18 at $\eta C'_\mu$

$(\partial C_L/\partial \theta)_\infty$, Figure 16 at $\eta C'_\mu$

$(\partial C_L/\partial \alpha)_\infty$, Figure 16 at $\eta C'_\mu$

	C_μ		
	1	2	3
ηC_μ	.76	1.52	2.28
$\eta C'_\mu$.895	1.79	2.68
F	.738	.717	.711
V	.962	.944	.937
$(\partial C_L/\partial \theta)_\infty$	3.80	5.75	7.32
$(\partial C_L/\partial \alpha)_\infty$	8.11	10.05	11.55

Contrails

Calculations - Continued

	1	C_{μ} 2	3
$(\Delta C_L)_{\theta} = F(1+t/c) \lambda (\partial C_L / \partial \theta)_{\infty} \sin \theta$	2.22	3.28	4.12
$C_{L\alpha} = F(1+t/c) V (\partial C_L / \partial \alpha)_{\infty}$	6.72	7.65	8.65
$(\Delta C_L)_{\Gamma} = (\Delta C_L)_{\theta} - \eta C_{\mu} \sin \theta$	1.59	2.02	2.23
$C_{L0} = (C_L)_B + (\Delta C_L)_{\theta} - C_{\mu} \sin \delta_T$	4.16	4.91	5.44
$(C_{LMAX})_{PL} = \frac{\frac{3}{4F} [1.15(\Delta C_L)_{\theta} \phi - (C_L)_B (1-\phi) + (C_{LMAX})_B]}{1 - \frac{3}{4F} (1-\phi)} - C_{\mu} \sin \delta_T$	5.87	7.16	8.32
$\Delta \alpha_{MAX} = \frac{(C_{LMAX})_{PL} - (C_L)_{\alpha=0}}{C_{L\alpha}} - \frac{(C_{LMAX})_{PO} - (C_L)_{PO, \alpha=0}}{(C_{L\alpha})_{PO}}$	3.57	5.78	7.80
$\alpha_{MAX} = (\alpha_{MAX})_{PO} + \Delta \alpha_{MAX}$	18.57	20.78	22.80
$(\Delta C_L)_{\alpha} = C_{L\alpha} (\alpha / 57.3)$ at $\alpha =$			
-5°	-.59	-.67	-.70
0°	0	0	0
10°	1.17	1.34	1.51
$C_L = C_{L0} + (\Delta C_L)_{\alpha}$ at $\alpha =$			
-5°	3.57	4.24	4.69
0°	4.16	4.91	5.44
10°	5.33	6.25	6.95
$\eta C_{\mu} \sin (\theta + \alpha)$ at $\alpha =$			
-5°	.59	1.18	1.77
0°	.63	1.26	1.89
10°	.69	1.39	2.08
$C_L - \eta C_{\mu} \sin (\theta + \alpha)$ at $\alpha =$			
-5°	2.98	3.06	2.98
0°	3.53	3.65	3.55
10°	4.64	4.86	4.87
$C_{Di} = \frac{[C_L - \eta C_{\mu} \sin (\theta + \alpha)]^2}{\pi A}$ at $\alpha =$			
-5°	.405	.426	.405
0°	.569	.608	.569
10°	.980	1.08	1.08
$(\Delta C_L)_{\alpha P.O.} = \frac{A(1+t/c) 2\pi \alpha}{(A+2)(57.3)}$			
= .48 at $\alpha = -5^{\circ}$			
= 0 at $\alpha = 0$			
= .96 at $\alpha = 10^{\circ}$			
$\eta C_{\mu} \cos (\theta + \alpha)$ at $\alpha =$			
-5°	.479	.906	1.435
0°	.425	.850	1.275
10°	.309	.618	.926
$C_D = C_{Df} + (\Delta C_D)_R + C_{Di} - \eta C_{\mu} \cos (\theta + \alpha)$ at C_L 's calculated above at $\alpha =$			
-5°	.071	-.335	-.885
0°	.289	-.095	-.561
10°	.816	.605	.295

Contrails

Calculations - Concluded

	C_{μ}		
	1	2	3
$[C_R - (x_{REF} - x_{LEc'})] / \bar{c} = .408$	1	2	3
$(\Delta C_m)_{RREF} = -\eta C_{\mu} \sin \theta [C_R - (x_{REF} - x_{LEc'})] / \bar{c}$	-.32	-.65	-.97
$(\Delta C_m)_{rREF} = -(\Delta C_L)_r [(C_m)_B / (C_L)_B] \alpha = 0$	-.67	-.85	-.94
$x_{CP} / \bar{c}_F = .25 - .01 \eta C_{\mu}$.24	.23	.23
$(x_{CP} / \bar{c}_F) (\bar{c}_F / \bar{c}) - (x_{REF} - x_{LEc'}) / \bar{c}$.04	.05	.05
$(\Delta C_m)_{\alpha REF} = - [(\Delta C_L)_{\alpha} - (\Delta C_L)_{\alpha P.O.}] \cdot$			
$\cdot \left[\left(\frac{x_{C.P.}}{\bar{c}_F} \right) \left(\frac{\bar{c}_F}{\bar{c}} \right) - \frac{(x_{REF} - x_{LEc'})}{\bar{c}} \right]$ at $\alpha =$.005	.010	.011
0°	0	0	0
10°	-.008	-.019	-.027
$(\Delta C_m)_{RD} = -(\Delta C_D)_R \Delta l_R / \bar{c}$	0	0	0
$C_m = (C_m)_B + (\Delta C_m)_R + (\Delta C_m)_r + (\Delta C_m)_{\alpha}$	-1.94	-2.44	-2.76
$+ (\Delta C_m)_{RD}$	-1.94	-2.45	-2.77
$\text{at } \alpha = \begin{cases} -5^\circ \\ 0^\circ \\ 10^\circ \end{cases}$	-1.95	-2.47	-2.80

Contrails

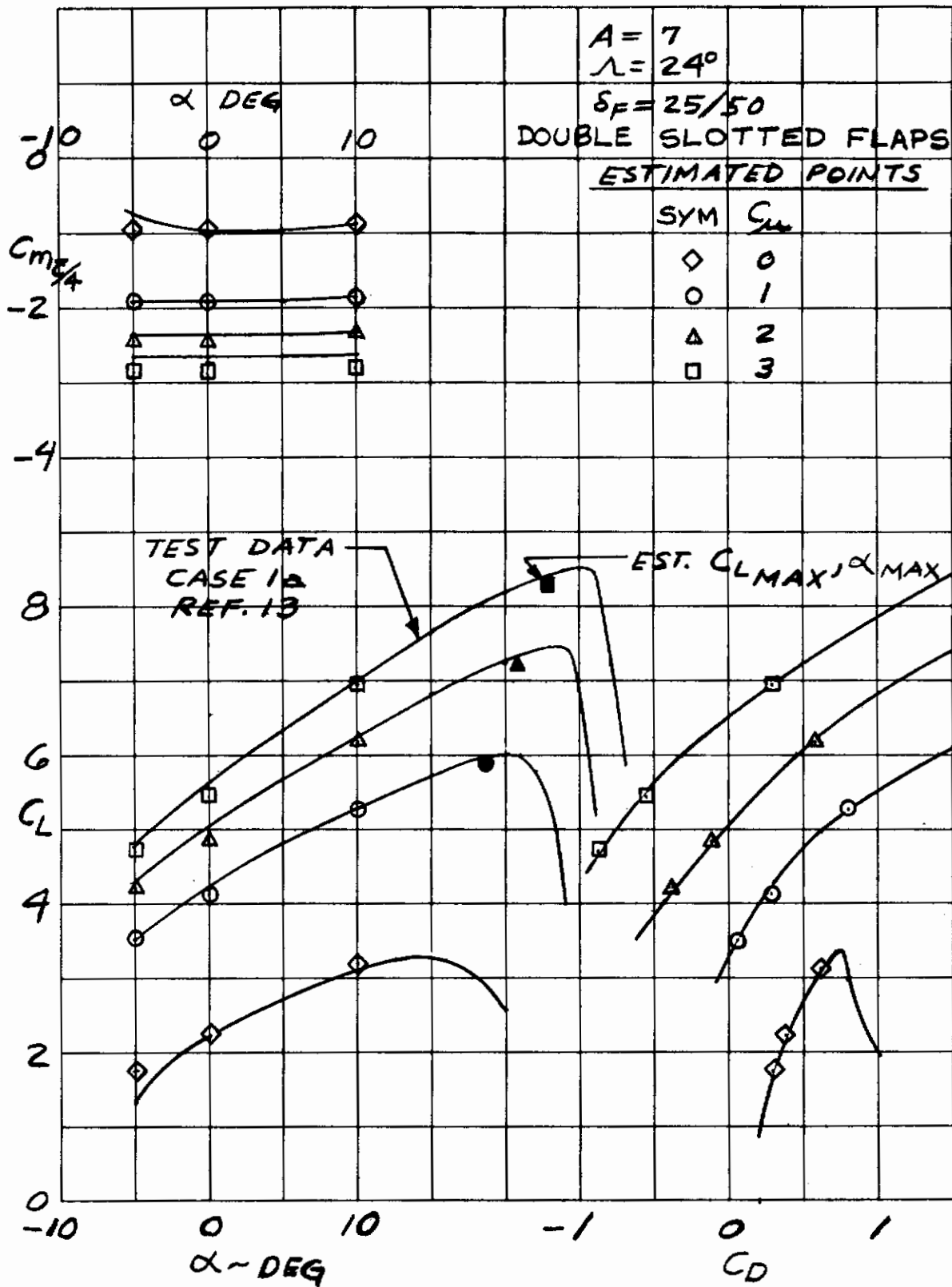


Figure 65 (a). Comparison of Estimated and Experimental Results

Contrails

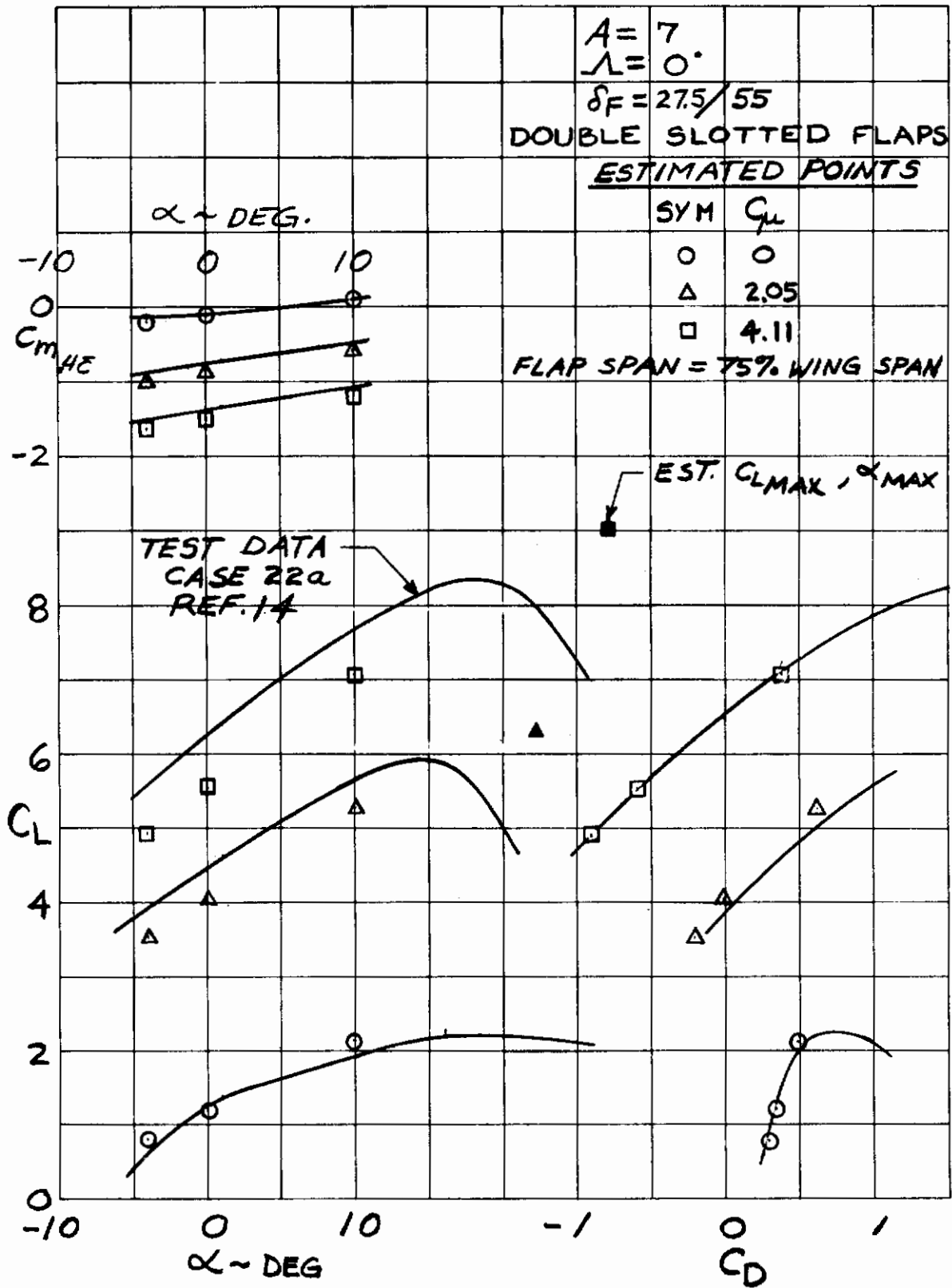


Figure 65 (b). Comparison of Estimated and Experimental Results

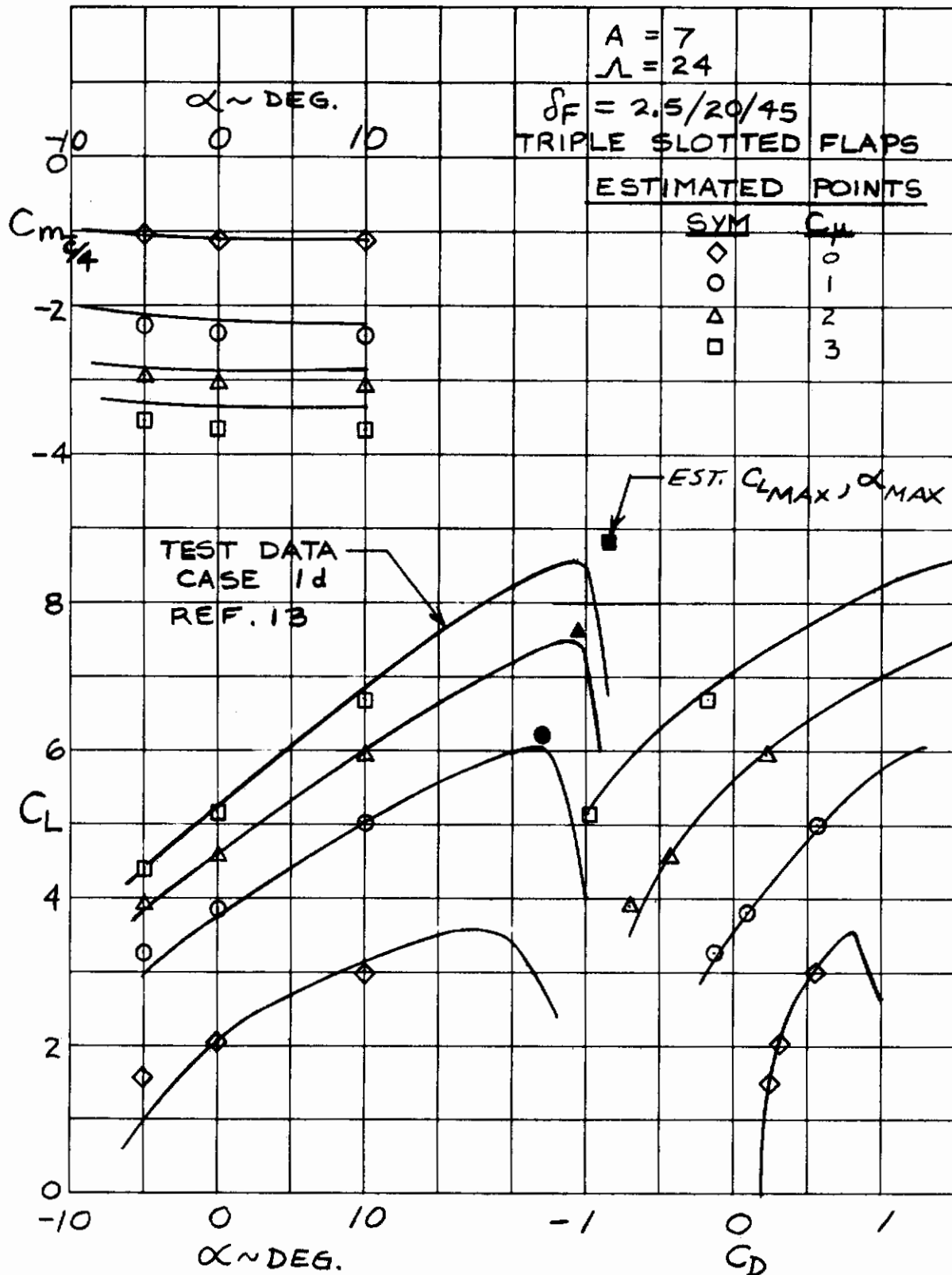


Figure 65 (c). Comparison of Estimated and Experimental Results

DEFINITION OF TEST CASES

CASE	REF.	FIG.	$\frac{\Lambda}{4} \frac{c}{4}$	A	% SPAN FLAPS	NO. FLAP SLOTS	NOMINAL FLAP ANGLE	NOZ. ANGLE OR DEFLEC.
1a	13	7	24	7	100	2	25/50	15°
1b	13	8	24	7	100	2	35/60	15°
1d	13	18	24	7	100	3	2.5/20/45	15°
1f	13	20	24	7	100	3	2.5/30/55	15°
2a	13	74/75	24	7	100	2	25/50	-15°
6a	13	104	24	7	100	2	25/50	0°
9a	13	97/98	9.33	8	100	2	25/50	15°
10a	13	97/99	30	6.6	100	2	25/50	15°
11a	13	139/140	24	10	100	2	25/50	15°
14a	13	129	24	7	75	2	25/50	15°
21a	14	13	0	7	100	2	27.5/55	0
22a	14	14	0	7	75	2	27.5/55	0
23a	14	15	0	5.25	100	2	27.5/55	0
91a	22	12a	25	7.84	50	0	30	-10°
61a	9	8a	25	7	75	2	20/60	0
24a	14	10	0	7	100	2	17.5/35	0
25a	14	11	0	7	75	2	17.5/35	0
51a	2	5b	24	7.75	100	2	30/60	NAC 3°
71a	20	8b	24	7.75	100	2	20/40	Defl.
81a	5	7	24	7.23	100	3	25/10/50	3°
51c	2	16	24	7.75	100	2	30/60	3°
51d	2	17	24	7.75	100	2	20/40	3°
101	4	12	24	7.75	75	2	30/60	3°
102	4	13	24	7.75	75	2	30/60	3°
103	4	14	24	7.75	75	2	30/60	3°

APPENDIX

FORTRAN IV PROGRAM FOR CALCULATING
AERODYNAMIC CHARACTERISTICS OF EXTERNALLY
BLOWN FLAP POWERED LIFT SYSTEMS

Contrails

INTRODUCTION

Aerodynamic characteristics of externally blown flaps are calculated by the program. The design compendium develops an analytical approach upon which the program is based.

The simple nature of the program means very little computer time is used. Fortran code was written to be easily understood and revised in support of analytical development.

Contrails

PROGRAM OPERATION

Data input consists of a set of six to twelve cards describing each case to be analyzed. After the cards are read in, the computations are performed followed by the printed and graphic output. After a case is finished the program attempts to process a new case terminating if there are no more input cards. Each case may contain as many as ten different angles of attack and ten different jet moment coefficients.

If graphic output is not desired, the main analytical routine will function by itself if the call subroutine "CRT CRT" is removed or the subroutine is replaced by a dummy routine.

ANALYTICAL METHODS

LIFT FORMULATIONS

Input data for lift

$$C_{\mu}, \lambda \text{ OR } S'/S, \eta, A, t/c, \theta, \alpha, (C_L)_B, \delta T, (C_{LMAX})_B$$

Jet momentum coefficient based on effective wing area

$$C_{\mu}' = \frac{C_{\mu}}{\lambda} \quad (\text{Eq. 1})$$

Two dimension gradient of lift with jet deflection angle

$$(C_{L\theta})_{\infty} = \left[4\pi\eta C_{\mu}' \left\{ 1 + 0.151(\eta C_{\mu}')^{1/2} + 0.139\eta C_{\mu}' \right\} \right]^{1/2} \quad (\text{Eq. 2})$$

Two dimensional lift curve slope

$$(C_{L\alpha})_{\infty} = 2\pi \left[1 + 0.151(\eta C_{\mu}')^{1/2} + 0.219\eta C_{\mu}' \right] \quad (\text{Eq. 3})$$

Lift curve slope correction for partial span blowing

$$\nu = \frac{S'}{S} + \left(1 - \frac{S'}{S} \right) \frac{2\pi}{(C_{L\alpha})_{\infty}} \quad (\text{Eq. 4})$$

Aspect ratio correction factor

$$F = \frac{A + 2\eta C_{\mu}' / \pi}{A + 2 + 0.604(\eta C_{\mu}')^{1/2} + 0.876\eta C_{\mu}'} \quad (\text{Eq. 5})$$

Increment of lift coefficient due to circulation due to power

$$(\Delta C_L)_r = \left[(1 + t/c) F \lambda (C_{L\theta})_\infty - \eta C_\mu \right] \sin \Theta \quad (\text{Eq. 6})$$

Gradient of lift due to angle of attack

$$\frac{\Delta C_L}{\Delta \alpha} = \left[F (1 + t/c) \gamma (C_{L\alpha})_\infty \right] \quad (\text{Eq. 7})$$

Increment of lift due to angle of attack, power on

$$(\Delta C_L)_\alpha = (\Delta C_L / \Delta \alpha) \alpha \quad (\text{Eq. 8})$$

Increment of lift due to jet turning

$$\begin{aligned} (\Delta C_L)_\theta &= \left[(1 + t/c) F \lambda (C_{L\theta})_\infty - \eta C_\mu \right] \sin \Theta + \eta C_\mu \sin \Theta \\ &= (\Delta C_L)_r + \eta C_\mu \sin \Theta \end{aligned} \quad (\text{Eq. 9})$$

Total lift coefficient

$$C_L = (C_L)_B + (\Delta C_L)_\theta + (\Delta C_L)_\alpha - C_\mu \sin \delta_T \quad (\text{Eq. 10})$$

Maximum lift coefficient

$$\begin{aligned} (C_{L\text{MAX}})_{\text{PL}} &= \left\{ \frac{\frac{3}{4F} \left[1.15 (\Delta C_L)_\theta \phi - (C_L)_{\text{PO}, \alpha=0} (1-\phi) \right] + (C_{L\text{MAX}})_B}{1 - \frac{3}{4F} (1-\phi)} \right\} - C_\mu \sin \delta_T \\ \phi &= (C_{L\alpha})_{\text{PO}} / C_{L\alpha} \end{aligned} \quad (\text{Eq. 11})$$

Maximum angle of attack

$$\alpha_{\text{MAX}} = (\alpha_{\text{MAX}})_B + \frac{(C_{L\text{MAX}})_{\text{PL}} - (C_L)_{\alpha=0}}{C_{L\alpha}} - \frac{(C_{L\text{MAX}})_B - (C_L)_{B, \alpha=0}}{(C_{L\alpha})_{\text{PO}}} \quad (\text{Eq. 12})$$

DRAG FORMULATIONS

Input data for drag

$$\eta, C_u, \theta, \alpha, A, (\Delta C_D)_R, C_{Df}$$

C_L from lift calculations

Coefficient of drag due to lift

$$C_{Di} = \frac{[C_L - \eta C_{\mu} \sin(\theta + \alpha)]^2}{\pi A} \quad (\text{Eq. 13})$$

Total drag coefficient

$$C_D = C_{Df} + C_{Di} - \eta C_{\mu} \cos(\theta + \alpha) + (\Delta C_D)_R \quad (\text{Eq. 14})$$

PITCHING MOMENT FORMULATIONS

Input data for pitching moment

$$\eta, C_{\mu}, \alpha, t/c, X_{c.p.}, \bar{c}_F, \bar{c}, (X_{REF} - X_{L.E.} \bar{c}_F), (\Delta C_{DR}), \\ (C_m)_B, \theta, c_R, (X_{REF} - X_{L.E.} c')$$

$\nu, (C_{L\alpha})_{\infty}, (\Delta C_L)_F$, from lift calculations

Center of pressure of additional load due to angle of attack

$$X_{c.p.} = (.25 - .01 \eta C_{\mu}) \bar{c}_F \quad (\text{Eq. 15})$$

Increment of lift due to angle of attack due to power

$$(\Delta C_L)_{\alpha_{PO}} = \alpha F (1 + t/c) \nu [(C_{L\alpha})_{\infty} - 2\pi] \quad (\text{Eq. 16})$$

Pitching moment coefficient of power effects on lift due to angle of attack about the moment reference center

(Eq. 17)

$$(\Delta C_m)_{\alpha_{REF}} = -(\Delta C_L)_{\alpha_{PO}} \left[\left(\frac{X_{c.p.}}{\bar{c}_F} \right) \left(\frac{\bar{c}_F}{\bar{c}} \right) - \left(\frac{X_{REF} - X_{L.E.} \bar{c}_F}{\bar{c}} \right) \right]$$

Pitching moment coefficient of ram drag about the moment reference center

$$(\Delta C_m)_{RD} = -(\Delta C_D)_R \frac{\Delta l_R}{\bar{c}} \quad (\text{Eq. 18})$$

Pitching moment coefficient due to circulation lift due to power about the moment reference center

$$(\Delta C_m)_{\Gamma_{REF}} = (\Delta C_L)_{\Gamma} \left[\frac{(C_m)_B}{(C_L)_B} \right]_{\alpha=0} \quad (\text{Eq. 19})$$

where $(C_m)_B$ is about moment reference.

Pitching moment coefficient due to jet reaction about moment reference center

$$(\Delta C_m)_{R_{REF}} = -\eta C_{\mu} \sin \Theta \left[\left(\frac{C_R}{C'} \right) \left(\frac{C'}{\bar{c}} \right) - \left(\frac{x_{REF} - x_{L.E.C'}}{\bar{c}} \right) \right] \quad (\text{Eq. 20})$$

Total pitching moment coefficient

$$C_m = (C_m)_B + (\Delta C_m)_R + (\Delta C_m)_{\Gamma} + (\Delta C_m)_{\alpha} + (\Delta C_m)_{RD} \quad (\text{Eq. 21})$$

NOMENCLATURE

SYMBOL	FORTTRAN NAME	DESCRIPTION
A	A	Aspect Ratio
α	ALPHA	Angle of Attack, Degrees
α	ALPHAR	Angle of Attack, Radians
\bar{c}	CBAR	Mean Aerodynamic Chord of Wing
\bar{c}_F	CBARF	Mean Aerodynamic Chord of Wing with Flaps Extended
C_D	CD	Total Drag Coefficient, Power On
C_{Df}	CDF	Minimum Drag Coefficient Extrapolated to Zero Lift
C_{Di}	CDI	Coefficient of Drag Due to Lift
C_L	CL	Total Lift Coefficient
$(C_L)_{\alpha}$	CLAI	Two Dimensional lift curve slope
$(C_L)_B$	CLB	Total Lift Coefficient, Power Off
C_{LMAX}	CLMAX	Maximum Lift Coefficient
$(C_{LMAX})_B$	CLMAXB	Maximum Lift Coefficient, Power Off
$(C_L)_{\theta}$	CLTI	Two Dimensional Gradient of Lift with Jet Deflection Angle
C_m	CM	Total Pitching Moment Coefficient
$(C_m)_B$	CMB	Total Pitching Moment Coefficient, Power Off
$(C_m)_B \alpha = 0$	CMBAO	Total Pitching Moment Coefficient, Power Off Zero Angle of Attack
C_{μ}	CMU	Jet Momentum Coefficient, or Thrust Coefficient
C_{μ}^*	CMUP	Jet Momentum Coefficient Based on Effective Wing Area
C_R	CR	Chordwise Distance from Intersection of Jet Reaction Vector with Reference Plane to Leading Edge of Chord at Thrust Centerline
$(\Delta C_D)_R$	DCDR	Ram Drag Coefficient
$(\Delta C_L)_{\alpha}$	DCLA	Increment of Lift Due to Angle of Attack
$\Delta C_L / \Delta \alpha$	DCLDA	Gradient of Lift Coefficient with Angle of Attack
$(\Delta C_L)_P$	DCLG	Increment of Lift Coefficient due to Circulation Due to Power
ΔC_{LMAX}	DCLMAX	Increment in Maximum Lift Coefficient due to Power
$(\Delta C_L)_{\theta}$	DCLT	Increment of Lift Coefficient due to Jet Turning
$(\Delta C_m)_{\alpha REF}$	DCMA	Pitching Moment Coefficient of Power Effects on Lift Due to Angle of Attack About the Moment Reference Center
$(\Delta C_m)_P REF$	DCMG	Pitching Moment Coefficient due to Circulation Lift Due to Power About the Moment Reference Center
$(\Delta C_m)_{R REF}$	DCMR	Pitching Moment Coefficient due to Jet Reaction About Moment Reference Center

Contrails

NOMENCLATURE

SYMBOL	FORTTRAN NAME	DESCRIPTION
$(\Delta C_m)_{RD}$	DCMRD	Pitching Moment Coefficient of Ram Drag About the Moment Reference Center
$(\Delta C_L)_{\alpha_{PO}}$	DDCLPO	Increment of Lift due to Angle of Attack due to Power
Δl_R	DLR	Moment Arm of Ram Drag about Moment Reference Center
Δl_T	DLT	Moment Arm of Thrust about Moment Reference Center Positive if Nozzle Axis is below Moment Reference Center
δ_{TD}	DT	Thrust Incidence Angle, Degrees
δ_T	DTR	Thrust Incidence Angle, Radians
ΔX_F	DXF	Chordwise Distance from Moment Reference Center to Flap Mid-Chord
ΔX_G	DXG	Chordwise Distance from Moment Reference Center to Leading Edge of Mean Aerodynamic Chord of Flapped Wing Area
ΔX_R	DXR	Chordwise Distance from Moment Reference Center to Leading Edge of Chord on Thrust Centerline
η	ETA	Jet Turning Efficiency
F	F	Aspect Ratio Correction Factor
λ or S/S	LAMDA	Area Ratio, Flapped Wing Area to Total Wing Area
	NA	Number of Alpha Values
	NC	Number of CMU Values
ν	NU	Lift Curve Slope Correction for Partial Span Blowing
π	PI	Ratio of Circumference of a Circle to its Diameter
t/c	TC	Airfoil Thickness Ratio
θ_D	THETA	Jet Turning Angle, Degrees
θ	THETAR	Jet Turning Angle, Radians
	TITLE	Title of Case
X_{cp}	XCP	Center of Pressure of Additional Load due to Angle of Attack

FORTRAN FIXED 10 DIGIT DECIMAL DATA

DECK NO.	PROGRAMMER	DATE	PAGE	of	JOB NO.
1	CASE	1A			
13					
25					
37					
49					
61					
1	2.25				CLB
13	0.76				ETA
25	56.0				THETA
37	0.125				TC
49	18.0				DT
61	7.0				A
13	0.85				LAMDA
25	0.145				CDF
37	6.6				DXR = XREF - X L.E.C'
49	14.6				CR
61	15.5				CBAR
1	3.9				DXG
13	19.6				CBARF
25	0.0				DLT
37	4.7				DLR
49	3.35				CLMAXB
61	15.0				AMAXB

TITLE

139

114-F-17 VET 1114

FORTRAN FIXED 10 DIGIT DECIMAL DATA

DECK NO. _____ PROGRAMMER _____ DATE _____ PAGE _____ of _____ JOB NO. _____

NUMBER	IDENTIFICATION	DESCRIPTION DO NOT KEY PUNCH	NA
1		NUMBER OF ALPHAS (MAXIMUM OF 10)	ALPHA(1)
13		OC D (ONE VALUE SHOULD BE ZERO)	CMB(1)
25		CMB	ALPHA(2)
37			CMB(2)
49			ALPHA(3)
61			CMB(3)
1			
13			
25			
37			
49			
61			
140			
1		NUMBER OF CMUS (MAXIMUM OF 10)	NC
13		CM	CMU(1)
25		Δ CDR	DCDR(1)
37			CMU(2)
49			DCDR(2)
61			CMU(3)
1			DCDR(3)
13			CMU(4)
25			DCDR(4)
37			
49			
61			

CASE 1A

INPUT DATA (PROGRAM VERSION 3A)

CLB	2.2500				
ETA	0.7600				
THETA	56.0000				
TC	0.1250				
DT	18.0000				
A	7.0000				
LAMDA	0.8500				
CDF	0.1450				
DXR	6.6000				
CR	14.6000				
CBAR	15.5000				
DXG	3.9000				
CBARF	15.6000				
DLT	0.0				
DLR	4.7000				
CLMAXB	3.3500				
AMAXB	15.0000				
ALPHA	-5.0000	0.0	10.0000		
CMB	-0.9500	-0.9500	-0.8600		
CMU	0.0	1.0000	2.0000	3.0000	
DCDR	0.0	0.0	0.0	0.0	

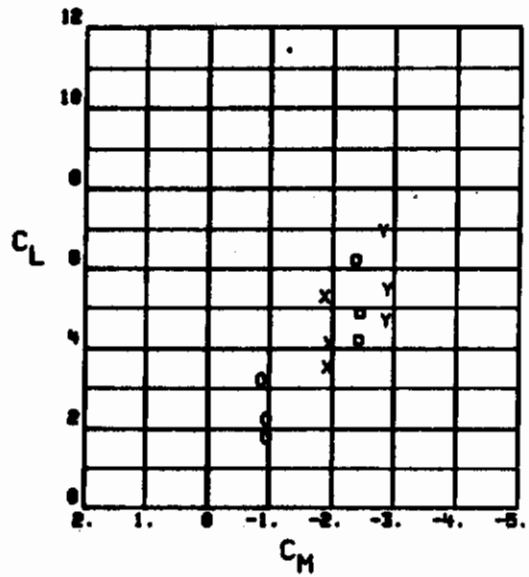
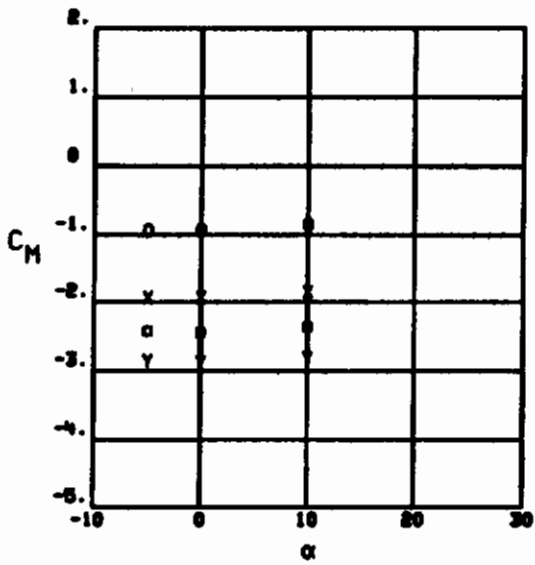
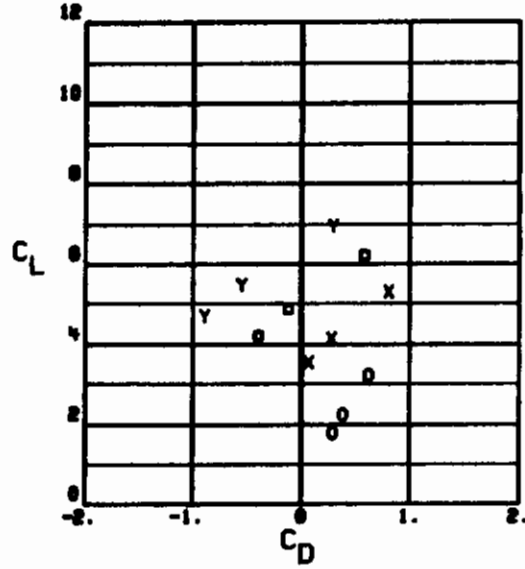
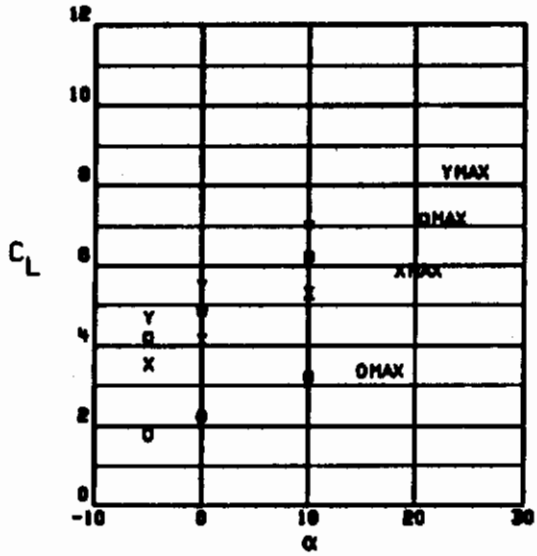
CASE 1A	ALPHA	-5.0000						
CMU		0.0	1.0000	2.0000	3.0000			
CL	1.7702	1.7702	3.5409	4.2064	4.7131			
CD	0.2875	0.2875	0.0641	-0.3954	-0.8965			
CM	-0.9500	-0.9500	-1.9243	-2.4245	-2.8610			
DCLT	0.0	0.0	2.1866	3.2385	4.1344			
DCLDA	5.4978	5.4978	6.6544	7.6094	8.5277			
CDI	0.1425	0.1425	0.3974	0.4161	0.3934			
DCLA	-0.4798	-0.4798	-0.5807	-0.6640	-0.7442			
DCLG	0.0	0.0	1.5565	1.9783	2.2441			
DCMR	0.0	0.0	-0.3252	-0.6504	-0.9750			
DCMG	0.0	0.0	-0.6572	-0.8353	-0.9475			
DCMA	0.0	0.0	0.0081	0.0112	0.0121			
DCMRD	0.0	0.0	0.0	0.0	0.0			
ETACMU	0.0	0.0	0.7600	1.5200	2.2800			

CASE	IA	ALPHA	0.0	0.0	1.0000	2.0000	3.0000
CMU	0.0	0.0	0.0	1.0000	2.0000	3.0000	3.0000
CL	2.2500	0.0	4.1276	4.8704	4.8704	5.4573	5.4573
CD	0.3752	0.0	0.2763	-0.1123	-0.1123	-0.5514	-0.5514
CM	-0.9500	-0.0	-1.9324	-2.4357	-2.4357	-2.8731	-2.8731
DCLT	0.0	0.0	2.1866	3.2385	3.2385	4.1344	4.1344
DCLDA	5.4978	0.0	6.6544	7.6094	7.6094	8.5277	8.5277
GDI	0.2302	0.0	0.5563	0.5927	0.5927	0.5786	0.5786
DCLA	0.0	0.0	0.0	0.0	0.0	0.0	0.0
DCLG	0.0	0.0	1.5565	1.9783	1.9783	2.2441	2.2441
DCMR	0.0	0.0	-0.3252	-0.6504	-0.6504	-0.9756	-0.9756
DCMG	0.0	0.0	-0.6572	-0.8353	-0.8353	-0.9475	-0.9475
DCMA	0.0	0.0	0.0	0.0	0.0	0.0	0.0
DCMRD	0.0	0.0	0.0	0.0	0.0	0.0	0.0
ETACMU	0.0	0.0	0.7600	1.5200	1.5200	2.2600	2.2600

CASE 1A

ALPHA	10.0000				
CMU	0.0	1.0000	2.0000	3.0000	
CL	3.2095	5.2890	6.1985	6.9457	
CD	0.6134	0.7559	0.5788	0.2929	
CM	-0.8600	-1.8585	-2.3681	-2.8073	
DCLT	0.0	2.1866	3.2385	4.1344	
DCLDA	5.4978	6.6544	7.6094	8.5277	
CDI	0.4684	0.9600	1.0520	1.0753	
DCLA	0.9595	1.1614	1.3281	1.4884	
DCLG	0.0	1.5565	1.9783	2.2441	
DCMR	0.0	-0.3252	-0.6504	-0.9756	
DCMG	0.0	-0.6572	-0.8353	-0.9475	
DCMA	0.0	-0.0161	-0.0224	-0.0242	
DCMRD	0.0	0.0	0.0	0.0	
ETACMU	0.0	0.7600	1.5200	2.2800	
CLMAXP	3.3500	5.8738	7.1605	8.3243	
AMAX	15.0000	18.5713	20.7796	22.7991	

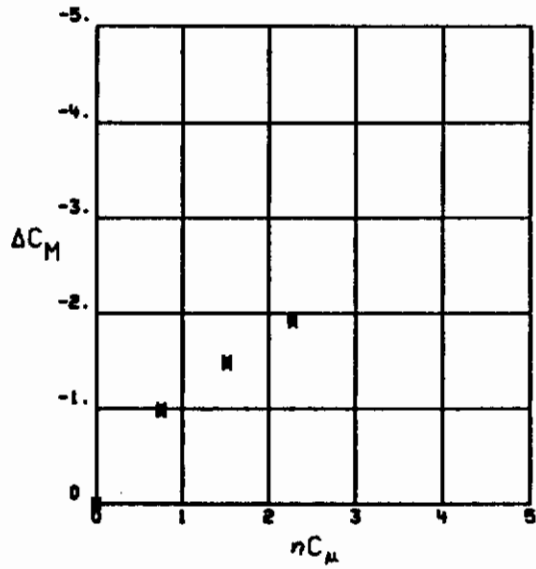
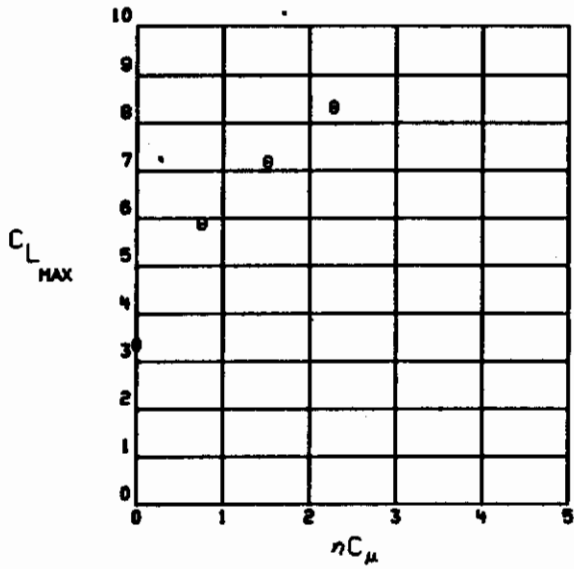
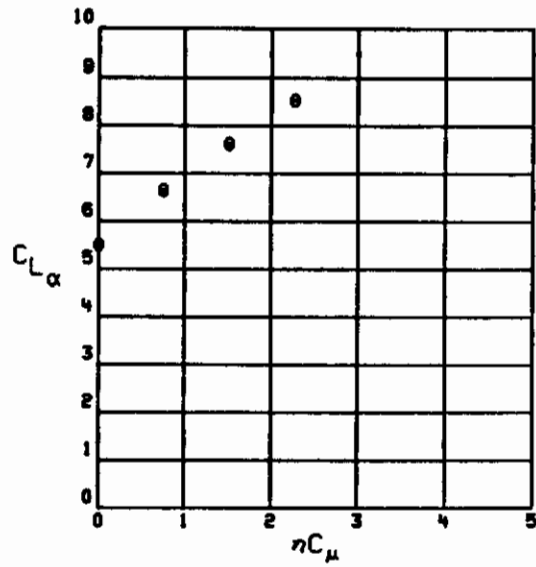
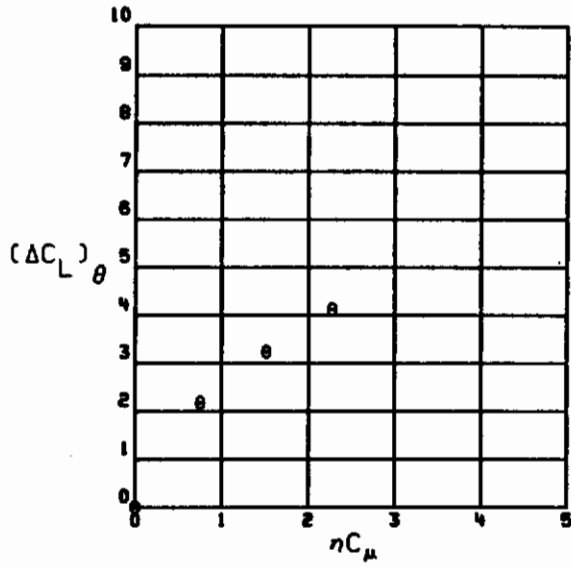
CASE 1A



SYMBOL	nC_M
O	0.6
X	0.7
□	1.5
Y	2.2

Contrails

CASE 1A



SYMBOL	α
X	-5.0
o	0.0
Y	10.0

EQUIPMENT REQUIREMENTS

HARDWARE

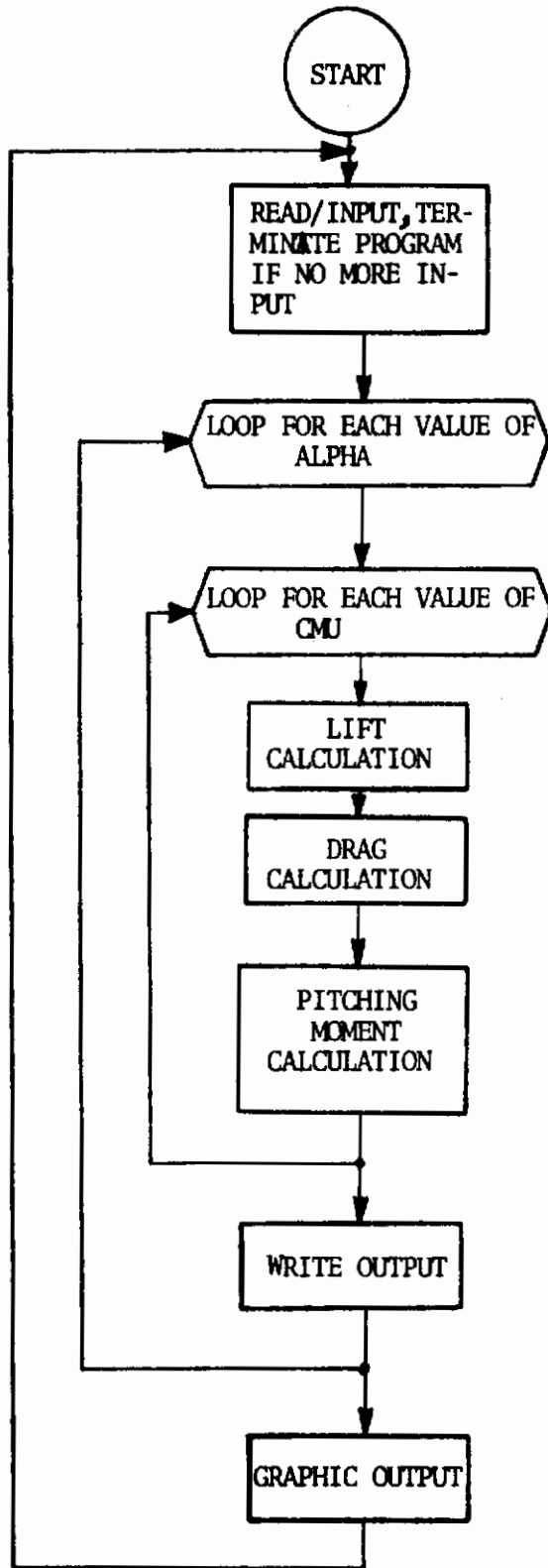
The program has been run on an IBM System 370 model 165KJ computer with graphic output processed on an Information International Incorporated FR-80 simulating a Stromberg-Datagraphics S-C 4020. Rms have also been made on a Control Data Corporation Model 6600 without graphic output.

SOFTWARE

A fortran IV compiler is required to translate the source code into object form. Standard Fortran library routines are required for mathematical operations, card reading and printing output.

Graphics output requires several NR library routines that generate instructions for the S-C 4020. Some reprogramming may be necessary for graphic output at another computer facility.

FLOW CHART OF PROGRAM FUNCTIONS



FORTRAN IV G LEVEL 20 MAIN DATE = 73110 00/26/45

PROGRAM FOR CALCULATING AERODYNAMIC CHARACTERISTICS OF
EXTERNALLY BLOWN FLAP POWERED LIFT SYSTEMS

0010
0020
0030

VERSION 3 WRITTEN NOVEMBER 29, 1972
REVISION A APRIL 19, 1973

0040
0050
0060

A ASPECT RATIO
ALPHA(J) ANGLE OF ATTACK, DEGREES
ALPHAR ANGLE OF ATTACK, RADIAN
AMAX(I) ANGLE OF ATTACK MAXIMUM, DEGREES
AMAXB ANGLE OF ATTACK MAXIMUM WITH POWER OFF, DEGREES
CBAR MEAN AERODYNAMIC CHORD OF WING
CBARF MEAN AERODYNAMIC CHORD OF WING WITH FLAPS EXTENDED
CD(I,J) TOTAL DRAG COEFFICIENT, POWER ON
CDF MINIMUM DRAG COEFFICIENT EXTRAPOLATED TO ZERO LIFT

0070
0080
0090

CDI(I,J) COEFFICIENT OF DRAG DUE TO LIFT
CL(I,J) TOTAL LIFT COEFFICIENT
CLAI TWO DIMENSIONAL WAVE SLOPE
CLB TOTAL LIFT COEFFICIENT, POWER OFF
CLMAXB MAXIMUM LIFT COEFFICIENT, POWER OFF
CLMAXP(I) MAXIMUM LIFT COEFFICIENT FOR POWERED LIFT

0100
0110
0120
0130
0140
0150

CLTI TWO DIMENSIONAL GRADIENT OF LIFT WITH JET DEFLECTION
ANGLE
CM(I,J) TOTAL PITCHING MOMENT COEFFICIENT
CMB(J) TOTAL PITCHING MOMENT COEFFICIENT, POWER OFF
CMBAO TOTAL PITCHING MOMENT COEFFICIENT, POWER OFF ZERO ANGLE
OF ATTACK
CMU(I) JET MOMENTUM COEFFICIENT, OR THRUST COEFFICIENT
CMUP JET MOMENTUM COEFFICIENT BASED ON EFFECTIVE WING AREA
CR CHORDWISE DISTANCE FROM INTERSECTION OF JET REACTION
VECTOR WITH REFERENCE PLANE TO LEADING EDGE OF CHORD AT
THRUST CENTERLINE

0160
0170
0180
0190
0200
0210
0220

DCDR(I) RAM DRAG COEFFICIENT
DCLA(I,J) INCREMENT OF LIFT DUE TO ANGLE OF ATTACK
DCLDA(I) GRADIENT OF LIFT COEFFICIENT WITH ANGLE OF ATTACK
DCLG(I) INCREMENT OF LIFT COEFFICIENT DUE TO CIRCULATION LIFT
DUE TO POWER
DCLT(I) INCREMENT OF LIFT COEFFICIENT DUE TO JET TURNING
DCMA(I,J) PITCHING MOMENT COEFFICIENT OF POWER EFFECTS ON LIFT DUE
TO ANGLE OF ATTACK ABOUT THE MOMENT REFERENCE CENTER

0230
0240
0250
0260
0270

0280
0290
0300
0310
0320
0330

0340
0350
0360
0370
0380
0390
0400

FORTRAN IV G LEVEL 20 MAIN DATE = 73110 00/26/45

C	DCMG(I)	PITCHING MOMENT COEFFICIENT DUE TO CIRCULATION LIFT DUE TO POWER ABOUT THE MOMENT REFERENCE CENTER	0410
C			0420
C	DCMR	PITCHING MOMENT COEFFICIENT DUE TO JET REACTION ABOUT MOMENT REFERENCE CENTER	0430
C			0440
C	DCMRO(I)	PITCHING MOMENT COEFFICIENT OF RAM DRAG ABOUT THE MOMENT REFERENCE CENTER	0450
C			0460
C	DDCLPO	INCREMENT OF LIFT DUE TO ANGLE OF ATTACK DUE TO POWER REACTION ABOUT MOMENT REFERENCE CENTER	0470
C			0480
C	DLR	MOMENT ARM OF RAM DRAG ABOUT MOMENT REFERENCE CENTER	0490
C	DLT	MOMENT ARM OF THRUST ABOUT MOMENT REFERENCE CENTER	0500
C	DT	THRUST INCIDENCE ANGLE, DEGREES	0510
C	DTR	THRUST INCIDENCE ANGLE, RADIAN	0520
C	DXF	CHORDWISE DISTANCE FROM MOMENT REFERENCE CENTER TO FLAP MID-CHORD	0530
C			0540
C	DXG	CHORDWISE DISTANCE FROM MOMENT REFERENCE CENTER TO LEADING EDGE OF MEAN AERODYNAMIC CHORD OF FLAPPED WING AREA	0550
C			0560
C	DXR	CHORDWISE DISTANCE FROM MOMENT REFERENCE CENTER TO LEADING EDGE OF CHORD ON THRUST CENTERLINE	0570
C			0580
C	ETA	JET TURNING EFFICIENCY	0590
C	ETACMP	PRODUCT OF ETA AND CMUP	0600
C	ETACMU(I)	PRODUCT OF ETA AND CMU()	0610
C	F	FACTOR	0620
C			0630
C	FFF(10)	TEMPORARY STORAGE FOR F VALUES	0640
C	I	INDEX ASSOCIATED WITH CMU()	0650
C	J	INDEX ASSOCIATED WITH ALPHA()	0660
C	K	SUBSCRIPT ASSOCIATED WITH ZERO CMU	0670
C	L	SUBSCRIPT ASSOCIATED WITH ZERO ALPHA	0680
C	LAMDA	AREA RATIO, FLAPPED WING AREA TO TOTAL WING AREA	0690
C	NA	NUMBER OF ALPHA VALUES	0700
C	NC	NUMBER OF CMU VALUES	0710
C	NU	LIFT CURVE SLOPE CORRECTION FOR PARTIAL SPAN BLOWING	0720
C	PI	RATIO OF CIRCUMFERENCE OF A CIRCLE TO ITS DIAMETER	0730
C	TC	AIRFOIL THICKNESS RATIO	0740
C	THETA	JET TURNING ANGLE, DEGREES	0750
C	THETAR	JET TURNING ANGLE, RADIAN	0760
C	TITLE(18)	TITLE OF CASE	0770
C			0780
C			0790
	COMMON	ALPHA(10) ,AMAX(10) ,CD(10,10) ,CDI(10,10)	0800

0001

FORTRAN IV G LEVEL 20 MAIN DATE = 73110 00/26/45

```

0002 COMMON CL(10,10) ,CLMAXP(10) ,CM(10,10) ,CMB(10) 0810
0003 COMMON CMU(10) ,DCDR(10) ,DCLA(10,10) ,DCLDA(10) 0820
0004 COMMON DCCLG(10) ,DCLT(10) ,DCMA(10,10) ,DCMG(10) 0830
0005 COMMON DCMK(10) ,DCMRD(10) ,ETACMU(10) ,TITLE(18) 0840
0850
0006 DIMENSION FFF(10) 0850
0007 REAL LAMDA, NU 0860
0008 DATA PI/ 3.14159265 / 0870
0009 60 READ(5,65) TITLE 0880
0010 65 FORMAT(18A4) 0890
0011 READ (5,70)CLB,ETA,THETA,TC,ET,A,LAMDA,CDF,DXR,CR,CBAR,DXG, 0900
1 CBARF,DLT,DLR,CLMAXB,AMAXB 0910
70 FORMAT (6F12.0) 0920
0012 READ (5,75) NA,(ALPHA(J),CMB(J), J=1,NA) 0930
0013 75 FORMAT (112,5F12.0,3(/6F12.0)) 0940
0014 READ(5,75) NC,(CMU(I),DCDR(I),I=1,NC) 0950
0015 WRITE(6,299) TITLE 0960
0016 299 FORMAT(1H1,18A4) 0970
0017 WRITE(6,350) 0980
0018 350 FORMAT(32HINPUT DATA (PROGRAM VERSION 3A) ) 0990
0019 WRITE(6,351)CLB 1000
0020 WRITE(6,352)ETA 1010
0021 WRITE(6,353)THETA 1020
0022 WRITE(6,354)TC 1030
0023 WRITE(6,355)DT 1040
0024 WRITE(6,356)A 1050
0025 WRITE(6,357)LAMDA 1060
0026 WRITE(6,358)CDF 1070
0027 WRITE(6,359)DXR 1080
0028 WRITE(6,360)CR 1090
0029 WRITE(6,361)CBAR 1100
0030 WRITE(6,362)DXG 1110
0031 WRITE(6,363)CBARF 1120
0032 WRITE(6,364)DLT 1130
0033 WRITE(6,365)DLR 1140
0034 WRITE(6,367)CLMAXB 1150
0035 WRITE(6,368)AMAXB 1160
0036 WRITE(6,370)(ALPHA(J),J=1,NA) 1170
0037 WRITE(6,371)(CMB (J),J=1,NA) 1180
0038 WRITE(6,372)(CMU (I),I=1,NC) 1190
0039 1200

```


FORTRAN IV G LEVEL 20 MAIN DATE = 73110 00/26/45

```

0077      850 CONTINUE
0078      K = 1
0079      852 CONTINUE
0080      DO 100 J = 1,NA
0081      DO 200 I = 1,NC
C
0082      DTR = DT * PI / 180.0
0083      THETA = THETA * PI / 180.0
0084      ALPHA = ALPHA(J) * PI / 180.0
C
0085      ETACMU(I) = ETA * CMU(I)
0086      CMUP = CMU(I) / LAMDA
0087      ETACMP = ETA * CMUP
0088      CLTI = (4.0 * PI * ETACMP * (1.0 + 0.151 * ETACMP**0.5 +
1          0.139 * ETACMP)**0.5
0089      CLAI = 2.0 * PI * (1.0 + 0.151 * ETACMP**0.5 + 0.219 * ETACMP)
0090      NU = LAMDA + (1.0 - LAMDA) * 2.0 * PI / CLAI
0091      F = (A + 2.0 * ETACMP / PI) / (A + 2.0 + 0.604 * ETACMP**0.5 +
1          0.876 * ETACMP)
0092      FFF(I) = F
0093      DCLG(I) = ((1.0 + TC) * F * LAMDA * CLTI - ETACMU(I)) *
1          SIN(THETA)
C
0094      DCLDA(I) = F * (1.0 + TC) * NU * CLAI
0095      DCLA(I,J) = DCLDA(I) * ALPHA
0096      DCLT(I) = DCLG(I) + ETACMU(I) * SIN(THETA)
0097      CL(I,J) = CLB + DCLT(I) + DCLA(I,J) - CMU(I) * SIN(DTR)
C
C
C      DRAG SECTION
0098      CDI(I,J) = (CL(I,J) - ETACMU(I)) * SIN(THETA + ALPHA)**2 / PI/A
0099      CDI(I,J) = CDF + CDI(I,J) - ETACMU(I) * COS(THETA + ALPHA) +
1          DCDR(I)
C
C      PITCHING MOMENT SECTION
0100      XCP = CBARF * (0.25 - 0.01 * ETACMU(I))
0101      DDCLPO = ALPHA * (F * (1.0 + TC) * NU * (CLAI - 2.0 * PI))
0102      DCMA(I,J) = -(DDCLPO) * ((XCP - DXG) / CBAR)
0103      DCMRD(I) = -DCDR(I) * DLR / CBAR
0104      DCMG(I) = DCLG(I) * CMBA0 / CLB
0105      DCMR(I) = -ETACMU(I) * SIN(THETA) * (CR / CBAR - DXR / CBAR)
0106      CM(I,J) = CMB(I,J) + DCMR(I) + DCMG(I) + DCMA(I,J) + DCMRD(I)
C
0107      200 CONTINUE

```

1610
1620
1630
1640
1650
1660
1670
1680
1690
1700
1710
1720
1730
1740
1750
1760
1770
1780
1790
1800
1810
1820
1830
1840
1850
1860
1870
1880
1890
1900
1910
1920
1930
1940
1950
1960
1970
1980
1990
2000

DATE = 73110 00/26/45

MAIN

20

FORTRAN IV G LEVEL

0108	WRITE(6,299) TITLE		2010
0109	WRITE(6,400) ALPHA(J)		2020
0110	400 FORMAT (7H0 ALPHA,F14.4)		2030
0111	WRITE(6,500)(CMU(I), I = 1,NC)		2040
0112	500 FORMAT (8H0CMU ,7F14.4)		2050
0113	WRITE(6,306)(CL (I,J),I=1,NC)		2060
0114	WRITE(6,307)(CD (I,J),I=1,NC)		2070
0115	WRITE(6,309)(CM (I,J),I=1,NC)		2080
0116	WRITE(6,304)(DCLT(I) ,I=1,NC)		2090
0117	WRITE(6,300)(DCLDA (I) ,I=1,NC)		2100
0118	WRITE(6,305)(CDI (I,J),I=1,NC)		2110
0119	WRITE(6,301)(DCLA (I,J),I=1,NC)		2120
0120	WRITE(6,308)(DCLG(I) ,I=1,NC)		2130
0121	WRITE(6,315)(DCMR(I) ,I=1,NC)		2140
0122	WRITE(6,310)(DCMG(I) ,I=1,NC)		2150
0123	WRITE(6,312)(DCMA (I,J),I=1,NC)		2160
0124	WRITE(6,311)(DCMRD (I) ,I=1,NC)		2170
0125	WRITE(6,302)(ETACMU(I) ,I=1,NC)		2180
0126	306 FORMAT(8F CL ,7F14.4)		2190
0127	307 FORMAT(8H CD ,7F14.4)		2200
0128	309 FORMAT(8H CM ,7F14.4)		2210
0129	304 FORMAT(8H DCLT ,7F14.4)		2220
0130	300 FORMAT(8H DCLDA ,7F14.4)		2230
0131	305 FORMAT(8H CDI ,7F14.4)		2240
0132	301 FORMAT(8H DCLA ,7F14.4)		2250
0133	308 FORMAT(8H DCLG ,7F14.4)		2260
0134	315 FCRMAT(8H DCMR ,7F14.4)		2270
0135	310 FORMAT(8H DCMG ,7F14.4)		2280
0136	312 FORMAT(8H DCMA ,7F14.4)		2290
0137	311 FORMAT(8H DCMRD ,7F14.4)		2300
0138	302 FORMAT(8H ETACMU ,7F14.4)		2310
0139	100 CONTINUE		2320
0140	DC 700 I = 1,NC		2330
0141	F = FFF(I)		2340
0142	CLMAXP(I) = ((0.75 / F * (DCLT(I) * 1.15 * DCLDA(K) / DCLDA(I) -		2350
	1 - CLB * (1.0-DCLDA(K) / DCLDA(I))) + CLMAXB) /		2360
2	(1.0 - 0.75/F * (1.0-DCLDA(K)/DCLDA(I))) - CMU(I)		2370
3	* SIN(UTR)		2380
0143	AMAX(I) = AMAXB + ((CLMAXP(I) - CL(I,1)) / DCLDA(I) -		2390
1	(CLMAXB - CLB) / DCLDA(K)) * 180.0 / PI		2400

00/26/45

DATE = 73110

MAIN

FORTRAN IV G LEVEL 20

0144	700	CONTINUE	2410
0145		WRITE(6,330)(CLMAXP(I),I=1,NC)	2420
0146		WRITE(6,331)(AMAX(I),I=1,NC)	2430
0147	330	FORMAT(8H0CLMAXP,7F14.4)	2440
0148	331	FORMAT(8H AMAX,7F14.4)	2450
0149		CALL CRTCRI(NA,NC)	2460
0150		GO TO 60	2470
0151		END	2480

FORTRAN IV G LEVEL 20 CRTCRT DATE = 73110 00/26/45

0001	SUBROUTINE CRTCRT(NA,NC)					2490
0002	COMMON ALPHA(10)	,AMAX(10)	,CD(10,10)	,CDI(10,10)		2500
0003	COMMON CL(10,10)	,CLMAXP(10)	,CM(10,10)	,CMB(10)		2510
0004	COMMON CMU(10)	,DCDR(10)	,DCLA(10,10)	,DCLDA(10)		2520
0005	COMMON DCLG(10)	,DCLT(10)	,DCMA(10,10)	,DCMG(10)		2530
0006	COMMON DCMR(10)	,DCMRD(10)	,ETACMU(10)	,TITLE(18)		2540
0007	EXTERNAL TABL1V, TABL2V, TABL3V					2550
0008	CALL CHSIZV(2,2)					2560
0009	ISPACE = 12					2570
0010	CALL CAMRAV(35)					2580
0011	CALL FRAMEV(3)					2590
0012	CALL RITE2V(100,1010,1023,90,1,72,1,TITLE,NLAST)					2600
	C					
0013	CALL SETMIV(180,500,610, 40)					2610
0014	CALL GRID2V(-2, 0, 5, 0, 10, 1, 1, 1, 1, -1, -1, 1, 2)					2620
0015	CALL DCLCRT(120,800,ISPACE)					2630
0016	CALL NUCURT(350,595,ISPACE)					2640
0017	DO 200 I=1,NC					2650
0018	X = ETACMU(I)					2660
0019	Y = DCLT(I)					2670
0020	CALL PDINIV(X,Y,I)					2680
0021	200 CONTINUE					2690
	C					
0022	PLOT DCLDA VS ETACMU					2700
0023	CALL SETMIV(600, 80,610, 40)					2710
0024	CALL GRID2V(-2, 0, 5, 0, 10, 1, 1, 1, 1, -1, -1, 1, 2)					2720
0025	CALL NUCURT(770,595,ISPACE)					2730
0026	CALL CLACRT(570,800,ISPACE)					2740
0027	DO 210 I=1,NC					2750
0028	X = ETACMU(I)					2760
0029	Y = DCLDA(I)					2770
0030	CALL POINTV(X,Y,I)					2780
0031	210 CONTINUE					2790
	C					
0032	PLOT DCLMAX VS ETACMU					2800
0033	CALL SETMIV(180,500,200,450)					2810
0034	CALL GRID2V(-2, 0, 5, 0, 10, 1, 1, 1, 1, -1, -1, 1, 2)					2820
0035	CALL CLMCRT(120,400,ISPACE)					2830
0036	CALL NUCURT(350,180,ISPACE)					2840
0037	DO 220 I =1,NC					2850
0038	X = ETACMU(I)					2860
0039	Y = CLMAXP(I)					2870
0040	220 CONTINUE					2880

00/26/45

DATE = 73110

CRTCRT

20

FORTRAN IV G LEVEL

```

0038 CALL POINTV(X,Y,I) 2890
0039 220 CONTINUE 2900
      C 2910
0040 PLOT DCM VS ETACMU 2920
0041 CALL SETMIV(600, 80,200,450) 2930
0042 CALL GRID2V(-2, 0, 5, 0,-5,1,1,-1,-1,1,2) 2940
0043 CALL NCUCRT(770,180,ISPAC) 2950
0044 CALL DLCMRT(570,400,ISPAC) 2960
0045 JY = 140 2970
      JX = 780
0046 CALL PRINTV(6,6,SYMBOL,JX-20,JY) 2980
0047 CALL VCHARV(90,1,JX+60,JY-5,0,TABL2V) 2990
0048 DO 240 J=1,NA 3000
0049 K = J + 1 3010
0050 DC 230 I=1,NC 3020
0051 X = ETACMU(I) 3030
0052 Y = CM(I,J) - CMB(J) 3040
0053 CALL POINTV(X,Y,-K) 3050
0054 230 CONTINUE 3060
0055 JY = JY - 13 3070
0056 CALL POINTV(JX,JY,-K,ANY) 3080
0057 CALL LABLV(ALPHA(J),JX+50,JY,4,1,2) 3090
0058 240 CONTINUE 3100
0059 CALL FRAMEV(3) 3110
0060 CALL RITE2V(100,1010,1023,90,1,72,1,TITLE,NLAST) 3120
      C PLOT CL VS ALPHA 3130
0061 CALL SETMIV(180,500,610, 40) 3140
0062 CALL GRID2V(-2,-10,30,0,12,10,1,1,2,-1,-2,2,2) 3150
0063 CALL CLLCRT(150,800,ISPAC) 3160
0064 CALL VCHARV(90,1,360,595,0,TABL2V) 3170
0065 DO 260 J=1,NA 3180
0066 X = ALPHA(J) 3190
0067 DO 250 I =1,NC 3200
0068 Y = CL(I,J) 3210
0069 CALL POINTV(X,Y,-I) 3220
0070 250 CONTINUE 3230
0071 260 CONTINUE 3240
      C PLOT CLMAXP VS AMAX 3250
0072 DO 265 I = 1,NC 3260
0073 X = AMAX(I) 3270
0074 Y = CLMAXP(I) 3280

```

00/26/45

DATE = 73110

CRTCRT

FORTRAN IV G LEVEL 20

```

0075 CALL POINTV(X,Y,-I)
0076 IX = IXV(X) + I0
0077 IY = IYV(Y)
0078 CALL PRINTV(3,3HMAX,IX,IY)
0079      265 CONTINUE
      C
0080      PLOT CL VS CD
0081 CALL SETMIV(600, 80,610, 40)
0082 CALL GRID2V(-2,-2,-2,0,12,1.0,1.0,1,2,-1,-2,2,2)
0083 CALL CLLCRT(580,800,ISPACE)
0084 CALL CDDCRT(770,595,ISPACE)
0085 DO 280 J=1,NA
0086   DO 270 I =1,NC
0087    X = CD(I,J)
0088    Y = CL(I,J)
0089    CALL POINTV(X,Y,-I)
0090      270 CONTINUE
      280 CONTINUE
      C
0091      PLOT CM VS ALPHA
0092 CALL SETMIV(180,500,200,450)
0093 CALL GRID2V(-2,-10,30,-5,2,10,1,1,-1,-1,2,2)
0094 CALL VCHARV(90,1,360,180,0,TABL2V)
0095 CALL CMMCRT(150,400,ISPACE)
0096 DO 300 J=1,NA
0097  X = ALPHA(J)
0098  DO 290 I=1,NC
0099  Y = CM(I,J)
0100  CALL POINTV(X,Y,-I)
0101      290 CONTINUE
      300 CONTINUE
      C
0102      PLOT CL VS CM
0103 CALL SETMIV(600, 80,200,450)
0104 CALL GRID2V(-2,2,-5,0,12,1,1,1,2,-1,-2,2,2)
0105 CALL CLLCRT(580,400,ISPACE)
0106 CALL CMMCRT(770,180,ISPACE)
0107 JY = 140
0108 JX = 750
0109 CALL PRINTV(6,6HSYMBOL,JX-20,JY)
0110 CALL NCUCRT(JX+50,JY,ISPACE)
0111 DO 310 I = 1,NC
      DO 320 J = 1,NA

```

FORTAN IV G LEVEL	20	CRTCRT	DATE =	73110	00/26/45
0112	X = CM(I,J)				3690
0113	Y = CL(I,J)				3700
0114	CALL POINTV(X,Y,-I)				3710
0115	320 CONTINUE				3720
0116	JY = JY - 13				3730
0117	CALL POINTV(JX,JY,-I,ANY)				3740
0118	CALL LABLV(ETACMU(I),JX+50,JY,4,1,2)				3750
0119	310 CONTINUE				3760
0120	RETURN				3770
0121	END				3780

FORTRAN IV G LEVEL 20 NCUCRT DATE = 73110 00/26/45

```
0001 SUBROUTINE NCUCRT(IX,IY,ISPACE) 3790
0002 EXTERNAL TABL1V,TABL2V 3800
      C DISPLAY NU LOWER CASE 3810
0003 CALL VCHARV(90,1,IX,IY,6,TABL2V) 3820
      C DISPLAY C 3830
0004 I=IX+ISPACE 3840
0005 CALL VCHARV (90,1,I,IY,19,TABL1V) 3850
0006 I=I+ISPACE 3860
0007 CALL VCHARV(90,1,I,IY-7,11,TABL2V) 3870
0008 RETURN 3880
0009 END 3890
```

FORTRAN IV G LEVEL 20

DATE = 73110

DLCMRT

00/26/45

0001	SUBROUTINE DLCMRT (IX,IY,ISPACE)	3900
0002	EXTERNAL TABLIV, TABL3V	3910
	DISPLAY DELTA	3920
0003	CALL VCHARV (90,1,IX,IY,3,TABL3V)	3930
	DISPLAY C	3940
0004	I = IX + ISPACE	3950
0005	CALL VCHARV(90,1,1,IY,19,TABL1V)	3960
	DISPLAY M LOWER CASE	3970
0006	I=I+ISPACE	3980
0007	CALL VCHARV(90,1,I,IY-10,36,TABL1V)	3990
0008	RETURN	4000
0009	END	4010

00/26/45

DATE = 73110

DCLCRT

FORTRAN IV G LEVEL 20

0001	SUBROUTINE DCLCRT (IX,IY,ISPACE)	4020
0002	EXTERNAL TABLIV, TABL2V, TABL3V	4030
	DISPLAY OPEN PARENTH	4040
0003	CALL VCHARV (90,1,IX,IY, 60, TABLIV)	4050
	DISPLAY DELTA	4060
0004	I = IX + ISPACE	4070
0005	CALL VCHARV(90,1,1,IY,3,TABL3V)	4080
	DISPLAY C	4090
0006	I = I+ISPACE	4100
0007	CALL VCHARV(90,1,1,IY,19,TABLIV)	4110
	DISPLAY L IN LOWER CASE	4120
0008	I = I+ISPACE	4130
0009	CALL VCHARV(90,1,1,IY-10,35,TABLIV)	4140
	DISPLAY CLOSE PARENTH	4150
0010	I = I+ISPACE	4160
0011	CALL VCHARV(90,1,1,IY,28,TABLIV)	4170
	DISPLAY THETA IN LOWER CASE	4180
0012	I = I+ISPACE	4190
0013	CALL VCHARV(90,1,1,IY-15,7,TABL2V)	4200
0014	RETURN	4210
0015	END	4220

FORTRAN IV G LEVEL 20 CDDCRT DATE = 73110 00/26/45

0001	SUBROUTINE CDDCRT(IX,IY,ISPACE)	4230
0002	EXTERNAL TABLIV, TABL2V, TABL3V	4240
	C DRAW CD	4250
	C DISPLAY C	4260
0003	CALL VCHARV(90,1,IX,IY,19,TABLIV)	4270
	C DISPLAY D	4280
0004	I = IX + ISPACE	4290
0005	CALL VCHARV(90,1,I,IY-10,20,TABLIV)	4300
0006	RETURN	4310
0007	END	4320

FORTRAN IV G LEVEL 20 CLACRT DATE = 73110 00/26/45

0001	SUBROUTINE CLACRT(IX,IY,ISPACE)	4330
0002	EXTERNAL TABL1V, TABL2V, TABL3V	4340
	C DRAW_GLA	4350
	C DISPLAY C	4360
0003	CALL VCHARV(90,1,IX,IY,19,TABL1V)	4370
	C DISPLAY L	4380
0004	J = IY - 8	4390
0005	I = IX + ISPACE	4400
0006	CALL VCHARV(90,1,I,J,35,TABL1V)	4410
	C DISPLAY ALPHA	4420
0007	J = IY - 16	4430
0008	I = I + ISPACE	4440
0009	CALL VCHARV(90,1,I,J,0,TABL2V)	4450
0010	RETURN	4460
0011	END	4470

FORTRAN IV G LEVEL 20 CMMCRT DATE = 73110 00/26/45

0001	SUBROUTINE CMMCRT(IX,IY,ISPACE)	4480
0002	EXTERNAL TABLIV, TABL2V, TABL3V	4490
	DRAW CM	4500
	DISPLAY C	4510
0003	CALL VCHARV(90,1,IX,IY,19,TABLIV)	4520
	DISPLAY M	4530
0004	I = IX + ISPACE	4540
0005	CALL VCHARV(90,1,1,IY-10,36,TABLIV)	4550
0006	RETURN	4560
0007	END	4570

FORTRAN	IV	G	LEVEL	Z6	CLLCRT	DATE =	73110	00/26/45	
0001					SUBROUTINE CLLCRT(IX,IY,ISPACE)				4580
0002					EXTERNAL TABL1V, TABL2V, TABL3V				4590
				C	DRAW_CL				4600
				C	DISPLAY C				4610
0003					CALL VCHARV(90,1,IX,IY,19,TABL1V)				4620
				C	DISPLAY L				4630
0004					I = IX + ISPACE				4640
0005					CALL VCHARV(50,1,I,IY-10,35,TABL1V)				4650
0006					RETURN				4660
0007					END				4670

FORTRAN IV G LEVEL 20 CLMCRT DATE = 73110 00/26/45

```
0001 SUBROUTINE CLMCRT(IX,IY,ISPACE) 4680
0002 EXTERNAL TABLIV, TABL2V, TABL3V 4690
      C DRAW CL MAX 4700
      C DISPLAY C 4710
0003 I = IX 4720
0004 CALL VCHARV(50,1,I,IY,19,TABLIV) 4730
      C DISPLAY L 4740
0005 I = I + ISPACE 4750
0006 CALL VCHARV(90,1,I,IY-10,35,TABLIV) 4760
      C DISPLAY MAX 4770
0007 I = I + ISPACE 4780
0008 CALL PRINTV(3,3HMAX,I,IY-20) 4790
0009 RETURN 4800
0010 END 4810
```

REFERENCES

1. Campbell, John P., and Johnson, Joseph L., Jr., "Wind Tunnel Investigation of An External-Flow Jet-Augmented Slotted Flap Suitable for Application to Airplanes with Pod-Mounted Jet Engines", NACA TN 3898, dated December 1956
2. Freeman, Delma C., Parlett, Lysle P., and Henderson, Robert L., "Wind Tunnel Investigation of a Jet Transport Airplane Configuration with an External Flow Jet Flap and Inboard Pod-Mounted Engines", NASA TND 7004, December 1970
3. Parlett, Lysle P., Fink, Marvin P., and Freeman, Delma C., Jr., "Wind Tunnel Investigation of a Large Jet Transport Model Equipped with an External Flow Jet Flap", NASA TND 4928, December 1968
4. Parlett, Lysle P., Freeman, Delma C., Jr., and Smith, Charles C., Jr., "Wind Tunnel Investigation of a Jet Transport Airplane Configuration with High Thrust Weight Ratio and an External Flow Jet Flap", NASA TND 6058, 1970
5. Parlett, Lysle P., Greer, H. Douglas, and Henderson, Robert L., "Wind Tunnel Investigation of an External Flow Jet Flap Transport Configuration Having Full Span Triple Slotted Flaps", NASA TND 6391, August 1971
6. Renselaer, D. J., "Analysis of Longitudinal STOL Data Obtained During a NR Wind Tunnel Test of Externally Blown Flaps with Various Geometries", North American Rockwell Corporation, NA-69-435, June 1969
7. Ribner, Herbert S., "Field of Flow About a Jet and Effect of Jets on Stability of Jet Propelled Airplanes", NACA ARC L6C13, April 1946
8. Smith, Charles C., "Effect of Engine Position and High Lift Devices on Aerodynamic Characteristics of an External Flow Jet Flap STOL Model", NASA TND6222, March 1971
9. Volger, Raymond D., "Wind Tunnel Investigation of a Four-Engine Externally Blowing Jet Flap STOL Airplane Model", NASA TND 7034, December 1970
10. Spence, D. A., "A Treatment of The Jet Flap by Thin Airfoil Theory", RAE Report Aero 2568, November 1955

Contrails

11. Maskell, E. C., and D. A. Spence, "A Theory of the Jet Flap in Three Dimensions", RAE Report Aero 2612, September 1958
12. Williams, J., S.F.J. Butler, and M.N. Wood, "The Aerodynamics of Jet Flaps", ARC R&M 3304, January 1961
13. Hughes, M. T., "Results of Low Speed Wind Tunnel Tests of A STOL Research Model", North American Rockwell Report, NA-72-670, August 1972
14. Smith, Charles C., Jr., "~~Effect of Wing~~ Aspect Ratio and Flap Span on Aerodynamic Characteristics of an Externally Blown Jet Flap STOL Model", NASA LWP 1068, July 1972
15. Perry, D. H., with Appendix by D. N. Foster, "A Review of Some Published Data on the External Flow Jet Augmented Flap", RAE Report Aero 3153
16. Fink, Marvin P., "Aerodynamic Characteristics, Temperature and Noise Measurements of a Large Scale External Flow Jet Augmented Flap Model with Turbojet Engines Operating", NASA TND 943, 1961
17. Spence, D. A., "The Lift on a Thin Airfoil with A Blown Flap", RAE Technical Note No. AERO 2450
18. Ross, A. J., "The Theoretical Evaluation of the Downwash Behind Jet-Flapped Wings", ARC R&M No. 3119
19. Thomas, H.H.B.M., and A. J. Ross, "The Calculation of The Rotary Lateral Stability Derivatives of a Jet-Flapped Wing," ARC R&M No. 3277.
20. Parlett, Lysle P., Charles C. Smith, Jr., and James L. Megrail, "Effects of Varying Reynolds Number Through the Range of 0.47×10^6 to 1.36×10^6 on the Aerodynamic Characteristics of an Externally Blown Jet Flap Configuration," NASA LWP 1054, May 1972.
21. Parlett, Lysle P., and James P. Shivers, "Wind Tunnel Investigation of an STOL Aircraft Configuration Equipped with an External Flow Jet Flap, " NASA TND-5364, August 1969
22. Phelps, Arthur E., "Preliminary Low Speed Wind Tunnel Investigation of a Semispan STOL Jet Transport Wing with an Upper Surface Blown Jet Flap," NASA LWP 1022, January 1972

Contrails

23. Moorhouse, D. J., "A Practical Look at the Stall and High Lift Operation of Externally Blown Flap STOL Transport Configurations," AGARD Conference Preprint No. 102 on Fluid Dynamics of Aircraft Stalling
24. McRae, D. M., "The Aerodynamics of High-Lift Devices on Conventional Aircraft, Part I," J. R. Al Soc, Vol 73, No. 702, pp 535-541, 1969

Security Classification		
DOCUMENT CONTROL DATA - R & D		
<i>(Security classification of title, body of abstract and indexing annotation must be entered when the overall report is classified)</i>		
1. ORIGINATING ACTIVITY <i>(Corporate author)</i> Los Angeles Aircraft Division Rockwell International Corporation Los Angeles International Airport, L. A., Calif. 90009	2a. REPORT SECURITY CLASSIFICATION Unclassified	
3. REPORT TITLE STOL Tactical Aircraft Investigation, Externally Blown Flap, Volume II Design Compendium		
4. DESCRIPTIVE NOTES <i>(Type of report and inclusive dates)</i> Final Report (10 June 1971 to 10 December 1972)		
5. AUTHOR(S) <i>(First name, middle initial, last name)</i> Marshall H. Roe Dirk J. Renselaer Ralph A. Quam		
6. REPORT DATE April 1973	7a. TOTAL NO. OF PAGES 182	7b. NO. OF REFS 24
8a. CONTRACT OR GRANT NO. F33615-71-C-1760 b. PROJECT NO. 643A - Task 0020 d.	9a. ORIGINATOR'S REPORT NUMBER(S) 9b. OTHER REPORT NO(S) <i>(Any other numbers that may be assigned this report)</i> AFFDL-TR-73-20 Volume II	
10. DISTRIBUTION STATEMENT Approved for public release; distribution unlimited.		
11. SUPPLEMENTARY NOTES	12. SPONSORING MILITARY ACTIVITY Air Force Flight Dynamics Laboratory (PTA) Wright Patterson AFB, Ohio, 45433	
13. ABSTRACT The basic objective of the work reported herein was to provide a broader technology base to support the development of a medium STOL Transport (MST) airplane. This work was limited to the application of the externally blown flap (EBF) powered lift concept. The technology of EBF STOL aircraft has been investigated through analytical studies, wind tunnel testing, flight simulator testing, and design trade studies. The results obtained include development of methods for the estimation of the aerodynamic characteristics of an EBF configuration, STOL performance estimation methods, safety margins for takeoff and landing, wind tunnel investigation of the effects of varying EBF system geometry parameters, configuration definition to meet MST requirements, trade data on performance and configuration requirement variations, flight control system mechanization trade data, handling qualities characteristics; piloting procedures, and effects of applying an air cushion landing system to the MST. From an overall assessment of study results, it is concluded that the EBF concept provides a practical means of obtaining STOL performance for an MST with relatively low risk.		

Security Classification

14. KEY WORDS	LINK A		LINK B		LINK C	
	ROLE	WT	ROLE	WT	ROLE	WT
STOL Transport Externally blown flaps Medium STOL Transport Aerodynamic Methods Lift Augmentation						